A NEW METHOD FOR ANALYSING THE MIXED LUBRICATION IN METAL ROLLING

BY

MOHAMMAD NAZMUL HOSSAIN KHAN

A thesis submitted in fulfilment of the requirements for the degree

of **Masters by Research** in 2012

School of Mechanical and Manufacturing Engineering

The University of New South Wales

Sydney, Australia

ORIGINALITY STATEMENT

‘I hereby declare that this submission is my own work and to the best of my knowledge it contains no materials previously published or written by another person, or substantial proportions of material which have been accepted for the award of any other degree or diploma at UNSW or any other educational institution, except where due acknowledgement is made in the thesis. Any contribution made to the research by others, with whom I have worked at UNSW or elsewhere, is explicitly acknowledged in the thesis. I also declare that the intellectual content of this thesis is the product of my own work, except to the extent that assistance from others in the project's design and conception or in style, presentation and linguistic expression is acknowledged.’

Signed …….....

Date …….....

(A) COPYRIGHT STATEMENT

‘ I hereby grant to the University of New South Wales or its agents the right to archive and to make available my thesis or discussion in whole or part in the University libraries in all forms of media, now or hereafter known, subject to the provision of the copyright Act 1968. I retain all proprietary rights, such as patent rights. I also retain the right use in future works (such as articles or books) all or part of this thesis or dissertation. I also authorise University Microfilms to use the abstract of my thesis in Dissertations Abstract International (this is applicable to doctoral thesis only). I have either used no substantial portions of copyright material in my thesis or I have obtained permission to use copyright material; where permission has not been granted I have applied/will apply for a partial restriction of the digital copy of my thesis or dissertation.’

Signed: .....

Date: .....

(B) AUTHORITY STATEMENT

‘I certify that the library deposit digital copy is a direct equivalent of the final officially approved version of my thesis. No emendation of content has occurred and if there are any minor variations in formatting, they are the result of the conversion to digital format.’

Signed: .....

Date: .....

ACKNOWLEDGEMENTS

I would like to express my sincerest appreciation to Professor Liangchi Zhang for his kind guidance, encouragement and every support during this project's progression.

Great thanks are due to Dr Haihui Ruan for his help and invaluable words of advice, especially in writing Subroutine by FORTRAN code. I would also like to thank Dr Thai Nguyen for his valuable advice and cooperation.

The continuous financial support from the Australian Research council (ARC) and State Key Laboratory for Rolling Technology, China is highly appreciated.

Finally, I would like to delicate this thesis to my mother for her continuous encouragement and mental support.

ABSTRACT

Mixed lubrication is an important lubrication mode in metal rolling, and if controlled properly, can improve the performance of a metal rolling process. However, the choice of appropriate processing parameters for realising proper mixed lubrication is a big challenge due to the complex solid-fluid interaction, surface asperity deformation, and the random nature of the asperity distributions through the rolling gap. A complete solution to mixed lubrication with full resolution down to the microscopic asperity level is formidable, although the fundamental fluid and solid mechanics have been established. A practical approach is to solve the problem in macroscopic scale but with sufficient ingredients of microscopic contact mechanics. A great deal of research efforts in the past decades has led to some implicit solutions, which include slab method in coupling with some asperity contact models. In these studies, film thickness and asperity contact are solved when an external pressure is obtained from the deformation of the strip. The load sharing by the liquid and the asperities are then solved in an iterative procedure. Such a process, however, often leads to divergence.

The aim of this thesis is to establish an explicit numerical approach to investigate mixed lubrication in metal rolling. The asperities on a slab surface were treated as contact springs with non-linear stiffness based on the Greenwood-Williamson's formulation, which relates the dry contact stress to the separation between the roll and slab's reference surfaces. The lubricant film thickness was assumed to be a function of the separation and the actual dry contact area. The lubricant pressure in every time step was obtained by solving the finite-difference form of modified Reynolds equation with input of nodal velocity and film thickness from the finite element (FE) simulation. This

approach was successfully implemented as a user-interface subroutine in the ABAQUS explicit FE code. It was found that the convergence problem could be easily avoided by simply reducing the time increment to an appropriate level. The developed of user interaction code was verified by Hertz contact problem. The results of a case study on strip rolling analysis were compared with the experimental results and a good agreement was found. A detailed parametric study was explored for the effect of the viscosity and rolling velocity on contact pressure, frictional force, friction reduction, hydrodynamic pressure in mixed lubrication.

Keywords: metal strip rolling, mixed lubrication, fluid-solid interaction, friction, random asperity, statistical modelling.

NOMENCLATURE

A	Real area of asperity contact
$A(d)$, $\overline{A}_a(d)$	Total integral area of asperity contact (mm^2)
a	Constant
C	Constant
d	Separation between two rough surfaces (mm)
E, E'	Young's modulus (MPa)
E_o	Expectancy operator
F_a	Individual asperity contact force (N)
$\overline{F}_a(d), F$	Total integral contact force per unit area (N)
g	Function
H	Ratio of separation to roughness
h	Asperity height (mm)
h_T	Average film thickness (mm)
h'	combined roughness (mm)
h_a	Height of individual asperity (mm)
m	Stiffness modification factor
n	Hardening coefficient
h_l	Local film thickness (mm)
h_T	Average film thickness (mm)
L	Length (mm)
$L_{0.5x,y}$	Length of x and y profile of asperity
N	The number of asperities per unit area
$p(h_a, x, y)$	Probability density function
P_a	Asperity contact pressure (MPa)
P_n	Normal pressure (MPa)

P_t	Frictional force per unit area (MPa)
p_f	hydrodynamic pressure (MPa)
P_f	Average hydrodynamic pressure (MPa)
R	Radius of the roller (mm)
r	Constant
t	Strip thickness (mm)
U_r	Roll speed m/s
U_s	Strip speed m/s
w_c	Critical interference
X	Contact length measured from the entry point (mm)
Y	Yield stress (GPa)
$\sigma,\sigma_{1,}\sigma_2$	Standard deviation of asperity height (mm)
σ_{11}	Normal stress in the transverse direction of the strip (MPa)
σ_{22}	Normal stress in the vertical direction of the strip surface (MPa)
β	Tip radius of asperity (mm)
γ	Surface characteristic number
δ	Function
Γ	Function
τ_a	Dry sliding frictional force per unit area (MPa)
τ_f	Shear force of the lubricant per unit area (MPa)
μ	Viscosity (Pa.s)
μ_o	Overall frictional coefficient
λ	Ratio of film thickness to RMS roughness
ϕ_x	Flow factor in the x direction
ϕ_s	Shear flow factor
ψ	Asperity distribution function
ζ	Plasticity index

τ	Uniaxial stress (MPa)
μ_a	Coulomb friction coefficient
μ_o	The resultant coefficient of friction
ε_p	Uniaxial plastic strain
v	Poisson ratio

LIST OF FIGURES AND TABLES

Fig. 2.1	Deformation pattern in different zones of deformed strip	9
Fig. 2.2	Sectional view of two sensors	11
Fig. 2.3	Pressure comparison for two friction model	18
Fig. 2.4	Pressure distribution: Experimental result of Al-Salehi *et al.* and FE result of Liu et al.	23
Fig. 2.5	Film thickness in rough surfaces contact	32
Fig. 2.6	Contact areas for different surface orientation	36
Fig. 2.7	Prediction of the normal pressure and hydrodynamic pressure	46
Fig. 3.1	The schematic of mixed lubrication in strip rolling	52
Fig. 3.2	Two rough surfaces contact	53
Fig. 3.3	The concept of equivalent film thickness	59
Fig. 3.4	The flow chart of numerical calculation	61
Fig. 3.5	Contact pressure distribution of a cylindrical indentation problem	63
Fig. 3.6	Hydrodynamic pressure comparison for constant velocity case	66
Fig. 3.7	Hydrodynamic pressure comparison for variable velocity case	67
Fig. 4.1	FE meshes and model	70
Fig. 4.2	Plastic stress-strain curve	71
Fig. 4.3	FE mesh sensitivity test	72
Fig. 4.4	Separation of two reference surfaces during rolling	73

Fig. 4.5 The distribution of frictional force: (a) friction coefficient 0.1 and (b) effect of friction coefficient 75

Fig. 4.6 Comparison of normal pressure and frictional force 77

Fig. 4.7 Distribution of the velocity perpendicular to the rolling direction 77

Fig. 4.8 Hydrodynamic pressure and resultant friction 79

Fig. 4.9 Comparison of normal pressure for 21.86 % reduction 81

Fig. 4.10 Comparison of normal pressure for 29.40 % reduction 81

Fig. 4.11 Hydrodynamic pressure and normal pressrue 84

Fig. 4.12 Distribution of real area of contact for different viscosity 86

Fig. 4.13 Real area of contact for different plasticity index 87

Fig. 4.14 Effects of separation on (a) force and (b) contact pressure 89

Fig 4.15 (a) The frictional force and (b) hydrodynamic pressure for different viscosity 91

Fig. 4.16 Effects of lubricant on (a) the resultant friction coefficient and (b) hydrodynamic pressure 92

Fig. 4.17 Hydrodynamic pressure for different rolling velocity 94

Table 3.1 Parameters used in the simulation 62

Table 3.2 Parameters used in the analytical calculation 66

Table 4.1 Parameters used in the rolling analysis 73

Table 4.2 Lubricants used in the parametric study 83

CONTENTS

Originality statement ii

Copyright statement iii

Authority statement iii

Acknowledgements iv

Abstract v

Nomenclature vii

List of figures and tables x

Chapter 1: Introduction 1

Chapter 2: Literature review 5

2.1 Introduction 6

2.2 Metal rolling 7

2.2.1 Experimental investigation 7

2.2.2 Theories of metal rolling 13

(a) Slip line theory 13

(b) Slab method 14

(c) The finite element method 19

2.3 Mixed lubrication 25

2.3.1 Asperity deformation model 26

2.3.2 Lubricant flow model 31

2.3.3 Coupling of asperity deformation and lubricant flow 38

2.4 Discussion and conclusions 47

Chapter 3: Methodology 50

3.1 Basic assumptions 51

3.2 Formulations 53

3.2.1 Asperity distribution and contact pressure calculation 53

3.2.2 Calculation of hydrodynamic pressure 57

3.3 Implementation 60

3.4 Approach verification 62
3.4.1 Hertz elastic contact problem 62
3.4.2 Verification of the solution of Reynolds equation 64

Chapter 4: Results and analysis 68

4.1 Rolling analysis 70
4.1.1 Numerical model and parameters 70
4.1.2 Neutral point 74
4.1.3 Contact pressure 76
4.1.4 Deformation in rolling 78
4.1.5 Hydrodynamic pressure and resultant friction coefficient 79
4.1.6 Different thickness reduction ratio 80
4.2 Parametric study 82
4.2.1 Effect of lubricant on contact pressure 83
4.2.2 Effect of lubricant on frictional force 90
4.2.3 Effect of lubricant on resultant friction 92
4.2.4 Effect of rolling speed on hydrodynamic pressure 93
4.3 Discussion and conclusions 94

Chapter 5: Conclusions 97

Bibliography 101
Appendix 116

Appendix-1 FORTRAN subroutine code 117
Appendix-2 List of publication 128

CHAPTER 1

INTRODUCTION

Metal strip rolling is a key metal forming process. The production of high-quality strip can only be achieved by applying improved manufacturing technique and thorough understanding of the rolling processes. However, metal rolling is a very complex mechanics problem, in which the surfaces are rough and the asperities that take part in the deformation process are of a much smaller scale compared with the strip dimensions. The asperities are deformed or flattened in the rolling process (Sutcliffe 1988; Wilson and Sheu 1988). Moreover, the effect of the microscopic asperity-asperity contact in the overall macroscopic deformation is not well understood.

The rolling process takes place with the aid of frictional force throughout the roll-strip rolling gap. However, the excessive frictional force may deteriorate the quality of the rolled surface due to wear, crack and edge crash in the surface. Different coolants are used in the production process to control the temperature and to reduce the friction coefficient in the rolling interface. Generally, water with different types of lubricants is used as coolant (Kosasih and Tieu 2007). However, the choice of appropriate lubricants is still a big challenge due to lack of a reliable mixed lubrication model. The consensus has been that the best way is to develop a stable rolling mode in mixed lubrication, because mixed lubrication can provide low friction and improved surface quality (Lu, Kiet Tieu *et al.* 2003; Sutcliffe and Johnson 1991; Wilson and Sheu 1988) Improving the performance of rolling and developing new products need a radical innovation in the fundamental theory that will lead to high precision and damage free surfacing.

In mixed lubrication, only the asperities are in solid-solid contact and the rest of the contact is under solid-liquid interaction. In the interface of rolling, significant hydrodynamic pressure may develop and share part of the total load applied for the

deformation. The total normal pressure is shared between the asperity contact pressure and hydrodynamic pressure in the contact interface (Sheu and Wilson 1994). The frictional force in mixed lubrication plays a vital role in reducing the overall coefficient of friction. There are frictional forces due to both solid shearing and liquid shearing. Therefore, total frictional force is also shared in the interface in mixed lubrication that must be addressed with an appropriate friction model.

The direct solution of mixed lubrication has posed a great difficulty due to multiscale modelling problems. The asperities and thin fluid films are in micro-scale; say 2-15 micrometer; whereas, the bulk material is in macro-scale. The numerical solution would produce millions of elements in the analysis, which makes it impossible to get a converged solution with existing computing capacity. There is a need to apply a novel technique to avoid these numerical difficulties but at the same time to consider the effects of micro and macro ingredients in the solution process.

In this study, an innovative numerical technique will be developed to explore mixed lubrication mechanics addressing the multi-scale modelling approach and load sharing principle in the interface. Specifically this study will accomplish the following outcomes:

(a) To develop a multi-scale modelling technique to account for the deformation of surface asperities and bulk material formation under mixed lubrication;
(b) To integrate this new technique with the FE method, through a user interface subroutine approach in a commercial code, for mixed lubrication analysis;

(c) To understand the effect of some key rolling parameters, including lubricant, rolling velocity, real area of contact, etc., on the pressure and friction of metal rolling.

CHAPTER 2

LITERATURE REVIEW

2.1 Introduction

The concept of rolling appeared at the end of 15th century (Roberts 1978). Since then, there has been a great deal of research initiatives into the mechanics of the rolling process, both theoretically and practically. Presently, the quality of product can be improved only by optimising the rolling conditions or parameters of the existing mills. Different solution techniques and experimental studies have been implemented by researchers in rolling analysis to study the contact pressure, shear traction, deformation of material, stress and strain. But these are not sufficient to meet the growing demand of quality products in the industry. It is crucial for the rolling industries to develop innovative rolling technologies with superior surface integrity and precision of rolling profile but at a low cost. However, despite the increase in research and investment of steel rolling plants, there remain many fundamental questions not yet answered. A method to choose appropriate processing parameters like rolling speed, lubricants and roll diameter, which are very important in the production process, remains elusive. The need for obtaining a reliable and accurate rolling model thus becomes emphasized.

The early rolling theories were based on some assumptions, for example the Von Karman's homogeneous theory (Von Karman 1925) and plane strain theory. However, the implementation of these theories leads to large discrepancy due to oversimplifications. Moreover, different lubricants are used in industry to control quality and economy production. The early analyses of rolling for dry contact (Fleck and Johnson 1987; Gratacos, Montmitonnet *et al.* 1992) have been extended to include lubricants and thus have involved more assumptions. Many of these assumptions are not realistic and have led to discrepancy. It has been revealed that a stable mixed lubrication mode can provide superior surface integrity by reducing the friction coefficient and

avoiding friction pick up (Chang, Marsault *et al.* 1996; Geike and Popov 2008; Ramamohana Rao and Mohanram 1994; Rao and Mohanram 1993; Sheu and Wilson 1994; Stiharu, Demian *et al.* 1994; Sutcliffe and Johnson 1991). However, mixed lubrication is a multi-scale modelling problem, which involves asperity deformation, strip plastic deformation, load sharing between solid and liquid, lubricant flow and complex friction mechanism. To develop a mixed lubrication model, the surface deformation mechanics must be addressed properly to include not only the macro but also the micro effect. Direct numerical simulation with details down to microscopic resolution is extremely difficult. Therefore, a reliable mixed lubrication model must be sufficiently abstractive and implementable but also include sufficient ingredients of statistical rough surface features, asperity-asperity contact mechanics, fluid flow between the rough surfaces, and the interaction between lubricant and asperities.

In this literature review, the experimental and theoretical works on metal rolling are discussed in Section 2.2. The details of mixed lubrication, which includes asperity contact models, lubricant flow models and different mixed lubrication models will be presented in Section 2.3. A discussion and conclusion will be presented in Section 2.4, which will highlight an innovative research direction of this study.

2.2 Metal rolling

2.2.1 Experimental investigation

Experimental techniques have been developed with varying degrees of success for metal rolling by many researchers. Few techniques have received widespread acceptance, though many techniques have contributed to a more complete understanding of the

rolling process. These studies were valuable to understand the rolling mechanism, deformation pattern, contact pressure, shear stress, coefficient of friction, rolling force and torque. At first, the experimental studies were limited to the observation of metal flow pattern in rolling. The earliest recorded experiment for rolling was done by Hollenburg (Hollenberg 1883). In this experiment, the internal flow of metal was investigated by drilling some holes in the strip surface, which are then filled up with wrought iron plugs. By inspecting the deformation of the plugs, the internal flow of metal was observed. The wrought iron plugs are replaced later by screws. This modification has facilitated the observation of compression at various heights and the axis of bending of the metal flow. In this study, the vertical section of the strip surface was found concave. This was in sharp contrast to the earlier theories, where the vertical section was assumed to remain as plane.

Multi-coloured plasticine bars were rolled by Orowan (Orowan 1943). This was one of the most important experimental works to represent broad ideas of the deformation pattern and to identify the different zones of the strip surface. The vertical section was found concave due to deformation which was similar to the study of Hollenburg. The material was deformed as the roll enters deeper into the strip surface during deformation. Along the strip surface in contact with the rolls is a point moving with the same velocity as the circumference of the roll surface. This is defined as the neutral point. The material that has not reached that point is moving slower than the roll periphery and after that it moves faster. Orowan indentified the four deformation zones in the deformed strip, as shown in Fig. 2.1: restricted deformation zone (zone I), plastic deformation zone (zone II) and rigid zones (zones III and IV). The idea of different deformation zones in rolling was inspiring to many authors.

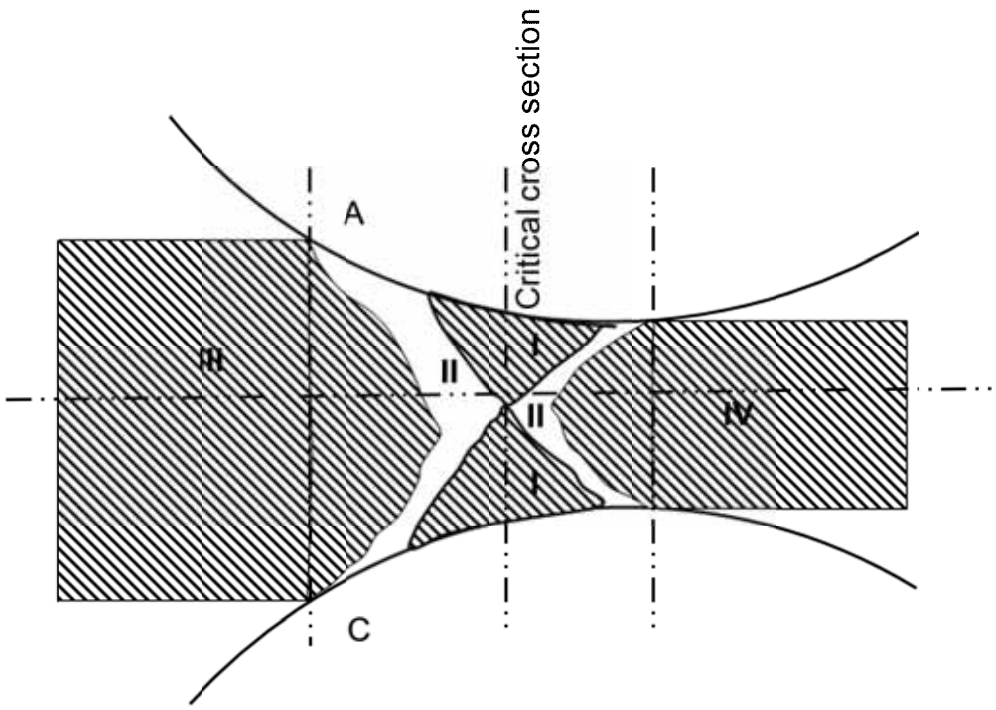

Figure 2.1: Deformation pattern in different zones of deformed strip (Orowan 1943)

Contact pressure, frictional force and the coefficient of friction are the important parameters that can address rolling mechanics in depth in comparison to studying the deformation of the flow pattern. The pin load cell technique was used by many authors to measure the contact pressure and frictional force distribution in the arc of contact. Siebel and Lueg (Seibel and Lueg 1933) were the first to use the large pin load cell technique to calculate the pressure variation in rolling for copper, iron and aluminium strip. A piezo-electric crystal with suitable detecting equipment was used in the experiment. The pin was carefully fixed into the recesses in the roll with their ends ground together with the roll surface. Force acting on the pin surface was measured by detecting the axial strain in the pin. A substantial correction factor was used due to the large ratio of pin width to arc length of contact. Pressure distribution along the arc of contact was obtained by using this method. This technique has been developed and applied widely by later workers, such as Smith *et al.*(Smith, Scott *et al.* 1952), Orowan

et al.(Orowan, Scott *et al.* 1950), Macgregor and Palme (McGregor and Palme 1959) and others. The pin load cell technique was further improved by introducing two pins, one in a normal direction and another in an oblique direction to measure the pressures by Van Rooyen and Backofen (Van Rooyen and Backofen 1957). Al-Salehi *et al*. (Al-Salehi, Firbank *et al.* 1973) applied pin-load-cell technique more extensively for calculating normal pressure and frictional force for different material strips. They used smaller transducer pins than those used in earlier experiments. Al-Salehi *et al*. conducted large numbers of experiments for aluminium, copper and mild steel materials with improved design of the transducer and increased sensitivity. It is the most detailed experiments so far available in the literature. This study has found more than one peak in the pressure distribution. There were also some discrepancies between the experimental result of Al-Salehi *et al*. and the theoretical results. Most of the discrepancies are in the areas of higher thickness reduction or when pressure distribution exhibits more than one peak.

More-than-one-peak pressure distribution was also found by McGregor and Palme (McGregor and Palme 1959). They explained this by referring to the fact that the conditions were not those of plane strain. This explanation is however inadequate as the ratio of strip width to strip thickness was always greater than 10. Their pressure distribution was wave-like for the rolling of aluminium, copper and steel bars. The pin-load-cell technique was also used by Lai-Send *et al*. (Lai-Send and Lenard 1984) to determine the coefficient of friction using an exponential relationship that was calculated from the experimental observation of high pressure tests.

More recently, a two-pin-load-cell technique was used by Jiang *et al*. (Jiang, Tieu *et al.* 2004) to determine the coefficient of friction as shown in Fig. 2.2 in an experimental rolling mill. In this experiment, one pin with a load cell and a strain gauge was mounted along the radius and the other pin was set at an oblique angle of 25^0 from the radially embedded pins. A thermocouple pin was also embedded to measure the temperature. The load cells and strain gauges signals are transmitted via a slip ring to an amplifier box, and the output was finally collected by a computer. The measured coefficient of friction was finally used in the 3D rigid plastic FE simulation. The measured friction coefficient from this study was used in the FE rolling contact simulation. The authors claimed that the study was a mixed film lubrication model; although a FE dry contact simulation was done by applying the measured variable coefficient of friction.

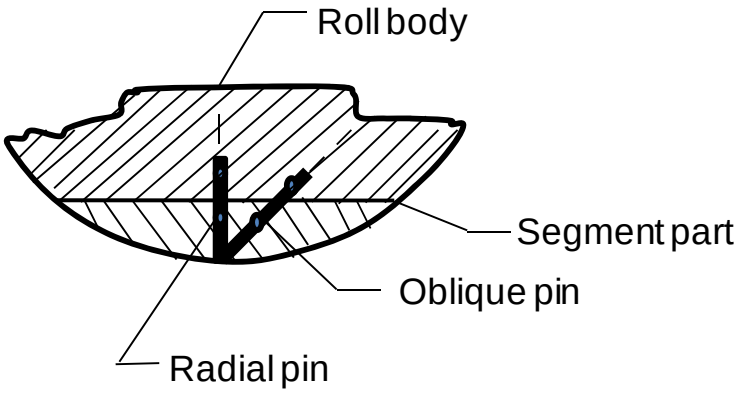

Figure 2.2: Sectional view of two sensors (Jiang *et al.* 2004)

A photo-elastic technique (Cole and Sansome 1968) was used in studying the deformation of strip in contact with roll for both normal and tangential pressure. In the arc of contact, a roll made of epoxy resin and a strip made of lead were used in the experiment. The rolling pressure was then measured. In this experiment, the pin was used to bear upon a photo-elastic dynamometer in addition to measuring pressure

distribution; the experimenters also investigated the errors associated with pin protrusion. A lead strip was also used by Khayyat and Lancaster (Khayyat and Lancaster 1969) as stock material. The rolls were made entirely of Araldite in order to establish the pressure and frictional force distribution in the arc of contact. The forward frictional force along the arc of contact was used for further refinements of this technique to establish true plane strain conditions and to enable a greater accuracy.

In 1983, Theocaris *et al*. (Theocaris, Stassinnkakis *et al.* 1983) used a caustic technique to measure normal and tangential pressure distributions in rolling. In this method, a light beam impinges on the specimen and the reflected light rays from the front end lateral face of the roll were concentrated along a highly illuminated surface in space. This is called the formation of a caustic surface, which was then cut by a reference plane placed at a distance from the work-piece. A potential function was developed from this relationship to calculate the normal and tangential pressure on the contact. When the caustic surface was cut by a reference screen, placed at some distance from the specimen, a singular curve, called a caustic was formed. The position of a point on the lateral surface of the deformed roll was related to that of a corresponding point on the screen.

Experimental techniques in rolling has been improved substantially from time to time in line with the improvements in technology. The earlier studies were limited to only analysis of the metal flow and deformation pattern of the strip surfaces. The pin-load-cell technique was an effective technique to find normal and tangential stresses and the coefficient of friction in the arc of contact. The measured pressure distribution, neutral point, and frictional force contribute to the understanding of rolling mechanics. The

single peak contact pressure distribution was initially found by Orowan. Experimental studies found multiple peaks later (Al-Salehi *et al.* 1973) in the pressure distribution. The coefficient of friction was also calculated experimentally which also helped to understand the rolling mechanics more precisely. But there were many limitations as well in the experimental works. For example, though lubricants are used in many experiments, exact information about such things as film thickness, lubricant pressure and contribution of lubricant pressure are still unknown.

2.2.2 Theories of metal rolling

Many theories have been devised for the analysis of both cold and hot rolling problems. These theories deal with elasto-plastic metal deformation, stress–stain relationship, contact pressure, frictional force, and effects of processing parameters in metal rolling. Many assumptions and simplifications have been necessary in the past analytical models due to the limitation of computational capacity. Modern metal rolling analyses and numerical methods still use those fundamental theories but with improved numerical accuracy and reliability.

(a) Slip line theory

Slip-line theory provides a good insight into the plastic flow of deformed strip. In the slip-line solution process, the plastically deforming regions are first identified. This is done by the presumed orthogonal lines. The paths of these lines are assumed to be the regions of maximum shear strain rate. Boundary conditions are applied to determine the limits of the slip-line field and the deformed geometry. The distribution of velocity can be constructed based on the slip-line field from where the metal flow can be determined.

Although slip-line field solutions are available for many metal forming processes, the method was not successfully applied until 1955, when Alexander (Alexander 1955) first successfully applied slip-line field solutions to the hot rolling process. Alexander identified the slip-line field satisfying both force and velocity boundary conditions through a trial-and-error method. Alexander made the slip lines meet the roll/strip interface either tangentially or normally. His first solution can only be applied for a single geometry. Alexander and other authors (Crane and Alexander 1968; Dewhurst, Collins *et al.* 1973) later developed a more comprehensive slip-line field solution which was capable of dealing with many different geometries.

The Slip-line solution has the advantage of determining stress and velocity distributions in the plastic zone. However, there is an uncertainty in slip-line theory as it may lead to more than one solution for the same boundary conditions. There are some difficulties in clearly identifying the region of plastic deformation. The accuracy of the slip line solution also depends on the analyser's experience and institution. Moreover, the solution is limited to plane strain conditions and rigid-perfectly plastic material behaviour.

(b) Slab method

In the slab method, the deformed strip is divided into a number of small slabs and a differential equation is then established from the equilibrium of forces acting on the deformed surface. In the slab method, the direct stress is uniform in the vertical section (in the thickness direction of the strip), which means that the vertical section remains plane. For the analysis of metal rolling problems, arc of contact is then divided into different zones; such as inlet, plastic or work and exit zones, where different conditions

for material deformation models are applied in the solution. This is the basic concept of the slab method. Researchers (Alexander 1972; Fleck and Johnson 1987) extended this basic concept for both thick and thin strip rolling problems that involved different friction models, slipping-sticking assumptions and the strain hardening model. The differential equations were solved by applying different numerical techniques. For example the Newton-Raphson method was used by Fleck and Johnson *et al.* solution (Fleck, Johnson *et al.* 1992) for simulating foil rolling.

Von Karman (Von Karman 1925) and Nadai (Nadai 1931) were the first to apply the slab method to determine roll pressure and force in rolling. Von Karman used the homogeneous deformation assumption in his rolling model. The slab method was then extended to inhomogeneous deformation by including perfectly plastic deformation and constant interfacial shear in the constitutive model. It can take both slipping and sticking friction into consideration. Orowan adapted the Prandle-Nadai (Nadai 1931) theory of metal compression between plane rough plates inclined at a small angle. The pressure distribution was calculated for the coefficient of friction of 0.14 and 0.4 and it was found in good agreement with the measurement results of Siebel and Lueg (Seibel and Lueg 1933) for the same geometric conditions. Alexander (Alexander 1972) introduced numerical integration to the equation of Orowan and found that the solution was computer resource sensitive. This equation was then further simplified by Bland and Ford (Bland and Ford 1943) by assuming the angle of roll-strip contact to be very small. The slab method was also used by many authors for thin strip (thickness less than 0.2 mm) or foil rolling analysis, for example by Alexander (Alexander 1972), Fleck *et al*. (Fleck and Johnson 1987) and Sutcliffe (Le and Sutcliffe 2003).

Fleck *et al.* (Fleck and Johnson 1987) developed a foil rolling model by using constant Coulomb friction law and treating rolls as elastic half space. The strain hardening of the strip surface was ignored in this study. The roll–strip contact interface was divided into five zones: elastic deformation at entry, plastic reduction at entry, no slip neutral zone, plastic reduction at exit and elastic deformation at exit. For the slipping zones, force equilibrium equations are applied to find the variation of pressure in the rolling direction. For the no slip neutral zone, a matrix equation was established with respect to roll deformation under normal pressure. The matrix equation was then inverted to find the variation of pressure in this no slip zone. A Newton-Raphson scheme was used to find the position between each of the two zones for applying continuity boundary conditions. Theoretical predictions of this model were in reasonable agreement with experiments with model materials used by Sutcliffe and Rayner (Sutcliffe and Rayner 1998). This model was then extended by Yuen *et al*. and co-workers (Dixon and Yuen 1995; Yuen, Dixon *et al.* 1996) to include strain hardening of the strip. Domanti *et al.* (Domanti, Edwards *et al.* 1994) used influence functions for circular rolls described by Jortner (Jortner, Osterle *et al.* 1960) for thin strip and temper rolling problems. They reported that each calculation time is only a very few seconds, although it is unclear how severe the roll flattening is for these calculation times.

Although these models described in the previous paragraph have gained widespread acceptance, they suffer from two major drawbacks. Firstly the identification of different zones, for which the boundaries have to be solved, is numerically unstable and time-consuming. Secondly the regime of roll deformation for the central flat region has to be indentified before starting the calculation. These deficiencies need to be overcome before friction modelling, which plays a key role in foil rolling. Zhang (Zhang 1995)

released the assumption of a flat no-reduction region, relating the shear stress to the roll shape and contact pressure in this region. This allows direct solution of the shear stress and contact pressure in the central region, giving much improved efficiency and less execution time. Alternatively, Gratacos *et al.* avoided this difficulty by defining a friction law, which simulates sticking friction in the neutral zone and slipping friction elsewhere (Gratacos *et al.* 1992).

Following the approach of Fleck *et al.*, Le *et al.*(Le and Sutcliffe 2001) developed a thin strip rolling model by relaxing the central neutral zone assumption by introducing a new explicit relation for pressure variation for the central no-slip zone. Moreover, this approach treats cases where the roll retains its circular arc or where there is significant roll deformation in the same way, greatly simplifying the solution process. This study found that the effect of equal entry and exit tension is equivalent to reducing the yield stress of the strip by this tension. This model predicts an increase in forward slip with increasing exit tension or decreasing entry tension, an effect well known from industrial practice.

Kumar *et al.* (Kumar and Dixit 2006) further developed the model of Le *et al.* (Le and Sutcliffe 2001) by introducing the friction model of Wanheim and Bay (Wanheim and Bay 1978) and strain hardening of material in the arc of contact. The authors claimed that Wanheim and Bay's friction model is more appropriate for the thin strip rolling problem compared to the Coulomb friction model. Fig. 2.3 shows the difference of pressure distribution in between the two friction models, where Coulomb friction model is showing higher pressure comparing to Wanheim and Bay's model. They also found

that the average value of flow stress in a non-hardening model does not yield correct results if the material strain hardening is significant during the process.

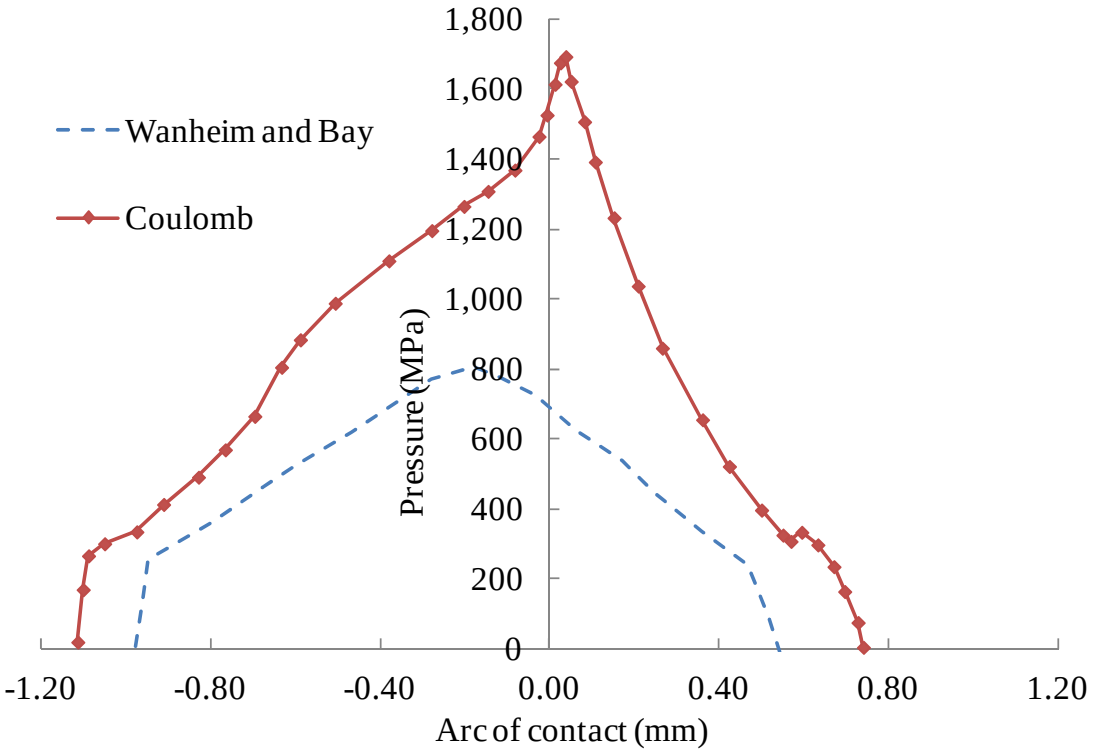

Figure 2.3: Pressure comparison for two friction model (Kumar and Dixit 2006)

The slab method is extensively used in symmetric and steady state rolling cases as discussed up to this paragraph. The method was also used in asymmetric and unsteady rolling models (Salimi and Kadkhodaei 2004; Salimi and Sassani 2002; Serajzadeh, Karimi Taheri *et al.* 2002; Tian, Guo *et al.* 2009). Recently, the slab method is used in the development of mixed lubrication model that will be discussed in Section 2.3.3. The assumptions and simplification in the dry contact models developed by the slab method will be retained in the mixed lubrication cases as well. Although the slab method gives a

reasonable accuracy, it is a simplified analysis with respect to modern numerical analysis (FE), where the application of continuum mechanics gives more accurate computational accuracy. For example, there is no need to define the different zones of deformation in the modern FE method. The assumptions for the different zones, slipping and sticking conditions and roll shape assumptions may lead to significant errors in the slab method calculation. Despite many limitations, the slab method is still a basic tool for rolling analysis as in many structural analyses and is used in the industry.

(c) The finite element method

The use of the FE method has become popular due to the easy use of boundary conditions, treatment for large deformation, meshing in fine elements, solution control, and numerical accuracy. The FE method is also proved to be powerful in metal forming simulation (Hwu and Lenard 1988; Liu, Hartley *et al.* 1985; Miguel, Marcela *et al.* 2001; Zhang, Zhang *et al.* 2010; Zienkiewicz, Jain *et al.* 1978). Two different approaches of the FE method have been used in the structural analysis, namely solid approach and fluid approach. In the solid approach, the metal behaviour is considered as rigid-plastic, elasto-plastic and elasto-viscoplastic. On the other hand, in the fluid approach, the material is considered to behave as non-Newtonian fluid. In the solid approach, two continuum formulations are used, namely updated Lagrangian formulation and Eulerian formulation. Most of the metal rolling problem was modelled by the Lagrangian formulation by conducting transient analyses until steady–state conditions are reached (Li and Kobayashi 1982; Mori, Osakada *et al.* 1982). The incremental equation is then solved according to FE mesh. In the Eulerian approach, the steady state response is reached by transient analyses, while mesh remains fixed in space. Moreover, the Eulerian method is used to refine the localized region of FE by

fine meshing in the crucial region rather than fine meshing for all regions. In the early FE analysis of the metal rolling problem, the elastic deformation of the roll was ignored by assuming roll as rigid due to this difficulty. The FE mesh refinement was difficult for the roll surface which would generate a large number of elements in the analysis by the Lagrangian method. But modern FE commercial softwares (ABAQUS, ANSYS) have the increased capability of addressing the large deformation problems and localised mesh refinement for the Lagrangian formulation too. The modern FE softwares are used by many authors and have proved to be effective in dealing with the large deformation metal rolling problem, for example by Jiang and Tieu (Jiang and Tieu 2002). This demonstrates that the FE technique has improved substantially and it can be applied in the rolling problem effectively.

The Viscoplastic FE method was the earliest one to model strip rolling in 1978 by Zienkiewicz *et al.* (Zienkiewicz *et al.* 1978) and Dawson (Dawson 1978), in which the elastic strain of the deformed metal was ignored and the flow of metal was considered as incompressible fluid. Friction was simulated in this approach by introducing a thin layer of elements at the roll/strip interface; the yield strength of these elements depends on the product of the friction coefficient and mean stress. In the pure, viscoplastic analysis the dynamic effects were ignored. Here, the shear modulus was equivalent to viscosity. The iterative scheme was developed to modify the velocity field and the distribution of viscosity until a convergent steady state solution was obtained. The viscoplastic analysis was also done by Thompson (Thompson 1982), where the elastic strain rate was included in the constitutive relation as a relation between the strain and the strain rate. The importance of elastic strain consideration was justified, when determining the residual stress left in the strip as it leaves the roll gap. The elasto-

viscoplastic approach had also been used by Grober (Grober 1986) for hot flat rolling and by Bertrand *et al*. (Bertrand, David *et al.* 1986) for edge rolling.

The rigid-plastic FE method was developed by Mori *et al*. (Mori *et al.* 1982) and Shima *et al*. (Shima, Mori *et al.* 1980) for both steady and non-steady state strip rolling. The material was considered slightly compressible in these studies based on the plasticity theory. For the neutral point definition, authors used relative velocity between the surfaces of the roll and strip as a positive functional and the neutral point was determined by minimization of this function. The front and back tensions were investigated in these studies. They found pressure distribution similar to that calculated by Bland and Ford (Bland and Ford 1943) for small reduction, but for the large reduction, the pressure was much higher. Mori *et al.* found two peaks in pressure distribution, one in the entry and the other in the exit. The rigid-plastic FE was also modelled by Li and Kobayashi (Li and Kobayashi 1982), but their material behaviour was assumed incompressible. For neutral point identification, Li and Kobayashi also used the modified functional relation by adding a term accounting for the frictional forces following the work of Chen and Kobayashi (Chen and Kobayashi 1978). Li and Kobayashi also found the double peak pressure distribution. The authors argued that the degree of homogeneity of the deformation and work hardening of the material contributed to the single peak or double peak in the pressure distribution curve.

The elastic–plastic FE method considers the elastic deformation as well as the plastic deformation of the strip material. The early elastic-plastic FE method was developed by Yamanda *et al*. (Yamanda, Ito *et al.* 1974), but their analysis was limited to small reduction rolling cases. The approach was later adapted by Rao and Kumar (Rao and

Kumar 1977), which was more applicable for plane strain rolling by elastic-plastic material assumption. But the roll, as in many analyses, was considered as rigid. Further studies of plane strain elastic-plastic were done by Yarita *et al*. (Yarita, Mallett *et al.* 1984) and Hirakawa *et al*. (Hirakawa, Fujita *et al.* 1984).

A more insightful elastic-plastic FE model was developed by Liu *et al.* (Liu *et al.* 1985; Liu, Hartley *et al.* 1985) following the friction layer approach developed by Pillinger *et al*. (Pillinger, C.E.N. *et al.* 1979). This layer was not any lubricant layer but an extra layer on the upper elements of the strip surface on which friction acted. The upper nodes on the elements of the layer were rigidly bonded to the roll surface. Thus any relative movement of the roll and the strip surface would cause shearing to the friction layer that induced a resisting force to the movement. This approach used a stiffness modification factor (s value), which was related with the shear factor (m value). The relationship between s and m was obtained by several experimental and FE studies of ring test simulation (Hartley, Sturgess *et al.* 1979; Pillinger *et al.* 1979). This is also known as the friction factor approach, which was different from the other earlier studies of FE analysis in rolling, where Coulomb friction law was used. This technique clearly identifies the elastic and plastic deformation zones and the effects of unloading. The stress and strain distributions throughout the strip surface were investigated together with the pressure distribution. The pressure distribution of this study was compared to the experimental result of Al-Salehi *et al*.(Al-Salehi *et al.* 1973) as shown in Fig. 2.4. The pressure distribution of the Liu *el al*. study shows good agreement with the experimental results near the exit zone of the arc contact. There is a large discrepancy of pressure at the entry region. Moreover, there is no pressure drop in the arc of contact

from the entry to exit the zone, which is a sharp difference from the experimental results.

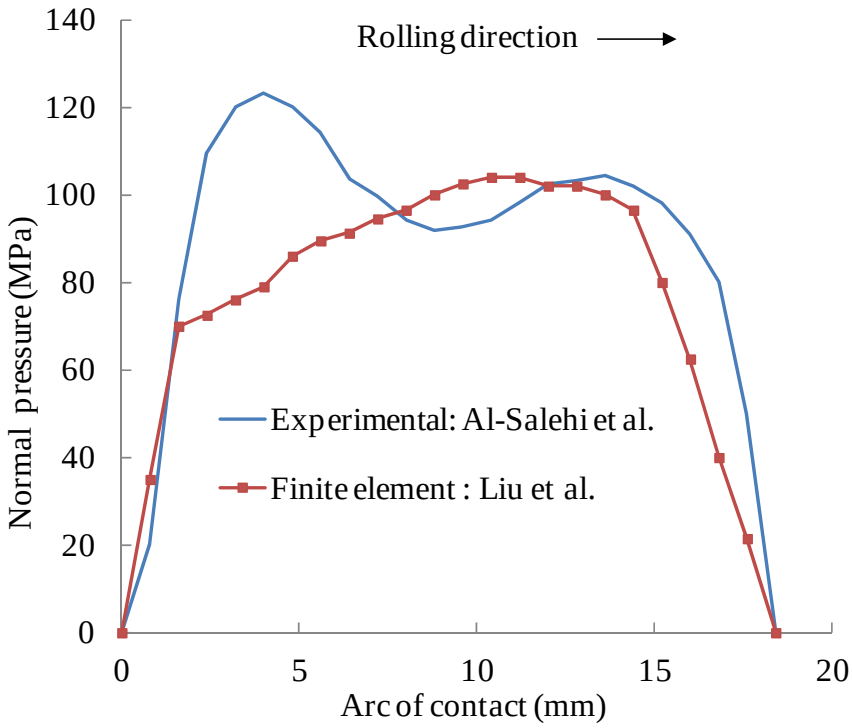

Figure 2.4: Pressure distribution : Experimental result of Al-Salehi *et al*. (Al-Salehi *et al.* 1973) and FE result of Liu *et al.* (Liu, Hartley et al. 1985

The discussion up to this point of FE models is based on the Lagrangian approach. The Eulerian approach was applied by Abo-elkhier (Abo-Elkhier 1997) to the elastic-plastic material rolling problem, which considered the elastic deformation of roll and elastic-plastic deformation of strip. This approach has improved the FE technique in metal rolling with due consideration of roll deformation in the analysis. The incremental equilibrium equations of the Eulerian formulation were developed. The material behaviour was assumed to follow the Von-Mises yield criteria associated with the Prandl-Reuss flow rule. The elements in the rolls that were in contact with the strip surface were considered to deform elastically, whereas the elements elsewhere were considered as rigid. Only 15 elements were considered in the roll surface, which

simplifies the solution process but considers the elastic deformation of the roll surface. The friction layer technique developed by Pillinger *et al*. was also used in this study. The contact pressure found in this study is a little bit higher compared to the results of Liu *et al*. and the differences with the measurement result of Al-Salehi *et al.* have reduced. The authors claimed that this was due to the consideration of elastic deformation of the roll, which was ignored in all the earlier studies (Liu *et al.* 1985; Rao and Kumar 1977). However, there was no drop of pressure in the arc of contact as appeared in the experimental measurement (Al-Salehi *et al.* 1973).

More recently, the FE method was used by Mancini *et al*. (Mancini, Campana *et al.* 2012) to study the surface defects or surface pit. The FE was used to identify the different positions in the arc of contact and the neutral point. The dry contact pressure was also used to calculate micro film by an empirical relation. The amount of fluid drawn during the rolling process was then calculated based on the micro film thickness. The process parameters like back tension, friction coefficient, reduction parameter, initial thickness and roll diameter were used to study the sensitivity of the recovery of the surface pit by expelling lubricant from the asperity valleys. The study used some process parameters and empirical relation with a simple model of the lubrication phenomenon, which was not justified by any experimental evidence. Moreover, the calculation of the micro film was based on the FE dry contact model. The film thickness in the mixed lubrication depends on many interrelated parameters like rough surface features, overall load sharing phenomenon and real area of contact, which were ignored in this study.

The FE studies discussed in this Section are based on dry contact analysis. Modern FE softwares like ABAQUS explicit and ANSYS LS-DYNA can solve metal rolling problems very easily for dry contact and smooth surface geometry. Rough surface geometry is not feasible to use in FE analysis, which would be computationally difficult and expensive. Though the FE is an important numerical tool to solve structural and fluid problems, it has the limitation of implementing the rough surfaces contact features and thin fluid interaction in the metal rolling problem.

2.3 Mixed lubrication

Lubrication in contact mechanics has attracted much attention due to its wide application in rotating components, for example, rolling element, gears, bearings, cams and traction drivers. These rotating mechanical components are usually operated in mixed lubrication mode. As the mixed lubrication involves solid-solid contact and solid-liquid interaction, the mechanics must be established based on real surfaces contact and thin film lubrication. The real surfaces are rough and the asperities come in contact if the lubricant film thickness is lower than the maximum asperity height. The asperity-asperity contact will start from the asperities with the highest height and then to those with the lower height as the two surfaces come closer. The applied load is then shared by the asperities and the hydrodynamic film. The direct asperity contacts are often the major cause of surface failure such as sliding wear, scuffing and pitting due to contact fatigue (Hu and Zhu 2000). Therefore, surface roughness and topography are very important factors in component failure analysis. It is necessary to develop a mixed lubrication model to understand contact mechanics, predict lubrication characteristics and improve component design/performance/reliability. There are three lubrication

regimes that can be found in fluid structure interaction mechanics, for example full film, mixed film and boundary lubrication. It has been widely accepted that the term “full film lubrication” refers to a condition under which the lubricant film is sufficiently thick so that there is no significant asperity contact. When the lubricant film is so thin that the load is supported mainly (or completely) by solid-to-solid asperity contact, it is known as in the region of “boundary lubrication” (dry contact). Between the full film and boundary lubrication, there is a transition region known as “mixed lubrication”, where neither the asperities nor the lubricant film can be ignored and the total load is shared by both (Hu and Zhu 2000; Wilson and Kalpakjian 1995). For developing mixed lubrication model, it is important to couple the asperity contact model and lubrication model to address load sharing in interface of contact. In the subsequent sections, different asperity contact models, lubricant flow model and coupling of the asperity contact model and the lubricant flow models (mixed lubrication models) are discussed.

2.3.1 Asperity deformation model

The asperities in rough surfaces contact play a leading role in microscopic deformation in a structure. The control of friction and lubrication is very important in such contact mechanics for stable processing conditions and modification of surface quality. The contact mechanics of surface asperities influence this frictional behaviour of the bulk underlying material. The real area of asperity-asperity contact is an important parameter to address the underlying bulk surface deformation, which is very small compared to the nominal area of the underlying material (Wilson and Sheu 1988). The asperities may be deformed or flattened and there will be growth of the real area of contact as the applied load increases. But this growth of the real area of contact would not continue to increase

indefinitely, i.e. the real area of contact will never be equal to the nominal area. The existing asperity deformation models are developed in two broad categories. One is to resolve full details by direct accounting for the random distribution of surface asperities and calculate asperity contact pressure and real area contact by the stochastic approach, for example the asperity deformation models of Greenwood-Williamson (Greenwood and Williamson 1966). The other one is based on the solid approach, where statistical ingredients are used to apply an energy minimization approach in the deformation analysis, for example the asperity deformation model of Wilson and Sheu (Wilson and Sheu 1988).

The microscopic asperity flattening model of Wilson and Sheu is one of the most popular concepts used in the study of both boundary and mixed lubrication problems. This was a solid approach, where an indentation analysis was developed by an upper bound energy method. The approach developed an empirical relationship among the real area of contact, strain rate and hardness of the underlying material. In this model, kinematically admissible continuous velocity fields were constructed based on deformation in one direction with no side spreads i.e. the upper bound approach. The indentation problem was then established based on the following assumptions: (a) Surface slopes must be small, (b) Pressure required for the indentation of the strip surface is equal to that for flattening of strip asperities assumed in the surface, (c) Uniform elongation rates in the rolling direction, (d) A rigid-plastic and incompressible material assumption of the strip surface. A semi-empirical relationship among the effective hardness, fraction of real area of contact and strain rate was then established by equating the external and internal energy dissipation in the assumed control volume. Wilson and Sheu (Wilson and Sheu 1988) found progressive asperity flattening and

monotonic growth of the real area of contact with the strain rate. The upper bound solution was applied in the load sharing concept for both mixed and boundary lubrication in metal forming. Wilson and Sheu established the effect of bulk plastic deformation on asperity flattening presuming arrays of roughness to lie in the direction parallel to the bulk strain. Whereas Sutcliffe (Sutcliffe 1988) proposed a model assuming the arrays of asperities to lie in the direction perpendicular to the bulk strain. Sutcliffe examined the crushing of asperities by a frictionless die under conditions of bulk deformation of the underlying material. Sutcliffe found a large increase in the contact area with bulk strain and a reduction in the load was needed for bulk yielding. This study used the energy minimization approach and constructed the slip-line field to find the real area of contact due to asperity crushing. Sutcliffe conducted experiments on random rough surfaces and found the asperity crushing roughly as expected. But the asperity flattening rate was found almost similar when considering both roughness arrays (parallel and perpendicular). Kimura and Childs (Kimura and Childs 1999) also developed a similar asperity flattening model using the energy minimization approach. According to this study, the growth of the real area of contact depends on contact friction and aspect ratios of the flow field. It was theoretically predicted that asperity crushing takes place with 0.02-0.08 of compressive strain at the start of the compression test. The theoretical real area of contact reaches between 75-90% of the tool area. The experimental compression test showed that the real area of contact is less (from 60-80% of the tool area) than the theoretical prediction. These were qualitative information for asperity deformation. Moreover, this method can be applied for combined material flow of asperity and bulk, which cannot be done by the slip- line field method.

One of the earliest stochastic asperity contact models was developed by Greenwood and Williamson (Greenwood and Williamson 1966), where the elastic deformation of asperities was solved by the Hertzian solution. The model used the solution of the contact of an elastic hemisphere and a rigid flat plane with Gaussian distribution of asperity heights. The study developed a set of relations which gives the total real area of contact, the number of microcontacts, the load and the conductance between the two surfaces in terms of the separation of their mean plane. This study found that the contact between the solids was controlled by material and surface topographic properties, for example, the plane stress elastic modulus, the hardness, the surface density of the asperities, the standard deviation of the height distribution of asperities, and the mean radius of asperities. As the load or interference increases, the stresses within the hemisphere also increase. These stresses eventually cause the material within the hemisphere to deform plastically. The critical interference ω_c was defined by the point of initial yielding after which the material will deform plastically. Supplementing the GW model, many elasto-plastic asperity models had been devised in this direction to consider the plasticity, for example elastic-plastic model of Chang *et al*.(Chang, Etsion *et al.* 1987), Zhao *et al*. (Zhao, Maletta *et al.* 2000), Kogut and Etsion (Kogut and Etsion 2003), and Robert and Green (Robert and Green 2005). Change *et al.* approximated the plastically deformed portion of a hemisphere by using volume conservation. The hemisphere below the critical interference behaves elastically. However, FEM results (Jackshon and Green 2005) shows that the Chang *et al*. model is unjustified, since the contact area can become larger than that predicted. Kogut and Etison used FE to account for the case of an elastic-perfectly plastic sphere in contact with a rigid flat. This study gives more detailed analysis of the stress distribution in the contact region, and empirical expressions are provided for the contact area and the

contact force. Applying the FE results of single asperity developed by Jackson and Green (Jackshon and Green 2005), Robert and Green developed a more comprehensive elastic-plastic asperity deformation model, which accounts for both geometry and material effect into the model. The most notable of these effects is that the predicted geometrical hardness found in fully yielded contact was not constant and changed with the evolving contact geometries and material properties. This single asperity model fully coincides with the Hertzian solution for up to 1.9 times of critical interference. For critical interference reaches above this value ($1.9\omega_c$), empirical expressions were provided by Robert and Green for the real area of contact and the contact force for a plastically deforming case. The solution for all asperities in a nominal area was then found simply by integrating over the entire range of asperity contact assuming the Gaussian distribution of asperity heights. It was found that there is significant increase of the real area of contact due to consideration of elasto-plastic deformation of asperities with regard to the elastic deformation assumption of the GW model.

The asperity deformation models discussed in this section give some insightful information about the real mechanics of asperity deformation. These are all stochastic asperity deformation contact models, where the statistical rough surface parameters and the random height distribution of asperities were used in the solution process. The deterministic asperity contact model was also used in contact analysis by some authors, where the real geometries of microscopic rough surfaces wre used in the solution process. The deterministic asperity deformation concept (Hu *et al.* 2001) was used in some real microscopic rough surfaces or shapes generated by computer, where some local deformation and effects were found in the solution. The deterministic models will be discussed in the Section 2.3.3.

2.3.2 Lubricant flow model

Since the mixed lubrication mechanics involves fluid flow in the rough surfaces, the fluid flow equation must be addressed with sufficient ingredients of rough surface features. There are basically two types of analysis available for fluid flow in between rough surfaces in literature. The first one is the stochastic concept, where some statistical parameters are used with random height distribution of asperities to model the roughness effect on lubricant flow. The second one is the deterministic approach, where real rough surface geometries are used to calculate the local film thickness, deformation and pressure .

The study of surface roughness effects in lubrication by the stochastic concept has gained attention from many researchers, for example Tzeng and Saibel (Tzeng and Saibel 1967), Christensen (Christensen 1970), Christensen and Tonder (Christensen and Tonder 1971), Tonder (Tonder 1977), and others. Christensen and Tonder developed the stochastic Reynolds equation for transverse and longitudinal roughness in slider and journal bearings. The effects of two-sided-striated roughness on bearing load carrying capacity was obtained by Rhow and Elrod (Rhow and Elrod 1974). Chow and Cheng (Chow and Cheng 1976) extended the stochastic theory of Rhow and Elrod to elastohydrodynamic (EHD) lubrication between two rollers. But most of these studies were limited to a specific type of roughness structures: one dimensional ridge oriented either transversely or longitudinally oriented. The extension to real rough surfaces was very difficult with the earlier stochastic theories.

Patir and Cheng developed a new approach by introducing pressure and shear flow factors in the steady state and isothermal Reynolds equation for fluid flow in 3D rough surfaces. The local film thickness h_l was defined (as shown in Fig. 2.5) by

$$h_l = d + ha_1 + ha_2 \tag{2.1}$$

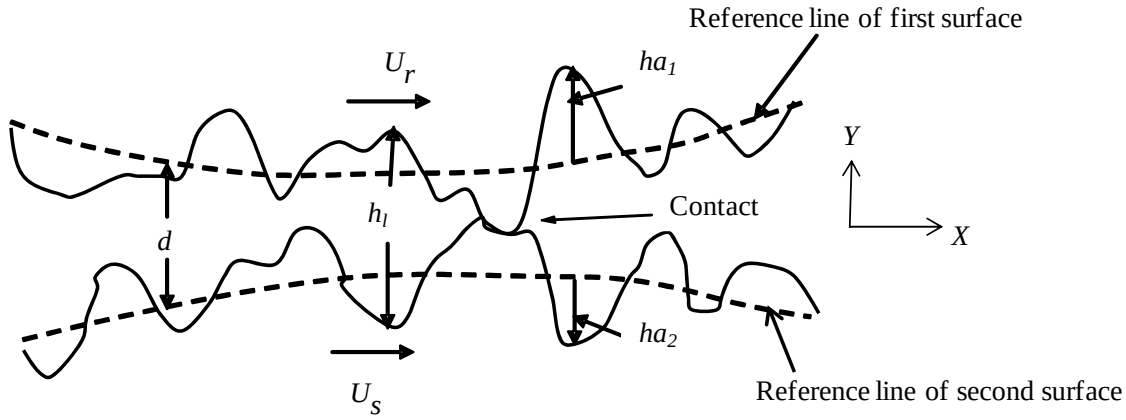

Figure 2.5: Film thickness in rough surfaces contact

where, d is the nominal film thickness or separation between the mean level of two surfaces in contact and ha_1 and ha_2 are the random roughness amplitude of the two surfaces measured from their respective reference line. The combined roughness h' was defined by

$$h' = ha_1 + ha_2 \tag{2.2}$$

For the Gaussian distribution of asperity height, the combined standard deviation σ was defined as

$$\sigma^2 = \sigma_1^2 + \sigma_2^2 \tag{2.3}$$

where, σ_1 and σ_2 are the standard deviation of the first and the second surfaces respectively. The ratio d/σ is an important parameter showing the effects of surface roughness. Three different conditions can be explained based on this d/σ ratio in the context of the roughness effect as

(a) $\frac{d}{\sigma} > 3$, the roughness effects are not important and smooth film theory is sufficiently accurate.

(b) $d/\sigma \to 3$, the roughness effects are important and asperities will start interacting

(c) $\frac{d}{\sigma} < 3$, the roughness effects are important and a partial or mixed lubrication condition is applicable.

For isothermal, incompressible and steady state elastohydrodynamic (EHD) contact, the lubricant pressure is governed by the Reynolds equation as

$$\frac{\partial}{\partial x}\left(\frac{h_l^3}{12\mu}\frac{\partial p_f}{\partial x}\right)+\frac{\partial}{\partial y}\left(\frac{h_l^3}{12\mu}\frac{\partial p_f}{\partial y}\right)=\frac{U_r+U_s}{2}\frac{\partial h_l}{\partial x}+\frac{\partial h_l}{\partial t} \tag{2.4}$$

where, p_f is the hydrodynamic pressure, μ is the viscosity of lubricant, ∂t is the time step, U_r and U_s are the velocity of two moving surfaces respectively. The classical Reynolds Eq. (2.4) is applicable for the fluid flow in smooth surfaces. This Reynolds

equation was modified by Patir and Cheng for fluid flow in between rough surfaces by introducing pressure flow factors in the flow direction. A control volume was assumed in the base area of a bearing, where the fluid was assumed to be flowing. The unit flows entering and leaving this control volume were analysed and the final form of the modified Reynolds equation for the rough surfaces flow was given as

$$\frac{\partial}{\partial x}\left(\phi_x \frac{d^3}{12\mu}\frac{\partial P_f}{\partial x}\right)+\frac{\partial}{\partial y}\left(\phi_y \frac{d^3}{12\mu}\frac{\partial P_f}{\partial y}\right)=\frac{U_r+U_s}{2}\frac{\partial h_T}{\partial x}+\frac{\partial h_T}{\partial t}+\frac{U_r-U_s}{2}\sigma\phi_s \tag{2.5}$$

where, P_f is average hydrodynamic pressure, h_T is the average film thickness, ϕ_S term represents the additional flow transport due to sliding, ϕ_X , ϕ_Y are the pressure flow factors in the x and y direction respectively. A simulation of flow was done by Patir and Cheng for the derivation of pressure flow factors. A bearing area was approximated as a number of small areas of the whole bearing. But this small area was large enough to include a large number of asperities. A mathematical relation was established to calculate the flow factors from the simulation of the bearing model. The engineering surfaces were assumed to have a Gaussian distribution of asperity height distribution. Apart from the height distribution, the directional properties of rough surfaces are very important that influence the flow factors. The directional properties of surface roughness were defined (Peklenik 1967) by surface characteristic parameter γ as

$$\gamma=\frac{L_{0.5x}}{L_{0.5y}} \tag{2.6}$$

where, γ is defined as the ratio of $L_{0.5}$ length of x and y profiles. The term $L_{0.5}$ is defined as the length at which the auto correlation function of a profile reduces 50 percent of its initial values. The directional properties of engineering surfaces have different patterns resulting from different manufacturing processes.

These directional patterns are mostly in the longitudinal or transverse direction. The flow factors of surfaces can be obtained by generating rough surfaces with different γ ratio. The value γ was visualized as the length to width ratio of a representative asperity. Based on the correlation lengths of a representative asperity, the following three orientations were found to be applicable as shown in Fig. 2.6 by characteristic number γ as

(a) Longitudinally oriented (γ >1),

(b) Isotropic (γ =1),

(c) Transversely oriented (γ <1)

The longitudinal oriented areas offer little resistance to pressure flow and permit only a small side flow. The resulting flow is larger than the similar smooth bearing if the average gap in the valleys is larger than the compliance. A decrease in d/σ is accompanied by a large increase in the mean gap (relative to d/σ), and hence large increase in the flow factor. A decrease in λ results in smaller valley lengths and increase in side flow, thereby decreasing the main flow and flow factors. When the surface is

isotropic, the local flow is of the same order of magnitude as the main flow. Hence the resistance to the main flow increases because the flow has to pass around the contact areas. This increase in resistance offsets the effects of a larger mean gap, resulting in flow factors less than 1. The side flow and resistance to the main flow is increased further as the surface becomes transversely oriented. A decrease in γ and or in d/σ increases this resistance, thereby reducing the flow factors.

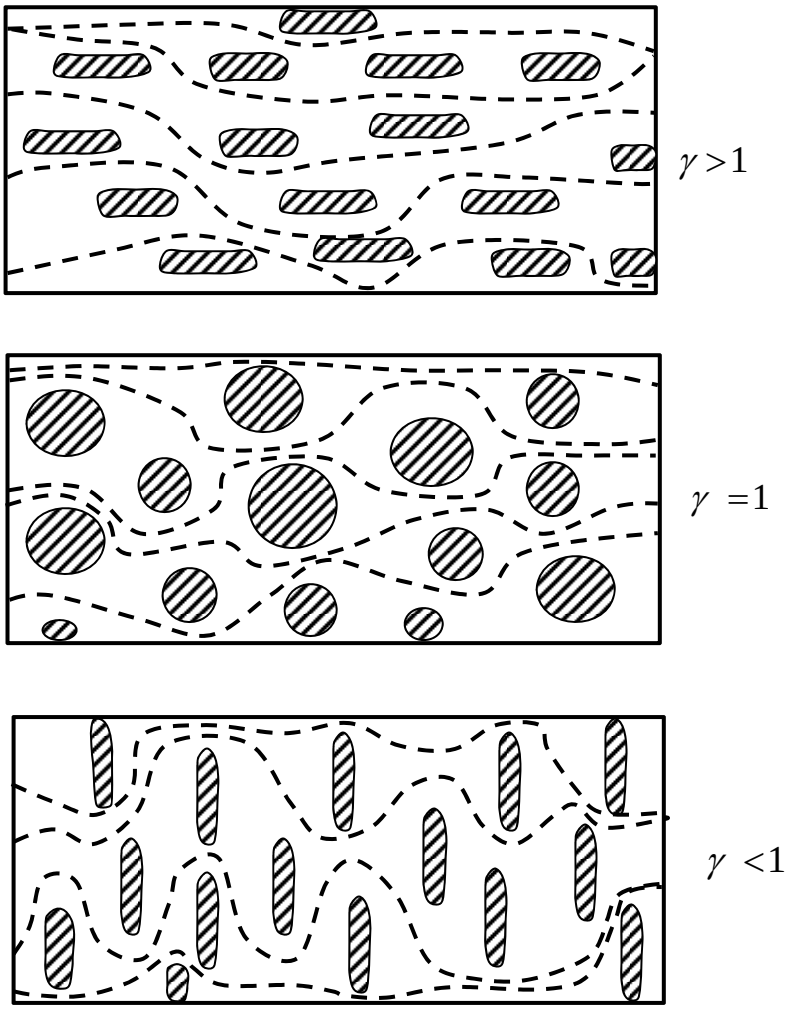

Figure 2.6: Contact areas for different surface orientations

The directional patterns are available mostly in the longitudinal and transverse directions. Patir and Cheng developed semi empirical equations for these three orientations and a respective pressure flow factor in the x direction as

$$\phi_x = 1 - CEo^{-rH} \text{ , for } \gamma \leq 1 \tag{2.7}$$

$$\phi_x = 1 + CH^{-r} \text{ , for } \gamma > 1 \tag{2.8}$$

where, $H=h/\sigma$, E_o is the expectancy operator, the constants C and r are calculated from the function of γ value and H range.

The stochastic models discussed above for fluid flow in rough surfaces can give only the global effects of rough surface topography. No details of local surface pressure peaks, film thickness fluctuations and asperity deformation pressure are available. However, local features are critical to study the lubrication breakdown and surface failure mechanisms. Deterministic models (Hu, Wang *et al.* 2001; Hu and Zhu 2000) can be valuable to find the local effects of rough surfaces. These are becoming popular due to improvements in computer technology. This type of analysis uses simplified or real surface profiles as an input of the numerical solutions. So, the statistical parameters are no longer needed in deterministic solutions. Both the stochastic and deterministic models are used in developing mixed lubrication model that will be discussed in Section 2.3.3.

2.3.3 Coupling of asperity deformation and lubricant flow

The mechanisms of mixed lubrication involve sharing of asperity contact pressure and hydrodynamic pressure in the contact zone. The coupling of the asperity deformation model and the lubrication model is necessary to apply the load sharing principle in contact. Some mixed lubrication models separately calculate the asperity contact pressure and the hydrodynamic pressure and then simply superimpose these to balance the applied load in the contact interface, for example Zhu and Cheng (Zhu and Cheng 1988). Alternatively, some mixed lubrication models use a unified numerical solution process with full coverage of all lubrication regions for asperity contact pressure and hydrodynamic pressure, for example Sheu and Wilson (Sheu and Wilson 1994).

Hu and Zhu (Hu and Zhu 2000) developed a mixed lubrication model in point contact by simplifying the load sharing principle and applying the same model for both the hydrodynamic film and the contact pressure calculation. The asperity contact was treated as a continuous decrease in film thickness. The transition between contact and non-contact was continuous. In the analysis of mixed lubrication, the contact zone was divided into two different types of area; the hydrodynamic regions where the two surfaces were separated by the lubricant film, and the asperity contact regions where two surfaces were in direct contact. In the hydrodynamic regions, the pressure was governed by the Reynolds equation (see Eq. (2.4)). For the asperity contact region, the pressure was governed by the thin film. The pressure over the thin films was assumed to obey the Reynolds equation and the solution was found as the film thickness approaches to zero, which was equal to the Hertz elastic contact pressure. To achieve the convergent and stable solutions, the Reynolds equation was modified, when the local film thickness approaches zero, leading to a reduced form of the Reynolds equation as

$$\frac{U_r + U_s}{2}\frac{\partial h_l}{\partial x} + \frac{\partial h_l}{\partial t} = 0 \tag{2.7}$$

This solution of Eq. (2.7) was treated as the solution for the asperity contact region. Pressure distributions over the entire computation domain were thus obtained through solving a unified Eq. (2.4) without identifying the hydrodynamic or asperity contact regions. A multi-level integration method was used to calculate surface deformation. Computations were conducted for several example cases and results show that the convergent solutions are achievable for different three-dimensional rough surfaces moving at different rolling and sliding velocities. The approach can handle cases under very severe conditions, covering the full range of λ ratio (λ is the ratio of film thickness to composite RMS roughness) from infinitely large down to nearly zero. The local roughness and film thickness effect on contact pressure or hydrodynamic pressure were captured by this study for elastic deformation of material. The analysis further included more study and verification by Hu *et al*. (Hu *et al.* 2001) as an extension of the previous work of Hu and Zhu. This study confirmed that the pressure distribution over the thin films between interacting asperities must obey the Reynolds equation, when the film thickness approaches to zero. This expectation had been confirmed by computation experiment. The converged solution was found for different roughness and over a wide range of λ ratios for lubricated contacts from full film to boundary lubrication for different film thickness and operation conditions. A similar deterministic model of point contact was developed by Wang *et al.* (Wang, Hu *et al.* 2007), which used thermal solutions from a moving point heat source to get the surface temperature provided that shear stresses in both the regions of hydrodynamic and asperity contacts had been predetermined. A rheology model based on the limit shear stress of the lubricant was

proposed while calculating the shear stress, which gives smooth transition of friction between the two regions. The computation seems to be powerful to give deterministic solutions for mixed lubrication over a wide range of film thickness, from full film to lubrications with very low λ ratio, even down to the region where asperity contact pressure dominates.

The deterministic approach of Hu and Zhu was then extended to the deterministic-stochastic modelling approach by Wang *et al*. (Wang, Zhu et al. 2004). This was also known as the macro-micro approach in the calculation of hydrodynamic pressure and asperity contact pressure in the two separate models. The final film thickness was then found from the resultant action of these two pressures. In this approach, the average flow model of Patir and Cheng (Patir and Cheng 1979) was employed to obtain the distribution of average flow pressure, where the roughness of two surfaces, flow factors and rough surface orientations were considered. A separate asperity contact model was used to incorporate the details of asperity contact pressure into the overall pressure distribution to reveal the severity of the surface interaction. The numerical calculations were done for different operating conditions and the results were compared to the full-scale mixed-EHL model of Hu and Zhu. It was found that the macro-micro approach predicts much thicker films and much more moderate and smoother pressure distribution for the larger roughness (greater than 0.4 micrometer). This indicated that the asperity deformation in the macro-micro model was underestimated compared to the full-scale model. The high peak of pressure in asperity contact was found in the full-scale mixed-EHL model due to the real surface consideration. The very thin film in the vicinity of the asperity contact was capable of producing high hydrodynamic pressure in full-scale mixed-EHL contact. This model (macro-micro) identifies the regions of

application of the macro-micro approach based on the λ values. For the higher λ ratio (greater than 1), the macro-micro approach may yield reasonable film thickness and pressure distributions on average operating conditions that can generate a sufficient amount of hydrodynamic action by higher velocity and smaller roughness. For the lower λ ratio (less than 1), the pressure may be simply estimated by an asperity dry contact model. The deterministic approach of Hu and Zhu was finally extended to deterministic-stochastic modelling or the macro-micro approach, which may be helpful in the study of mixed lubrication involving a large interaction area.

The full-scale mixed-EHL model of Hu and Zhu had been improved and the final improvement of this approach was the macro-micro approach, which was capable of taking the microscopic asperity contact pressure into consideration. However, the use of this approach in mixed lubrication is still not feasible due to complex geometry, large area of surface interaction and rough surface features. Moreover, its implementation for large plastic deformation problems will be difficult due to the elastic material assumption. The treatment for large deformation and plastic material constitutive behaviour is still absent in the deterministic approach of Hu and Zhu as many mixed lubrication mechanics involve large plastic deformation, for example metal rolling in mixed lubrication.

The FE was also used in developing the mixed lubrication model. Ongun *et al.* (Ongun, André *et al.* 2008) developed a FE mixed lubrication model, which included the effects of hydrodynamic fluid in highly deformable rubber seal. The hydrodynamic interface fluid elements were developed in order to achieve a strong coupling of the fluid

dynamics and the deformation of the solid structure. The fluid was represented by the two dimensional steady state Reynolds equation and the structural deformation by standard FE procedures. The fluid elements were developed in the FE framework by an ABAQUS user-subroutine material model. The user-subroutine was used to calculate the fluid stiffness matrix by the Euler integration method with the increment in space. The global stiffness matrix was then assembled and the systems of equations were solved by the Newton-Raphson iteration step. This method enabled the application of arbitrary, non-linear material models provided by FE programs. The capability of this approach was tested by modelling a dynamic O-ring seal. The fluid film thickness and the pressure profiles were presented for mixed lubrication and fully lubricated state. Finally, a computational Stribeck curve was developed which demonstrates the frictional behaviour of the seal at different sliding velocities. Though the modern FE computational techniques had been used in this study but the mixed lubrication features of asperity-asperity contact pressure, real area of contact and fluid flow in the rough surfaces were not considered in this approach. It seems that the load sharing in the contact interface was not addressed properly with due consideration of rough surfaces contact. The fluid elements were generated based on the steady state Reynolds equation for fluid flow in between smooth surfaces, which means that the roughness effects on the fluid flow were not considered. Asperity contact pressure was calculated based on an exponential relationship given in the ABAQUS software, which may deviate significantly from the real rough surface asperity contact models as discussed in Section 2.3.1.

Following the approach of Ongun *et al.*, the lubrication effects of reciprocating hydraulic rod seals were studied by Schmidt *et al*. (Schmidt, André *et al.* 2010). This

study introduced some further enhancements of the Ongun *et al*. model as follows: (a) Squeeze terms were added to the Reynolds equation to account for time-dependent effects in the fluid film, (b) flow factors were incorporated into the transient Reynolds equation to consider the surface roughness effects, (c) Any ABAQUS default materials were allowed to use for the structural part. Though the flow factors were considered in the fluid flow model of Patir and Cheng, the real area of contact and load sharing in the contact interface were not addressed properly. Moreover, the asperity contact model was still based on the default exponential relationship of ABAQUS. The maximum hydrodynamic pressure was found 2.75 MPa (approximately), which is reasonable as the low viscosity 0.01 Pa s was used, but the analysis was not extended for higher viscosity values. Since the hydrodynamic effect with such a low pressure will be almost negligible in the interface, this approach may fail with higher viscosity values as the higher viscosity values result in higher hydrodynamic pressure and the load sharing will be difficult without considering the real area of contact.

The above discussion up to this paragraphs is based on the different coupling approaches of dealing with mixed lubrication problems, where the investigations were based on both deterministic and stochastic models. Although these models are not rolling problems, these studies are important to understand some fundamental techniques of modelling mixed lubrication. It is found that the deterministic models are able to predict microscopic local deformation, film thickness and pressure considering the real geometry in the analysis. However, this approach has a big limitation to apply complex geometry in the solution process as it can only be applied for computer generated microscopic geometry. On the other hand, the stochastic models used statistical parameters of rough surfaces but this type of analysis gives a global solution

for the average film thickness and contact pressure. It may be better to apply both the deterministic and the stochastic approach to develop a mixed lubrication model.

Mixed lubrication involves large plastic deformation of the underlying material as well as microscopic asperity deformation in sharing with liquid. To apply the load sharing concept in the interface of rolling, the real area of contact, asperity contact pressure and hydrodynamic pressure must be calculated based on the mechanics of mixed lubrication. Chang *et al*. (Chang *et al.* 1996) developed such a mixed lubrication model based on the upper bound asperity deformation concept. In the interface of rolling, the mass conservation law was applied to combine microscopic asperity deformation and bulk material deformation by a load sharing relation. This was based on the material hardness, which was assumed as the difference between the asperity contact pressure and hydrodynamic pressure. This load sharing relation was established among the total interface normal pressure, strain rate, real area of contact and hydrodynamic pressure. Chang *et al.* used an empirical relation for separation values for different regions, which was derived from the asperity geometry. The values of nominal separation initially were guessed and adjusted until evaluations yield equal results to a sufficient degree of accuracy. The interface normal pressure was calculated from the slab method by applying a force equilibrium concept. The hydrodynamic pressure was calculated from a similar form of modified Reynolds equation proposed by Patir and Cheng (Patir and Cheng 1978). Since the exit zone was assumed similar to inlet zone solution, the solution was attempted for inlet zone only. For the inlet zone, average film thickness was calculated in two regions; one region, where the surfaces were in contact and another region, where the surfaces were not in contact (boundary between work zone and inlet zone). The numerical procedure was a two point boundary value problem

associated with the double shooting technique. The boundary condition was applied for the hydrodynamic pressure calculation according to the upper bound assumption; the hydrodynamic pressure was assumed zero for the elastic entry zone due to the rigid plastic material assumption. According to the rigid plastic material assumption, the material would not deform in the elastic entry zone. At the exit, hydrodynamic pressure was assumed to be zero. Though the mixed lubrication model developed by Chang *et al*. was a insightful work, which combines microscopic and macroscopic deformation in a unified solution process by introducing a load sharing model, there were too many assumptions in both the upper bound microscopic and mixed lubrication models. The results of this study may deviate from actual reality. For the boundary lubrication (when there is no liquid and only solid-solid contact), the upper model is found satisfactory experimentally, but for the mixed lubrication, the mechanics is too complex and the hydrodynamic effect may not satisfy with the all the upper bound assumptions. Moreover, the hydrodynamic pressure assumed at the entry region due to the boundary condition was too high. There is no experimental evidence that such a high hydrodynamic pressure may generate at the beginning of the rolling process. Saniei *et al*. (Saniei and Salimi 2006) also used a similar approach to Chang *et al*. by introducing some modification. Saniei *et al.* used a second order average Reynolds equation for hydrodynamic pressure, Roelands relation (Roelands 1996) for variation of viscosity with respect to temperature and pressure and the effect of front and back tension for more accurate calculation. The Runge Kutta method was used for solving slab equations and load sharing equations. The Central Difference method was used for solving the average Reynolds equation. The overall relaxation method was used for solving the final equation. The results of these two mixed lubrication models (the model of Change *et al*. and Saniei *et al.)* are shown in Fig 2.7. It seems that with low viscosity value (0.02

Pa.s), the hydrodynamic pressure is roughly equal to the interface normal pressure in some regions of the contact area. There is no experimental validation of such high hydrodynamic pressure in rolling with such a low viscosity value. If this is true, such a high hydrodynamic pressure may lead to very low frictional force and the rolling process may fail due to insufficient friction.

Although the frictional force and the coefficient of friction are very important parameters of mixed lubrication, these studies did not include any discussion in this regard. Some authors developed the mixed lubrication model following a similar concept to Chang *et al.*, for example the mixed lubrication model of Lu *et al.*(Lu *et al.* 2003), Stephany *et al.* (Stephany, Ponthot *et al.* 2004), Kosasih *et al.*(Kosasih and Tieu 2007), and Tieu *et al*. (Tieu, Liu *et al.* 2002).

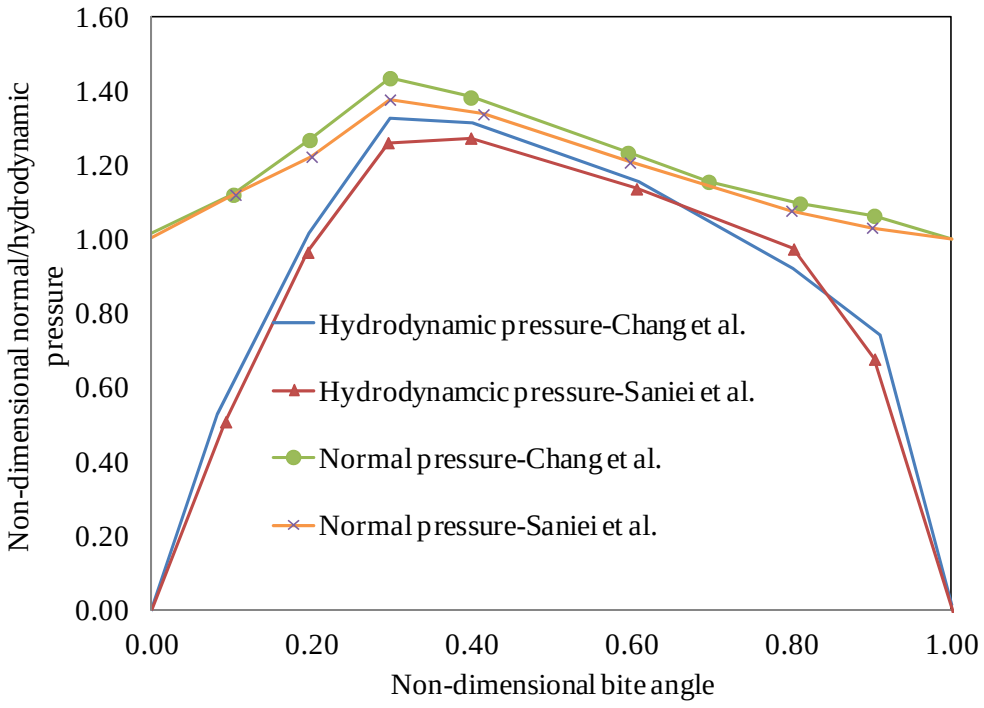

Figure 2.7: Prediction of the normal pressure and the hydrodynamic pressure (Chang *et al.* 1996; Saniei and Salimi 2006)

Though extensive research initiatives have taken place in the last two decades to develop the mixed lubrication rolling model, the development is still not sufficient to address a mixed lubrication phenomenon. In particular, the mixed lubrication rolling models discussed in this section are based on the concept of a microscopic upper bound model. The results of these upper bound microscopic model may deviate significantly from the real mechanics due to many simplified assumptions as explained. The results of this mixed lubrication models are not validated by any authentic experimental evidence. A complete mixed lubrication by addressing important features like real area of contact, load sharing, effect of viscosity and effect of rolling velocity needs a more realistic approach, which is close to real mechanics.

2.4 Discussion and conclusions

Mixed lubrication is a complex mechanics, which needs both microscopic and macroscopic ingredients including fluid flow in the rough surfaces. Some deterministic models (Hu *et al.* 2001; Hu and Zhu 2000) used real rough surface geometry and applied the Reynolds equation (for smooth surface) to develop a mixed lubrication model. But these analyses are limited to microscopic local effects of deformation, film thickness and pressure in mixed lubrication. Moreover, these analyses used a single model for both asperity contact and lubricant interaction, which accounts for the elastic deformation of the constitutive material only. These approaches were further improved by applying deterministic-stochastic (Wang, Zhu *et al.* 2004) approaches by considering two separate models for asperity contact and fluid interaction. But the asperity contact model was still based on the reduced form of a modified Reynolds equation. These

simplified analyses are strictly dependent on computer generated microscopic geometry and give some information about local effect. These analyses are limited to elastic deformation of the material constitutive behaviour, which may fail for the metal rolling problems, where large plastic deformation occurs during rolling.

Microscopic asperity contact models as discussed in Section 2.3.1 are used in both boundary and mixed lubrication models (Chang *et al.* 1996). Some mixed lubrication models (Chang *et al.* 1996; Kosasih and Tieu 2007) used an upper bound model for microscopic asperity deformation and a slab method for macroscopic deformation, which combines both microscopic and macroscopic material deformation into a single computation scheme. But there are many assumptions as explained in Section 2.3.3, which may deviate significantly from the real mechanics of rolling.

On the other hand, the FE technique was used by many authors for dry contact and smooth surfaces rolling contact analysis. The FE technique is more powerful and reliable comparing to any other methods like slab method that applied in rolling model. However, for mixed lubrication, the FE technique needs special treatment for rough surfaces contact and solid-liquid interaction. Very few attempts are found to develop mixed lubrication by the FE method, for example Schmidt *et al*. (Schmidt *et al.* 2010). Although the mixed lubrication model of Schmidt *et al*. used a user material model subroutine to represent the effect of fluid flow in rough surfaces, the load sharing phenomenon was not applied properly. In the interface of contact, load sharing must be addressed based on the real area of contact, which is not done in this study.

For the metal rolling problem, mixed lubrication features involving asperity deformation, large plastic deformation and load sharing in the interface need special treatment to apply in a unified model of multi-scale modelling. The rough surface features for both asperity contact pressure and hydrodynamic pressure must be incorporated including macroscopic bulk material deformation and the load sharing concept. Moreover rolling mechanics is a dynamic problem and explicit FE analysis is powerful to solve this type of dynamic problem. A multi-scale modelling technique with sufficient microscopic ingredients can turn this micro to macro deformation problem into a unified solution, if the load sharing phenomenon is established in the interface properly. This study will take up such a challenge to develop an explicit stochastic-deterministic FE approach by a user subroutine, which will introduce an artificial layer in the interface. The interface contact mechanics will be controlled by the user subroutine by updating interface contact pressure and frictional force. This innovative technique will calculate the real area of asperity contact, asperity contact pressure and hydrodynamic pressure explicitly in the user subroutine for every time step and apply the load sharing phenomenon in the FE simulation.

CHAPTER 3

METHODOLOGY

Mixed lubrication involves solid-solid contact and solid-fluid interaction between rough surfaces. The theoretical implementation of this complex interaction is a big challenge. The classical analytical method, developed by Wilson *et al*. (Sheu and Wilson 1994) and others (Chang *et al.* 1996; Kosasih and Tieu 2007; Saniei and Salimi 2006), was based on the rigid-plastic assumption and the presumed deformation field of slabs and asperities, which may significantly deviate from the actual scenario. In order to minimize the assumptions, we resort to the FE analysis for the elasto-plastic deformation of the material and only tackle the interface mixed lubrication with our own model. The fundamental idea and assumption is first introduced in Section 3.1. Detailed formulations and implementation are discussed in Sections 3.2 and Section 3.3 respectively. Section 3.4 gives verifications of the approach of our simulation protocol.

3.1 Basic assumptions

A schematic of strip rolling is shown in Fig. 3.1. Zooming into the micro-scale at the interface, the load transfer in a mixed lubrication scenario is through direct contact pressure or dry pressure for shorthand, and the pressure of the liquid. Denoting *A* is the fraction of area for direct asperity contact, then (1-*A*) is the fraction that is due to liquid contact. Therefore, the total normal contact pressure acting on the strip surface is simply a combination of dry contact pressure and liquid pressure following the load sharing principle as

$$P_n = AP_a + (1-A)P_f \,, \tag{3.1}$$

where, P_n , P_a and P_f are the average normal pressure acting on the strip surface, the dry pressure and the liquid pressure, respectively.

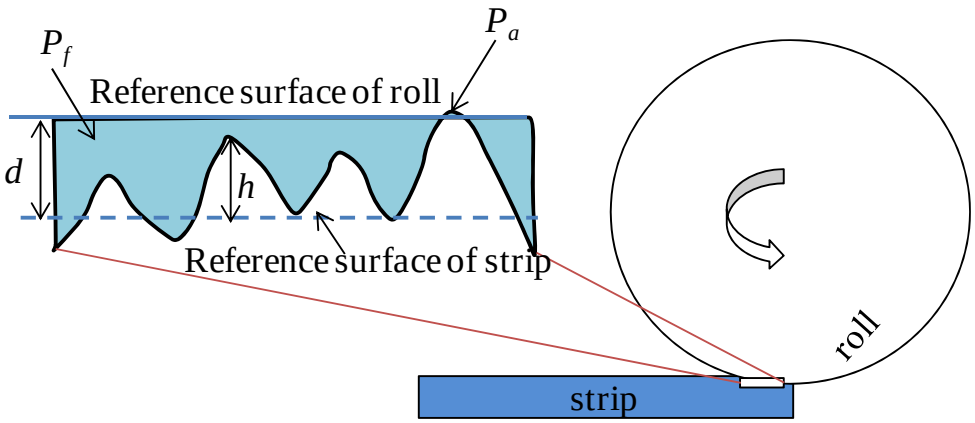

Figure 3.1: The schematic of strip rolling in mixed lubrication

Correspondingly, the unit area shear force P_t acting on the strip surface is also assumed to be the direct combination of dry and liquid contribution, namely

$$P_t = A\tau_a + (1-A)\tau_f \tag{3.2}$$

where, τ_a is the dry sliding frictional force and τ_f the shear stress of the lubricant when it was shared by the two solid surfaces. The keynote of our work is then to determine P_a, P_f, τ_a, τ_f through a proper interface model. After that, the calculation of P_n and P_t is trivial and the deformation of the elasto-plastic strip under P_n and P_t is solved by the conventional FE method. To establish the interface model, the following fundamental assumptions are relied on.

(i) Any two patches of the rough surface are statistically identical in terms of asperity distribution. Hence a unified description of asperity distribution can be obtained.

(ii) The lubricant is incompressible and isothermal and can flow in the interface. The steady state of the fluid can be reached in a very short duration. Therefore the Reynolds equation is applicable.

(iii) The interaction between fluid and asperity is negligible. Therefore the total pressure and frictional force is simply a combination of solid and liquid components (Eq. (3.1) and (3.2)).

3.2 Formulations

3.2.1 Asperity distribution and contact pressure calculation

Real surfaces are rough on a microscopic scale. The contact between two rough surfaces starts from their highest asperities and then successively develops to include the lower asperities with increasing contact force. Now, let us delineate two rough surfaces by reference smooth surface (e.g., the dashed line in Fig. 3.2) and discrete asperities with peaks higher or lower than this reference surfaces.

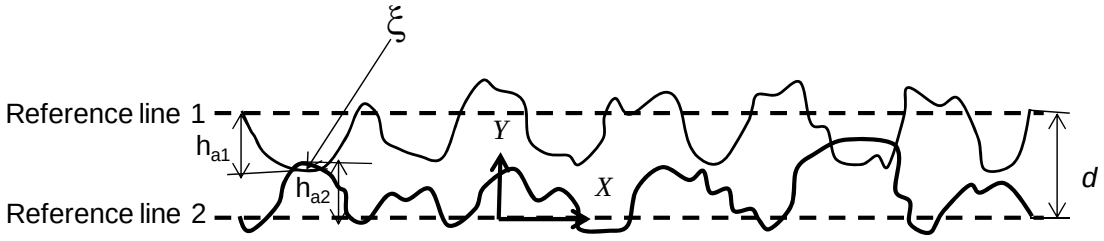

Figure 3.2: Two rough surfaces contact

The relative distances between the peak and reference surfaces are defined as the asperity height h_{a1} *and* h_{a2} respectively. The distribution of h_{a1} is denoted by the probability density function (PDF) $p(h_{a1}, x, y)$, where x and y are the position in the interface. Given the PDF of asperities, the probability to find an asperity with a height between h_{a1} and $h_{a1}+dh_{a1}$ in the infinitesimal area dx_1dx_2 centred at position (x, y) is given by $p(h_{a1}, x, y)\, dh_{a1}dxdy$. For this microscopic contact between two asperities of heights h_{a1} and h_{a2} on two rough surfaces, the contact force F_a and contact area function A_a are both functions of the overlap $\xi=h_{a1}+h_{a2}-d$ (see Fig. 3.2), where d (see Fig. 3.1) is the distance between two reference surfaces, the subscripts 1 and 2 designate two surfaces, e.g., the roller surface and the strip surface, respectively. The total contact force of unit surface is then given by

$$\overline{F}_a(d) = F = \int_{h_{a1}+h_{a2}>d} \iint_{x\ y} N_1 N_2 p_1(h_{a1},x,y) p_2(h_{a2},x,y) F_a(\xi) dh_{a1} dh_{a1} dxdy \tag{3.3}$$

where N_1 and N_2 are the total number of asperities on the unit surfaces 1 and 2 respectively and the overhead bar means total.

Let us define the density of the asperity pair of the total height $h(h=h_{a1}+h_{a2})$ as

$$\psi(h) = \int_{h_{a1}+h_{a2}=h} \iint_{x\ y} N_1 N_2 p_1(h_{a1},x,y) p_2(h_{a2},x,y) dxdy dh_{a1} dh_{a2} \tag{3.4}$$

Eq. (3.3) is recast as

$$\overline{F}_a(d) = \int_d^\infty \psi(h) F_a(h-d) dh \tag{3.5}$$

Similarly, the total contact area is given by

$$A(d) = \overline{A}_a(d) = \int_d^{\infty} \psi(h) A_a(h-d) dh \tag{3.6}$$

Because of the assumption (I), the PDF p can be independent of position (x, y). Eq. (3.4) can be further simplified as

$$\psi(h) = N_1 N_2 \int_{h_{a1}+h_{a2}=h} p_1(h_{a1}) p_2(h_{a2}) dh_{a1} dh_{a2} \tag{3.7}$$

If one of the surfaces is an ideally smooth surface, $N_1 p_1(h_{\backslash a1}, x, y)$ reduces to a delta function $\delta(h_{a1}, x, y)$, and the asperity pair distribution $\psi(h)$ reduces to $\psi(h) = \int N_2 p_2(h, x, y) dxdy$. Involving the assumption (I) and Eq. (3.7), $\psi(h) = N_2 p_2(h)$. In the subsequent derivations, the roller surface is generally assumed to be smooth. Therefore the distribution of the asperity height on the strip surface is used to establish statistical relations between the contact force/area and the distance between two surfaces d. But it should be emphasised that if both surfaces are rough, it only complicates the expression of $\psi(h)$ and has no effect on the general methodology.

Detailed expressions for asperity contact force and area $A_a(\xi)$, $F_a(\xi)$ are available in the literature. If the asperity contact is assumed to be elastic, the Hertz contact theory leads to (Greenwood and Williamson 1966) as

$$A_a(\xi) = \pi \beta \xi \tag{3.8}$$

for the contact area of individual microscopic asperity contact, where β is the tip radius of asperity.

and

$$F_a(\xi) = \frac{4}{3} E' \beta^{\frac{1}{2}} \xi^{\frac{3}{2}} \tag{3.9}$$

for the asperity contact force, where, E' is the equivalent modulus of elasticity of materials, defined by

$$\frac{1}{E'} = \frac{1-\nu_1^2}{E_1} + \frac{1-\nu_2^2}{E_2} \tag{3.10}$$

where, E and ν are Young's modulus and Poisson's ratio, respectively. Substituting Eqs. (3.9) and (3.10) into Eqs. (3.5) and (3.6) leads to

$$A(d) = \pi N \beta \int_d^\infty (h-d)\psi(h)dh \tag{3.11a}$$

$$\overline{F}_a(d) = \frac{4}{3} N E' \beta^{1/2} \int_d^\infty (h-d)^{\frac{3}{2}} \psi(h)dh, \tag{3.11b}$$

respectively. And the asperity contact pressure is

$$P_a = \overline{F}_a(d) / A(d) \tag{3.12}$$

Suppose that distribution of asperity is a Gaussian, i.e.

$$\psi(h) = \frac{1}{\sigma\sqrt{(2\pi)}} e^{-\frac{1}{2}(h/\sigma)^2}, \tag{3.13}$$

where, σ is the standard deviation of the asperity height or the roughness of the surface. The above asperity contact model is then reduced to the Greenwood - Williamson mode.

3.2.2 Calculation of hydrodynamic pressure

For mixed lubrication in rolling, fluid flow is governed by the rough surface features. The classical Reynolds equation for incompressible, steady state and isothermal fluid flow in between the two moving smooth surfaces was modified by Patir and Cheng (Patir and Cheng 1978) to accommodate the case of fluid flow associated with rough surfaces. Recasting Eq. (2.5) for 2D fluid flow between rough surfaces leads to

$$\frac{\partial}{\partial x}\left(\phi_x \frac{d^3}{12\mu}\frac{\partial P_f}{\partial x}\right) + \frac{\partial}{\partial y}\left(\phi_y \frac{d^3}{12\mu}\frac{\partial P_f}{\partial y}\right) = \frac{U_r + U_s}{2}\frac{\partial h_T}{\partial x} + \frac{\partial h_T}{\partial t} + \frac{U_r - U_s}{2}\sigma\phi_s \tag{3.14}$$

where, ϕ_S term represents the additional shear flow transport due to sliding. The additional flow term is negligible and can be ignored. After removing this addition shear flow, Eq. (3.14) takes the following form,

$$\frac{\partial}{\partial x}\left(\phi_x \frac{d^3}{12\mu}\frac{\partial P_f}{\partial x}\right) + \frac{\partial}{\partial y}\left(\phi_y \frac{d^3}{12\mu}\frac{\partial P_f}{\partial y}\right) = \frac{U_r + U_s}{2}\frac{\partial h_T}{\partial x} + \frac{\partial h_T}{\partial t} \tag{3.15}$$

Sheu and Wilson (Sheu and Wilson 1994) introduced an empirical relation for ϕ_x for metal rolling in 1D fluid flow, which was:

$$\phi_x = 1 + 3\left(\frac{\sigma}{h_T}\right)^2, \text{ for } h_T \geq \sqrt{3}\sigma \tag{3.16}$$

$$\phi_x = \frac{2\sqrt{3}\sigma}{h_T}, \text{ for } h_T < \sqrt{3}\sigma \tag{3.17}$$

The above flow factors Eqs. (3.16) to (3.17) will be used in this study.

For a plane-strain analysis and 1D flows factor consideration as mentioned in the Eqs. (3.16) to (3.17), the Reynolds equation, Eq. (3.15), can be further simplified to:

$$\frac{\partial}{\partial x}\left(\phi_x \frac{d^3}{12\mu}\frac{\partial P_f}{\partial x}\right) = \frac{U_r + U_s}{2}\frac{\partial h_T}{\partial x} \tag{3.18}$$

where term $\partial h_T/\partial t$ is dropped due to the steady state of rolling (Chang *et al.* 1996). The relation between the thickness of lubricant film h_T and that of interfacial layer d, following Patir and Cheng (Patir and Cheng 1978), is illustrated in Fig. 3.3. Assuming that only the lubricant between the tip of the asperity and the roll surface can flow, the equivalent film thickness of the lubricant is then the average of this height, (d - h), which is given by

$$h_T = \int_{-\infty}^{d} (d-h)\Gamma(h)dh. \tag{3.19}$$

Eq. (3.18) can be further simplified if the separation d is close to or larger than 3σ. In this case the integration $\int_{d}^{\infty} (d-h)\Gamma(h)dh$ is much smaller than $\int_{-\infty}^{d} (d-h)\Gamma(h)dh$ (*e.g.*, when $d = 2\sigma$, the former integration gives only 0.5% of the latter).

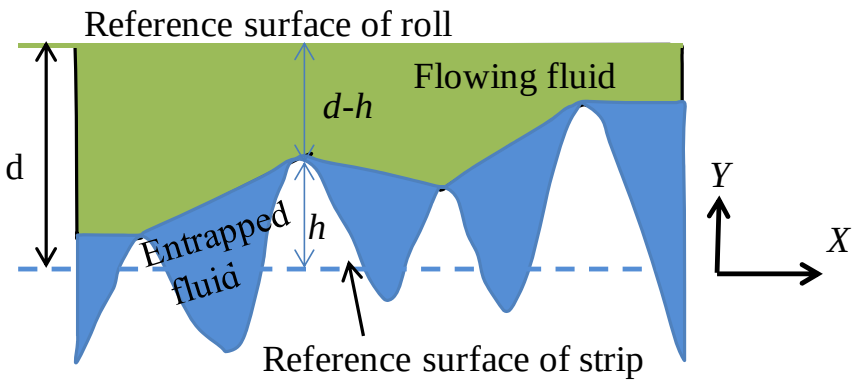

Figure 3.3: The concept of equivalent film thickness

Therefore, it is reasonable to change the upper integration limit of Eq. (3.19) to infinity, *i.e.*

$$h_T = \int_{-\infty}^{\infty} (d-h)\Gamma(h)dh. \tag{3.20}$$

This integration then gives $h_T = d$. In our simulation of metal rolling, even without lubricant, d is always larger than 3σ. Therefore, the approximation $h_T = d$ is always applicable, and the hydrodynamic pressure of fluid flow between the smooth roll surface and the rough strip surface can be found by solving Eq. (3.18).

For the shear traction, Eq. (3.2) is used which includes the frictional force due to solid-solid asperity contact and the frictional force due to viscous fluid. They are respectively given by

$$\tau_a = \mu_a P_a \tag{3.21}$$

$$\tau_f = \mu \frac{U_r - U_s}{h_T} \tag{3.22}$$

where, μ_a is the Coulomb friction coefficient for solid-solid sliding. The resultant coefficient friction μ_0 is defined as

$$\mu_0 = P_t / P_n \tag{3.23}$$

3.3 Implementation

A user-subroutine was written in FORTRAN language to calculate the contact pressure P_n from Eqs. (3.1), (3.12) and (3.18), and shear traction P_t from Eqs. (3.2), (3.11), (3.21) and (3.22). The separation d and the relative velocity between the roller and strip surfaces vary from node to node. These two variables can be automatically calculated by the user FE code. Eqs. (3.11), (3.12), (3.18), (3.20) and (3.21) can be calculated explicitly. The Reynolds Eq. (3.18), can be solved by the finite difference method

(Saniei and Salimi 2006). The Tri-diagonal Diagonal Matrix Algorithm (TDMA) is used in solving the second order Reynolds equation in the subroutine explicitly.

The flow chart of numerical calculation is shown in Fig. 3.4. The solution starts from the initial values of separation and other parameters from the input file under the definition of contact zone. Once the numerical calculations are done for the initial values, it proceeds automatically for the successive time steps.

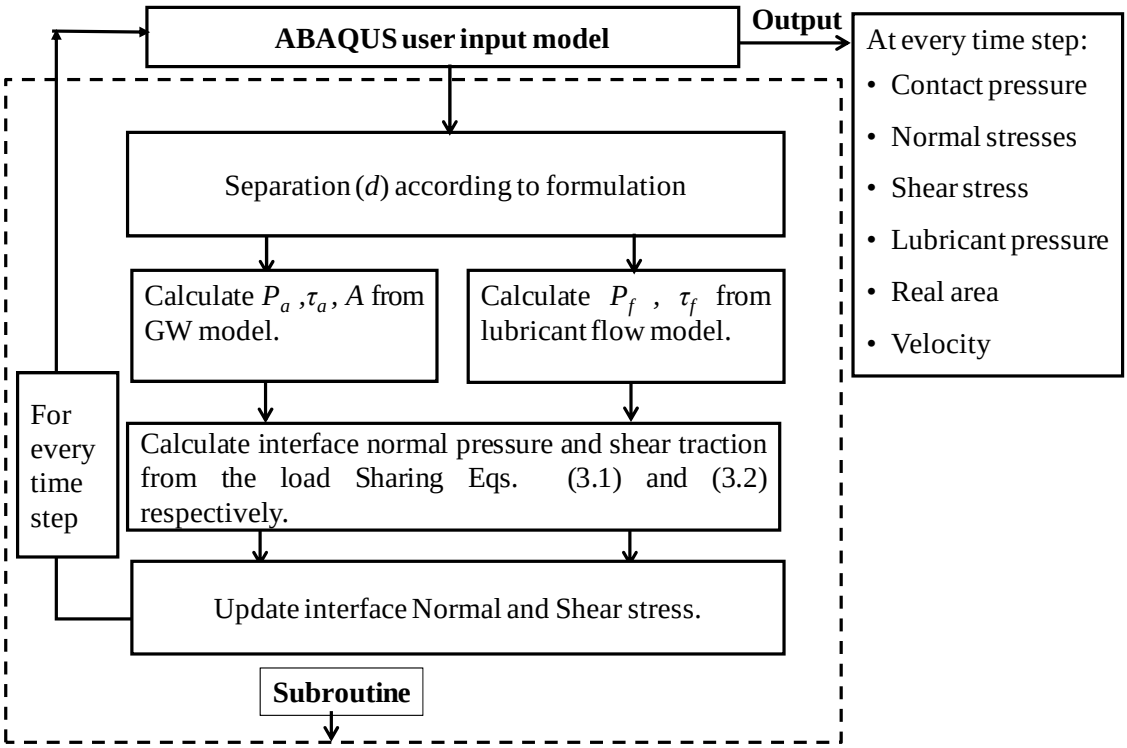

Figure 3.4: Flow chart of numerical calculation

The nodal values are updated in the FE model as explained in the formulation. The nodal forces will cause deformation of the material. The material response will follow the plastic stress-strain relation of the aluminium material model (Hartley, Sturgess *et al.* 1979). The deformation and stress of the FE solution are stored in the post

processing. The new separation values are used in the subroutine and are used for the solution of subsequent steps. The convergence problem is solved by simply reducing the time step of solution. The parameters used in the subroutine and in the FE model are shown in table 3.1.

Table 3.1: Parameters used in the simulation

Name	Symbol	Value
Young's Modulus	E	70 GPa (Liu *et al.* 1985)
Poisson's ration	v	0.35 (Liu *et al.* 1985)
Roll radius	R	150 mm (Liu *et al.* 1985)
Strip thickness	t	6 mm (Liu *et al.* 1985)
Coefficient of friction	μ_a	0.1 (Al-Salehi *et al.* 1973)
Viscosity	μ	0.04 ~ 5 Pa.s (Le and Sutcliffe 2006)
Asperity density	N	$10^7/mm^2$ (Robert and Green 2005)
Roughness	σ	0.005 mm (Robert and Green 2005)
Asperity summit radius	β	0.006 mm (Robert and Green 2005)

3.4 Approach verification

3.4.1 Hertz elastic contact problem

To verify the formula developed above and examine the user subroutine, let us examine a cylindrical indentation problem whose analytical solution is available. The numerical model is shown in the inset of Fig. 3.5. A displacement boundary condition is applied to

the rigid indenter to indent into the deformable strip. The strip material was assumed to be isotropic and linearly elastic, such that the Hertz contact theory can be applied. The resulting contact pressure distribution under the indenting force of 4602 N is shown in Fig. 3.5, where the pressure distributions due to the Hertz theory are also presented.

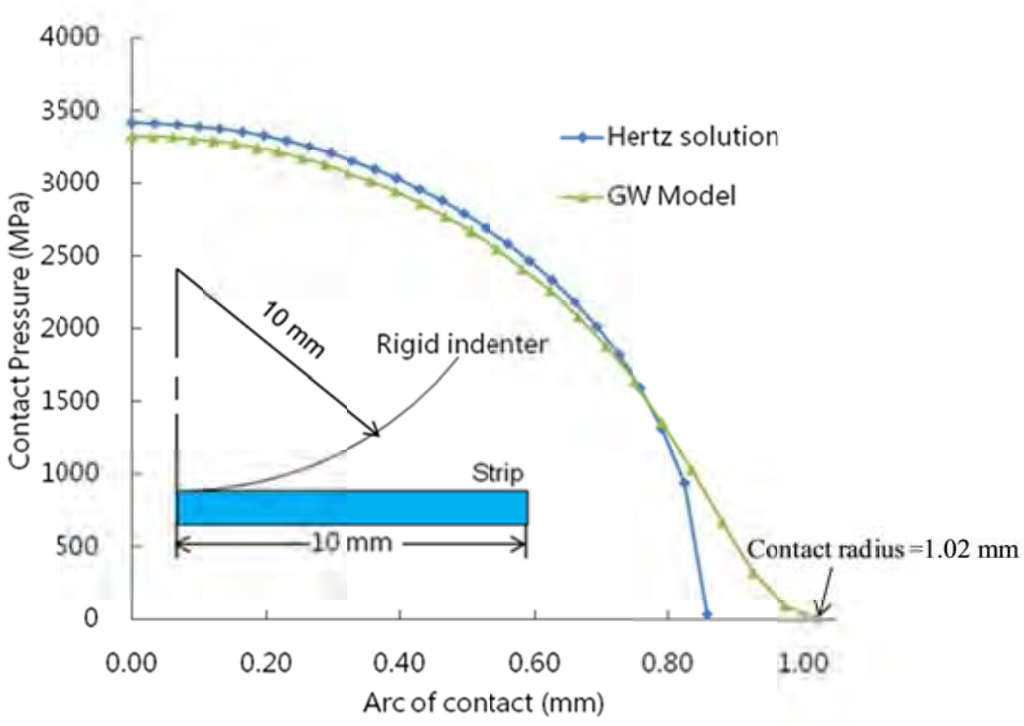

Figure 3.5: Contact pressure distribution of a cylindrical indentation problem

It is noted that the contact pressure in the central contact area calculated based on our model is smaller than the theoretical, but has a bigger radius of contact area. This discrepancy actually reflects the effect of the asperities in contact with a rough surface. At the edge of the contact zone, for a smooth surface contact problem, the pressure reduces more precipitously. For a rough surface, the separation between two reference surfaces must be larger than 3σ to ensure the condition of noncontact. This is because

asperities higher than 3σ can still be found with the probability larger than 0.1% according to Eq. (3.13). As a result, the contact pressure is not vanishing, according to Eq. (3.12). Fig. 3.5 shows that the contact radius for the rough surface contact is about 1.02 mm, which gives rise to the nominal distance between the two reference surfaces at the edge of contact area to be 0.0153 mm, slightly larger than 3σ (σ = 0.005 mm in this case). That is why the rough surface contact led to a wider contact pressure distribution.

3.4.2 Verification of the solution of Reynolds equation

The modified Reynolds equation for fluid flow between rough surfaces is solved by the finite difference method. This solution is verified by a manual calculation based on the analytical solution technique. The Reynolds equation used in this study is given by

$$\frac{\partial}{\partial x}\left(\phi_x \frac{d^3}{12\mu}\frac{\partial P_f}{\partial x}\right) = \frac{U_r + U_s}{2}\frac{\partial d}{\partial x} \tag{3.24}$$

where ϕ_x was defined by Sheu and Wilson (Sheu and Wilson 1994) as following,

$$\phi_x = 1 + 3(\sigma/d)^2 \tag{3.25}$$

The value of $(U_r + U_s)/2$ is assumed constant and steady state. By integrating Eq. (3.24) and using flow factor relation from the Eq. (3.25)

$$\frac{\partial P_f}{\partial x} = \frac{6\mu}{d^2 + 3\sigma^2}(U_r + U_s) + \frac{C}{d(d^2 + 3\sigma^2)} = g_1 + Cg_2 \tag{3.26}$$

where, g_1 and g_2 are the two functions defined by

$$g_1 = \frac{6\mu}{h^2 + 3\sigma^2}(U_r + U_s) \tag{3.27}$$

and

$$g_2 = \frac{6\mu}{h^2 + 3\sigma^2}(U_r + U_s) \tag{3.28}$$

respectively. Integration is then calculated from the Eq. (3.26), which will give the pressure distribution curve for each nodal point as following,

$$P_f(\bar{x}) = \int_0^L (g_1 + Cg_2)dx \tag{3.29}$$

where *L* is the arc length. Noting that boundary condition: $P_f(L) = 0$, the value of constant C can be calculated from the Eq. (3.29) by

$$C = -\frac{\int_0^L g_1 dx}{\int_0^L g_2 dx} \tag{3.30}$$

Eq. (3.26) is solved according to the integration rule in the excel spread sheet. The function used in the calculation is shown in the inset of Fig. 3.6 from Eq. (3.26). The same parameters are used to calculate hydrodynamic pressure by our own code.

Table 3.2: Parameters used in the analytical calculation

Name	Symbol	Value
Viscosity	μ	0.671 Pa.s
Total speed	$U_r + U_s$	10 m/s
Roughness	σ	0.005 mm
Step size		0.5 mm

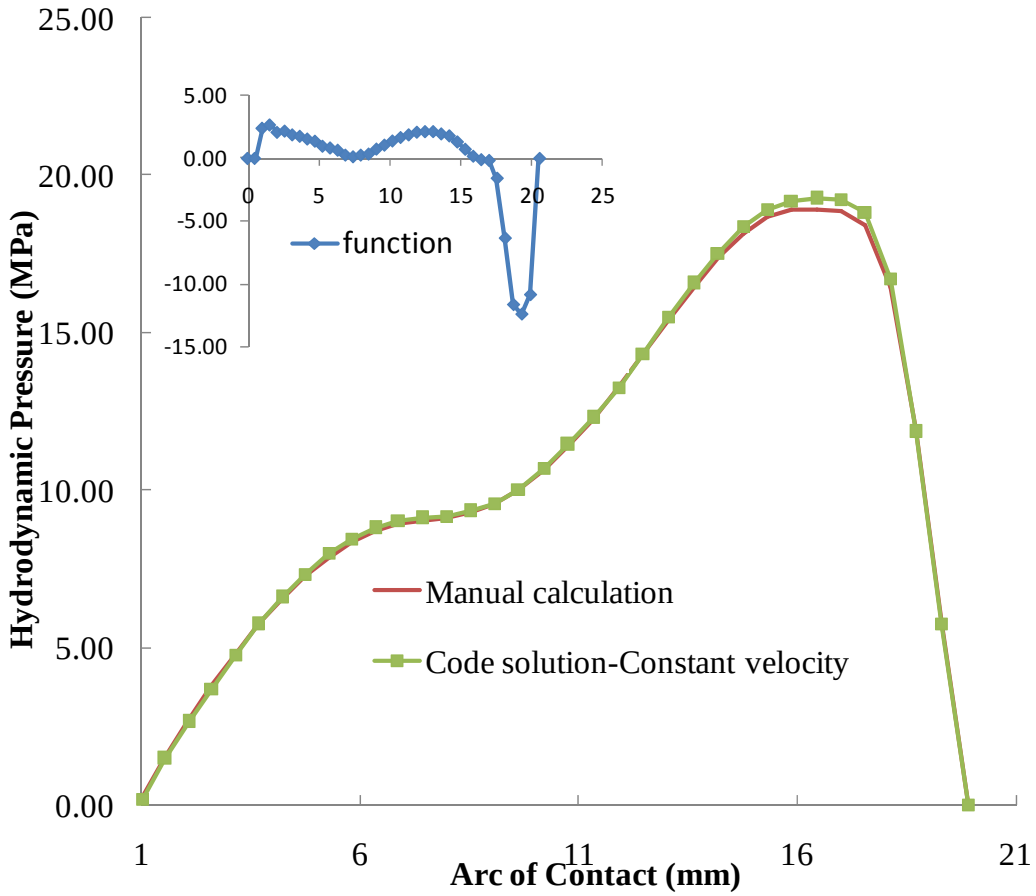

Figure 3.6: Hydrodynamic pressure comparison for constant velocity case

The velocity parameters will vary from entry to exit in a real simulation. The variation of this value ranges from 0.8-1 m/s as shown in the inset of Fig. 3.7. The actual simulation solution considering variable velocity is compared with analytical solution as shown in Fig. 3.7. It is found that the value of the real solution is higher than the analytical calculation as the variable speed is considered in the code solution. But the hydrodynamic pressure distribution pattern is very similar. It clearly demonstrates that our code solution is correct.

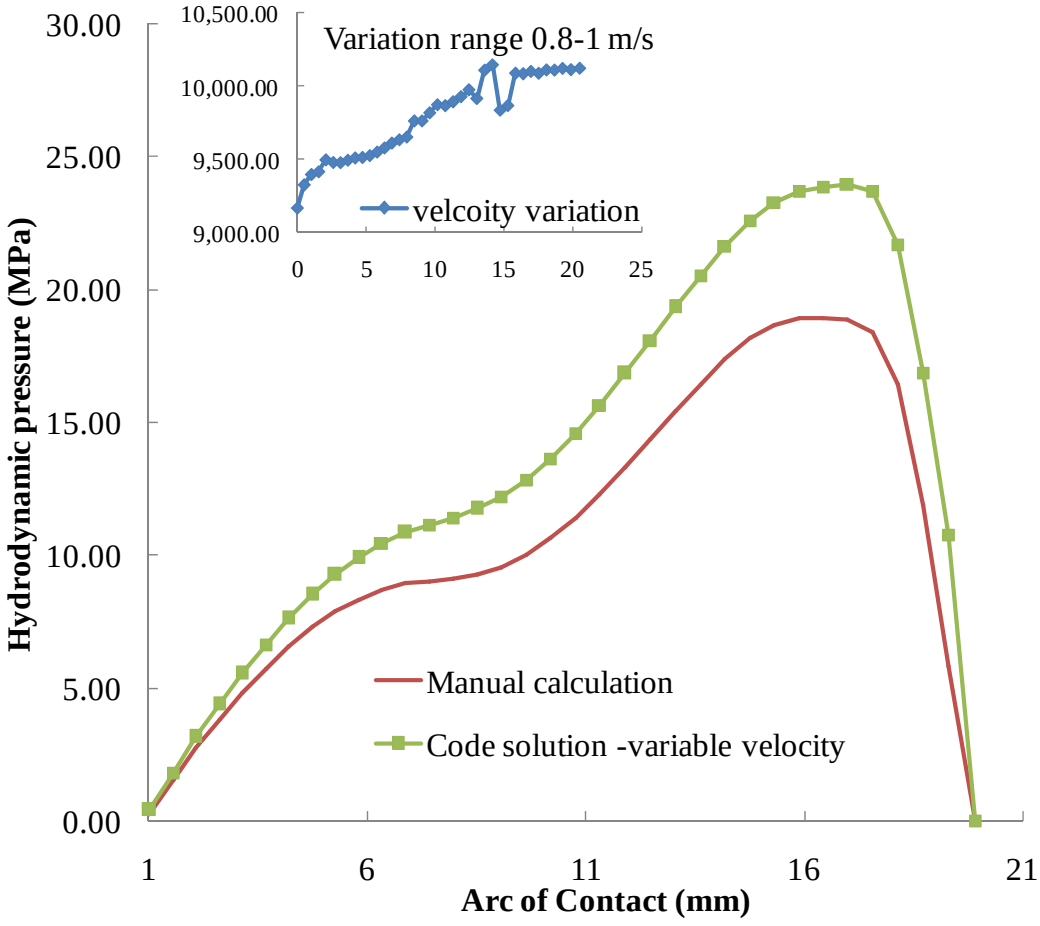

Figure 3.7: Hydrodynamic pressure comparison for variable velocity case (velocity variation range 0.8-1 m/s in the code solution)

CHAPTER 4

RESULTS AND ANALYSIS

Mixed lubrication in strip rolling is a complex mechanics, which needs the optimization of a group of parameters for quality roll products. In this study, a new numerical technique is applied to analyse different important parameters like rolling velocity, thickness reduction and lubricant viscosity that may influence the roll products. In industry, different lubricants are used mainly to reduce the coefficient of friction and to avoid friction pick up during production. Lubricant plays a significant role in determining the rolled strip surface quality, low power consumption and low wear rate (Al-Salehi *et al.* 1973; Kosasih and Tieu 2007; Le and Sutcliffe 2006). The roles of lubricants depend on the extent of hydrodynamic pressure developed in the rolling process. It doesn't mean that an increase of hydrodynamic pressure always favours the rolling process. An increase of hydrodynamic pressure may decrease the frictional force significantly and the rolling process may fail due to lack of sufficient frictional force to drag the strip in the roll bite. An optimum frictional force is needed to drag the strip and the rolling process to take place. So the optimum choices of lubricant, rolling velocity and thickness reduction ratio are needed to get the desired frictional force and hydrodynamic pressure for a rolling operation.

In this chapter, a case study based on our mixed lubrication rolling model will first be presented in Section 4.1. The effects of different rolling parameters will then be explored in Section 4.2, followed by discussion and conclusion in Section 4.3.

4.1 Rolling analysis

4.1.1 Numerical model and parameters

The numerical model generated by ABAQUS CAE for the FE explicit simulation is shown in Fig. 4.1. The contact between the roll and the strip was modelled by the user subroutine implementing surface to surface contact in penalty formulation. A 4-node bilinear plane strain quadrilateral element (CPE4R) with reduced integration point and hourglass control was used for meshing the strip, as shown in Fig. 4.1. The total number of elements in strip surface was 1920.

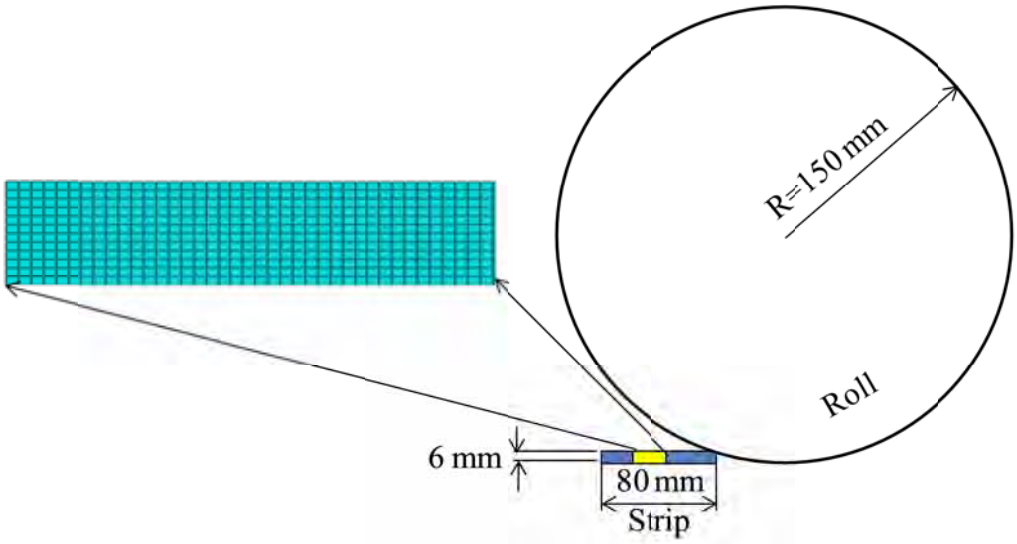

Figure 4.1: FE mesh and model

A symmetric half was analysed in this study and the symmetry boundary condition was applied at the bottom of the strip. An angular velocity was applied in the centre of the roll. The initial velocity, which was equal to roll circumferential velocity, was applied to the strip for a smooth engagement of the strip into the rolling region. The model was for 2D plane-strain rolling. In the simulation, the roll was assumed to be rigid and the

strip material was assumed to be isotropic and elasto-plastic with a constitutive relation (Hartley *et al.* 1979) between the uniaxial stress τ and the uniaxial plastic strain ε_p as

$$\tau = Y\left(1+\frac{\varepsilon_p}{\varepsilon_0}\right)^n \tag{4.1}$$

where Y is the yield stress, and n and ε_0 are the hardening coefficients. The strip material considered here was aluminium whose mechanical properties are Y = 50.3 MPa, n = 0.26, and ε_0 = 0.05 (Hartley *et al.* 1979). This uniaxial stress and plastic strain relation is shown in Fig. 4.2.

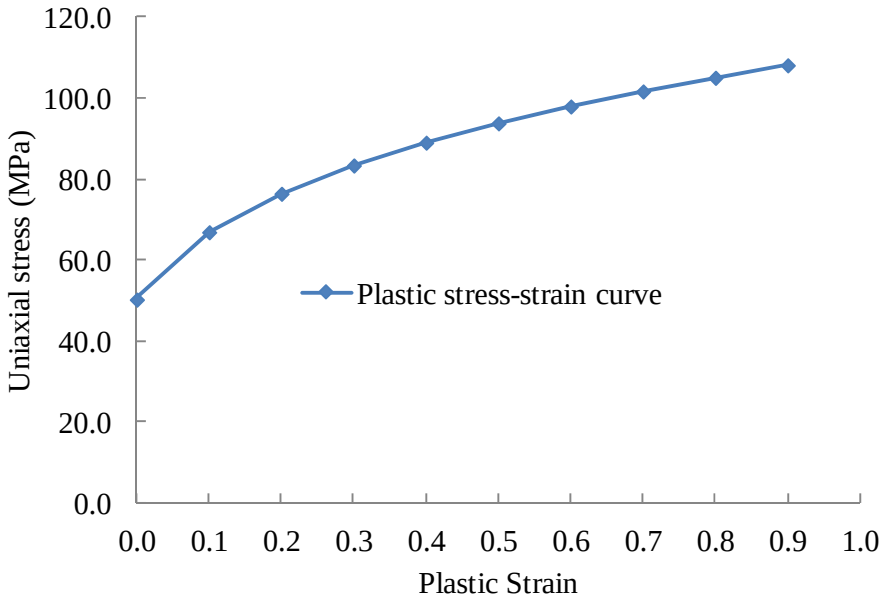

Figure 4.2: Plastic stress-strain curve (Hartley *et al.* 1979).

In simulation, the element size is 0.5 mm. A further reduction of the mesh size by half the element dimension gives an identical result of contact pressure as shown in Fig. 4.3, indicating that the mesh size used was appropriate. The separation value was updated automatically to the user subroutine at every time step and the normal pressure and shear surface traction were updated by the subroutine according to the formulations introduced in Chapter 3. The thickness of lubricant film h_T was assumed (see Chapter 3) to be equal to the separation of two reference surfaces d under the condition that d was much larger than the roughness σ.

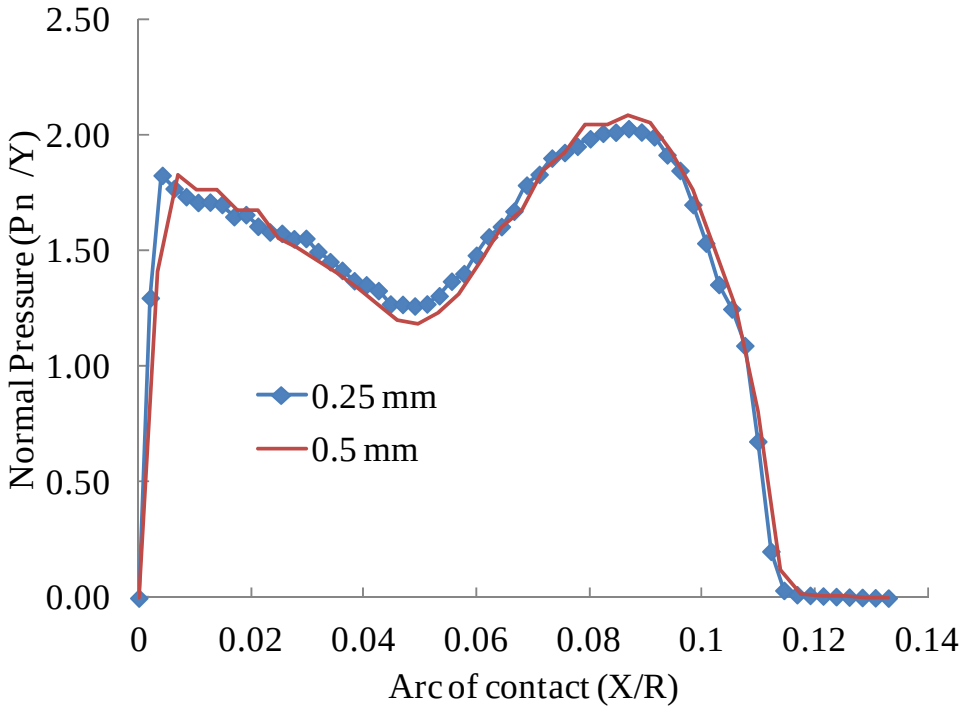

Figure 4.3: FE mesh sensitivity test

Fig. 4.4 shows that the minimum d/σ is about 4 in this study, which verifies the applicability of Eq. (3.20). The parameters used in the rolling are listed in Table 4.1.

Other parameters have been listed in Table 3.1. The results of this case study are described below.

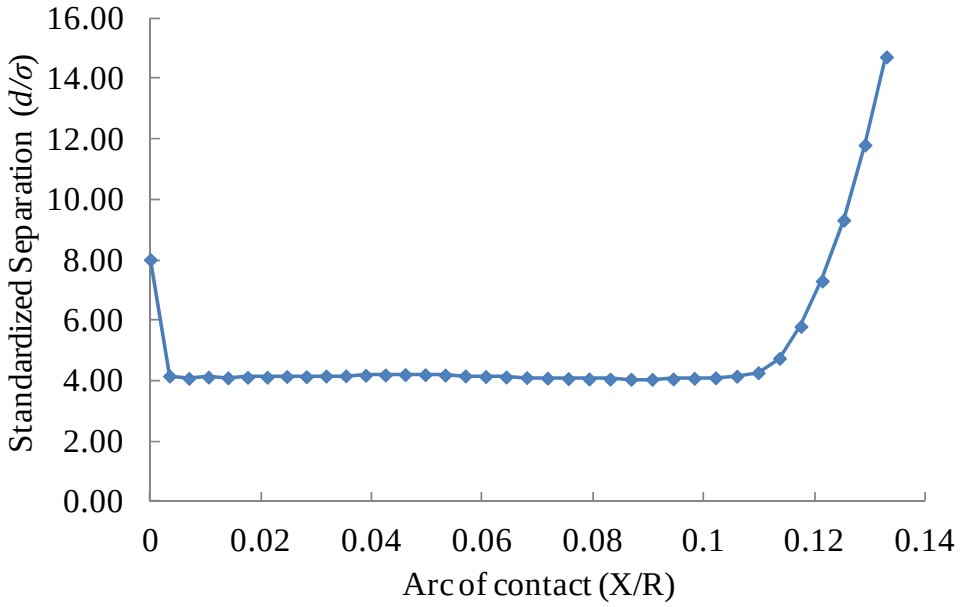

Figure 4.4: Separation of two reference surfaces during rolling

Table 4.1: Parameters used in the rolling analysis

Name	Symbol	Value
Rolling velocity	U_r	3 m/s
Viscosity	μ	0.04 Pa.s
Thickness reduction	t	15-30%

4.1.2 Neutral point

The neutral point is the cross section of the strip at which the roll and strip surfaces have the same velocity; or in other words, at which the relative velocity of the two surfaces is zero. This is also known as the no-slip point. In the present case, the neutral point is not at the middle of the arc of contact but some place close to the exit, as shown in Fig. 4.5a. Before this point, the roll moves faster than the strip, and after this point, the roll moves slower. The frictional force P_t advances the strip under the roll before the neutral point, while it retards the strip motion after the neutral point. Since the neutral point is close to the exit, the net frictional force acting on the roll tends to reduce its speed. Therefore, the rolling process may become unstable and the roll will skid over the strip and the strip will stop altogether (Avitzur 1980). The position of the neutral point apparently depends on the friction coefficient. If the solid-solid frictional coefficient μ_a increases, the neutral point moves away from the exit point, as shown in Fig. 4.5b. The net friction force on the roll reduces from 79.22 to 32.87 N when the friction coefficient increases from 0.1 to 0.3, leading to a more stable rolling process.

Although a larger friction coefficient may stabilize the rolling, it reduces the quality of the surface finish. Therefore, a reduction of frictional force through hydrodynamic lubrication is still desired. The higher the thickness reduction is attempted, the greater frictional force is needed and the closer is the neutral point to the exit. The maximum thickness reduction is reached when the neutral point reaches the exit point.

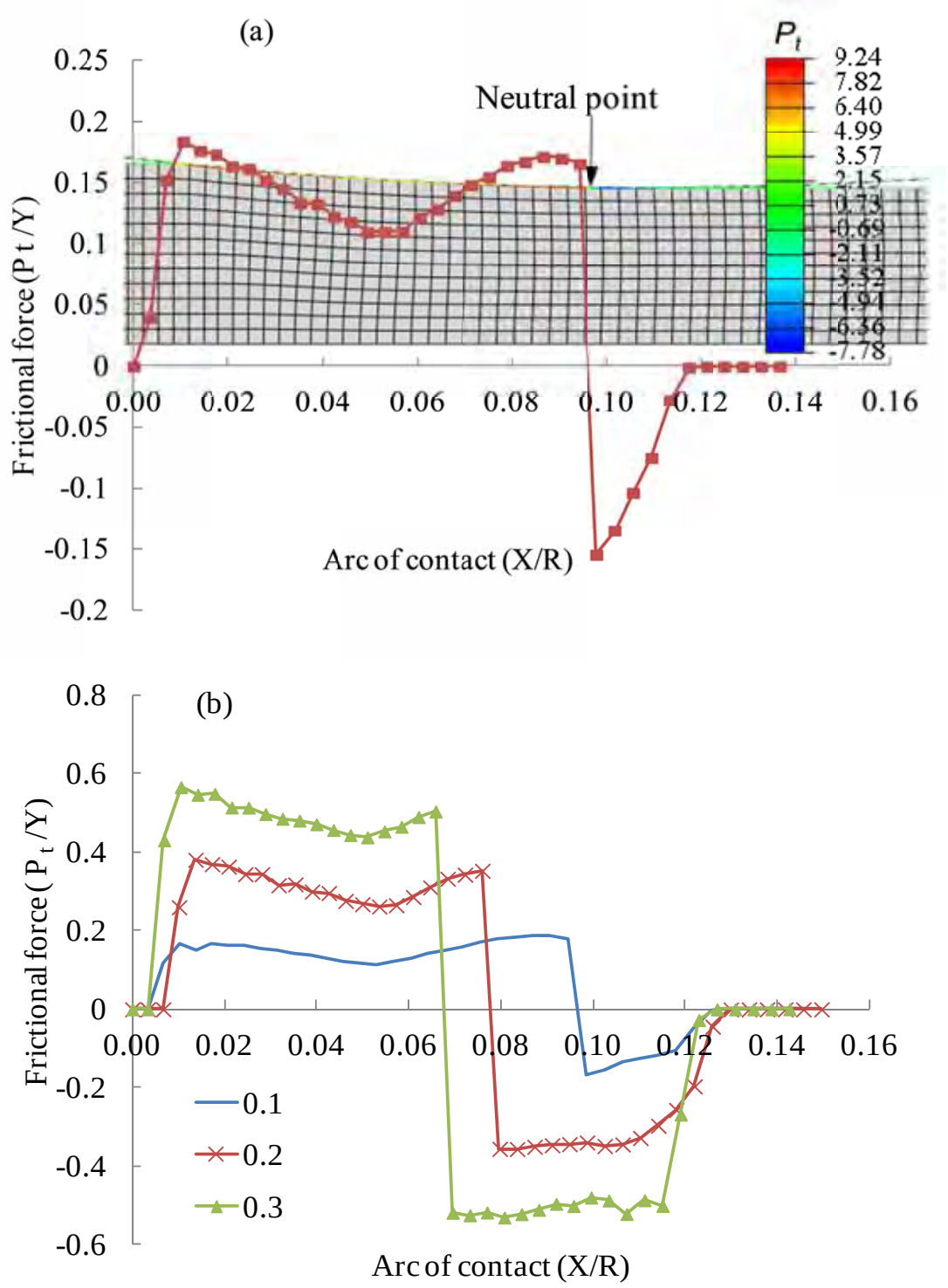

Figure 4.5: The distributions of frictional force :(a) friction coefficient = 0.1 and (b) effect of friction coefficient, where X is the contact length measured from the entry point

4.1.3 Contact pressure

Fig. 4.6 shows the variations of the contact pressure P_n and frictional force P_t along the arc of rolling contact. The experimental results obtained by Al-Salehi *et al* (Al-Salehi *et al.* 1973) are also included for comparison. It can be seen that in the region close to the entry point, the pressure obtained by this method is smaller than the experimentally measured. The discrepancy at the entry region can be ascribed to two reasons. Firstly, the strain rates ($\dot{\varepsilon}_{22}$) at the entry region, especially along the strip thickness direction, are much larger than those at the region of the second pressure peak. $\dot{\varepsilon}_{22}$ can be calculated from the velocity map shown in Fig. 4.7. It is found that $\dot{\varepsilon}_{22}$ is about -700 s^{-1} at the entry region but reduces to -10 ~ -100 s^{-1} in the region close to the exit. However the constitutive model adopted only counts for the strain hardening. The strain rate effect is not considered. This was treated similarly in the work of Al-Salehi *et al*. (Al-Salehi *et al.* 1973) and in other related papers (Hwu and Lenard 1988; Liu *et al.* 1985). Secondly, it is noted that the total normal load measured by a load cell in the roll (Al-Salehi *et al.* 1973) was smaller than the integral of the normal pressure. This could indicate that the contact pressure measured by Al-Salehi *et al*. was probably over-estimated especially at the entry region. The significant drop of the contact pressure at roughly the middle of the contact observed in the experiment is also captured by our model prediction.

In the inset of Fig. 4.6, the deformation of the strip and the distribution of the normal stresses σ_{11} and σ_{22} along the transverse and normal directions are also shown. Corresponding to the drop of the rolling pressure, σ_{11} and σ_{22} reach their respective maxima in tension and compression.

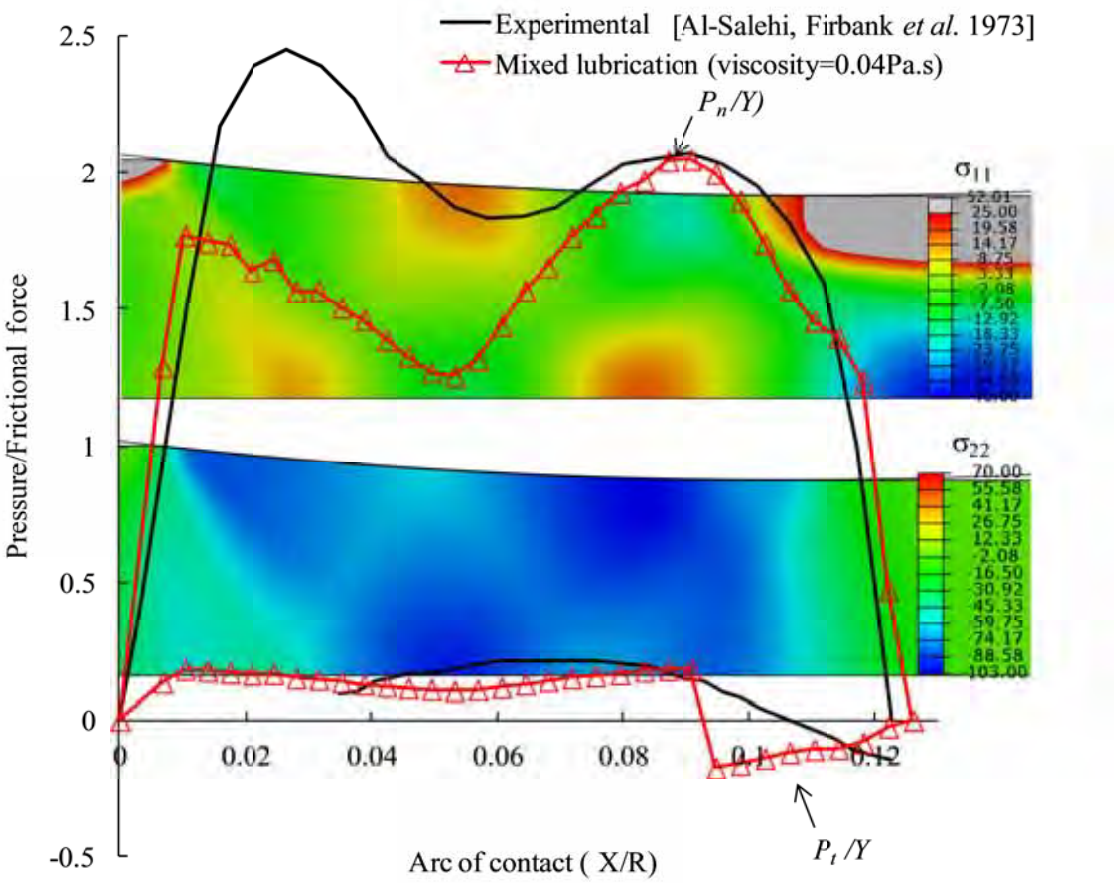

Figure 4.6: Comparison of normal pressure and frictional force

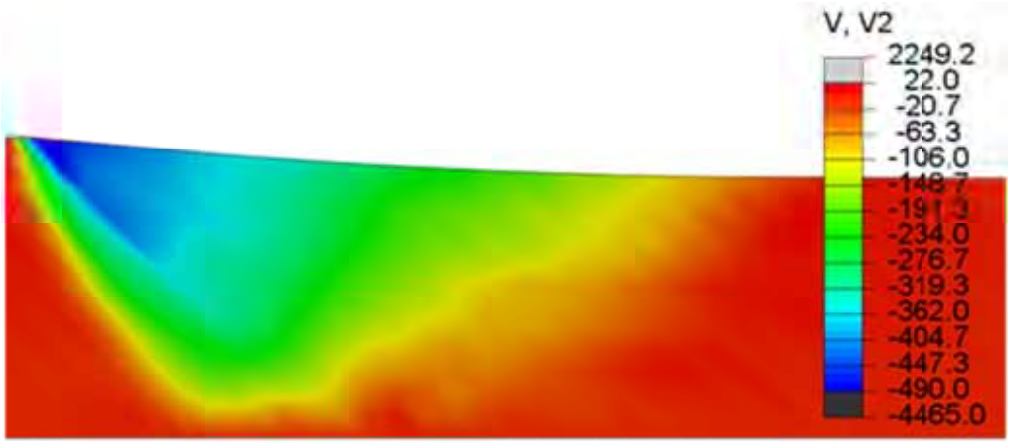

Figure 4.7: Distribution of the velocity perpendicular to the rolling direction

Therefore at the middle region of the contact arc, the top surface of the strip experiences maximum tension due to the non-uniform displacement field. This tensile stress in the horizontal direction deteriorates the capacity to sustain the pressure in the normal direction. It should be noted that at roughly the middle of the arc of the contact, the strip material is subjected to maximum stretch. This is different from the neutral point, at which the strip velocity reaches the maximum.

4.1.4 Deformation in rolling

Deformation in rolling is complex due to the presence of both normal and shear stress in the underlying material with large plastic deformation. In metal rolling, both tensile and compressive normal stresses are found due to material deformation. The normal stresses σ_{22} and σ_{11} in the vertical and transverse directions are shown in the inset of Fig. 4.6. σ_{22} and σ_{11} are in tension and compression respectively in the region close to the surface. It is noted that σ_{11} in the regions before and after the contact zone is larger than that inside the contact zone. This is because of the dragging of the frictional force. σ_{22} follows the distribution of the normal pressure, increases precipitously at the entry point, reduces to the minimum at roughly the middle of the contact region and reaches the maximum at roughly the neutral point. It should be noted that as the strip proceeds underneath the roll, it is subjected to increasingly larger thickness reduction. But the stress σ_{22} does not increase monotonically. This is due to the same reason as the drop in the contact pressure, as discussed in the last section. More specifically, this is because of the material yielding. In the simulation, the Von Mises yield criterion is used, which combines both σ_{22} and σ_{11} in the equivalent stress (τ). For the plane strain condition used in the simulation, τ is proportional to $\sqrt{\sigma_{11}^2+\sigma_{22}^2-a\sigma_{11}\sigma_{22}}$, where a is a positive

constant depending on the Poisson's ratio. When the material yields, the equivalent stress τ does not change much with the plastic strain. An increase in the tensile stress σ_{11} must lead to the reduction of the compressive stress σ_{22}.

4.1.5 Hydrodynamic pressure and resultant friction coefficient

The hydrodynamic pressure and the resultant friction reduction rate defined as μ_0/μ_a, are shown in Fig. 4.8. In this study, first, a small viscosity 0.04 Pa.s is used to see the effect of resultant friction according to the formulation of this study (see Eqs. (3.21) to (3.23)). It is found that for such a low viscosity, the hydrodynamic pressure is very small. The effect of such a lubricant on the resultant friction coefficient is negligible.

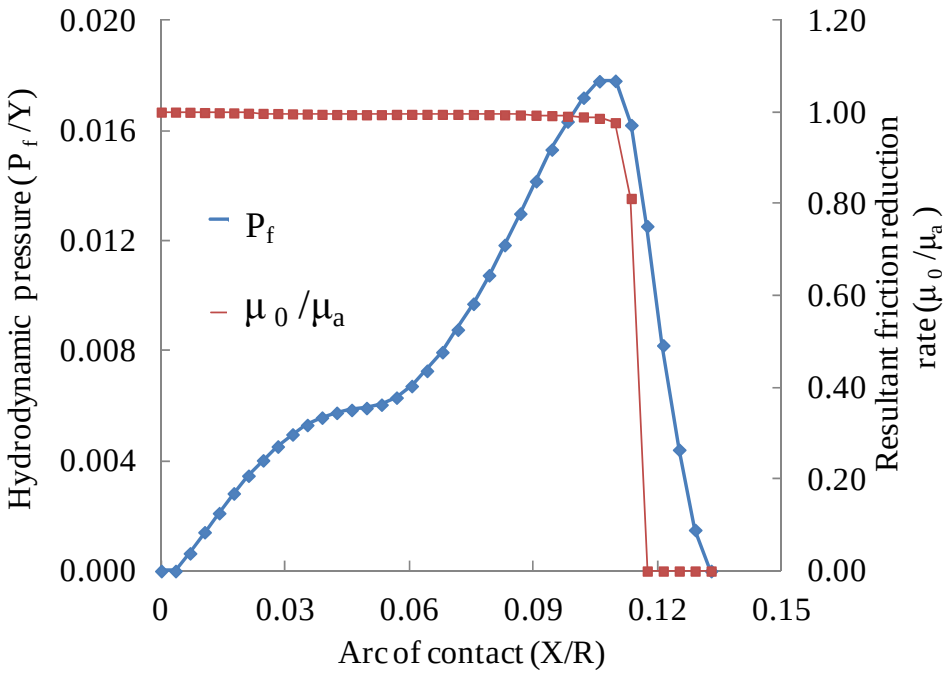

Figure 4.8: Hydrodynamic pressure and resultant friction

Some analytical models (Kosasih and Tieu 2007; Saniei and Salimi 2006) also used very low viscosity (0.02 ~ 0.04 Pa.s) in their calculation. The resulting hydrodynamic pressure from their models was almost equal to the total normal pressure. Although the same Reynolds equation is used, the result of this study is in sharp contrast to theirs. This is probably because of the difference in defining the boundary condition for solving the Reynolds equation. In their model, the contact pressure was solved from the material deformation at a certain point which was misinterpreted as the hydrodynamic pressure. The resultant hydrodynamic pressure was found almost equal to the total normal pressure. If their result is sensible, the frictional force must be almost negligible due to the high hydrodynamic pressure with low viscosity value. However, such a phenomenon did not occur in the experiments (Al-Salehi *et al.* 1973). However, in this study, the Reynolds equation is solved under the boundary condition that the hydrodynamic pressures at the entry and exit point are zero. This result is reasonable and can reflect the effect of viscosity and rolling velocity, as will be discussed shortly.

4.1.6 Different thickness reduction ratio

The simulation is done for a higher thickness reduction ratio and the results are compared with the experimental results of Al-Salehi *et al*. With the further increase of thickness reduction ratio, the normal pressure is generally expected to be higher as the material undergoes large deformation. The normal pressure distribution for 21.86 % and 29.40 % reduction is shown in Fig. 4.9 and Fig. 4.10 respectively for both the experiment and this study.

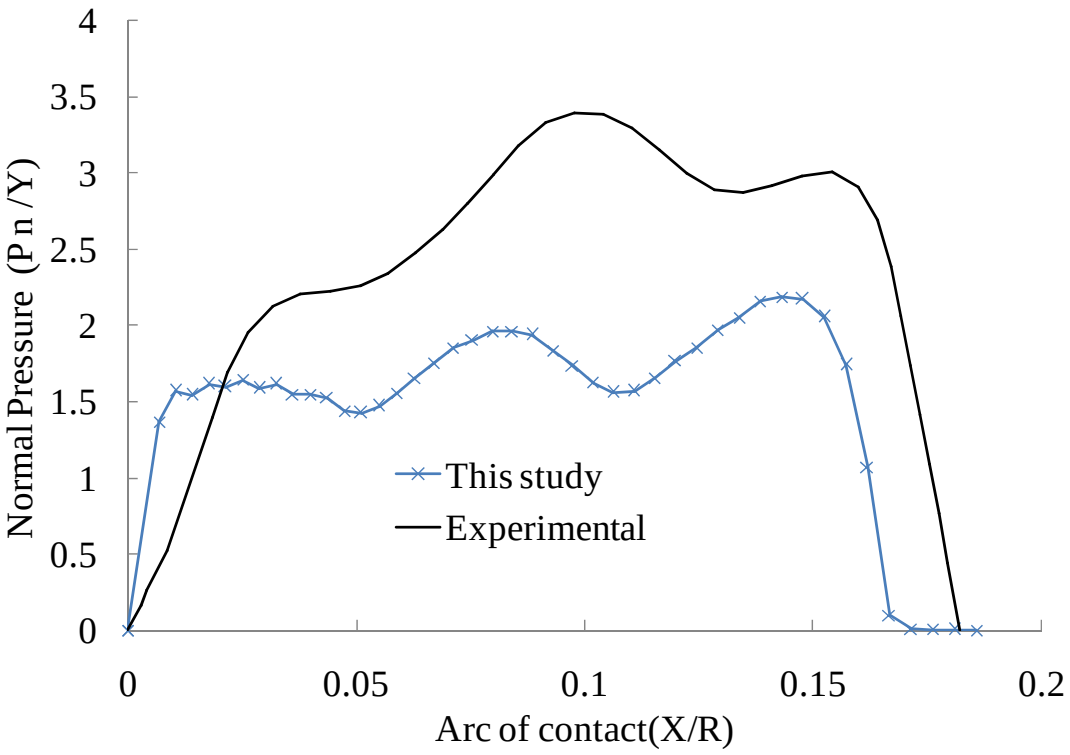

Figure 4.9: Comparison of normal pressure for 21.86% reduction

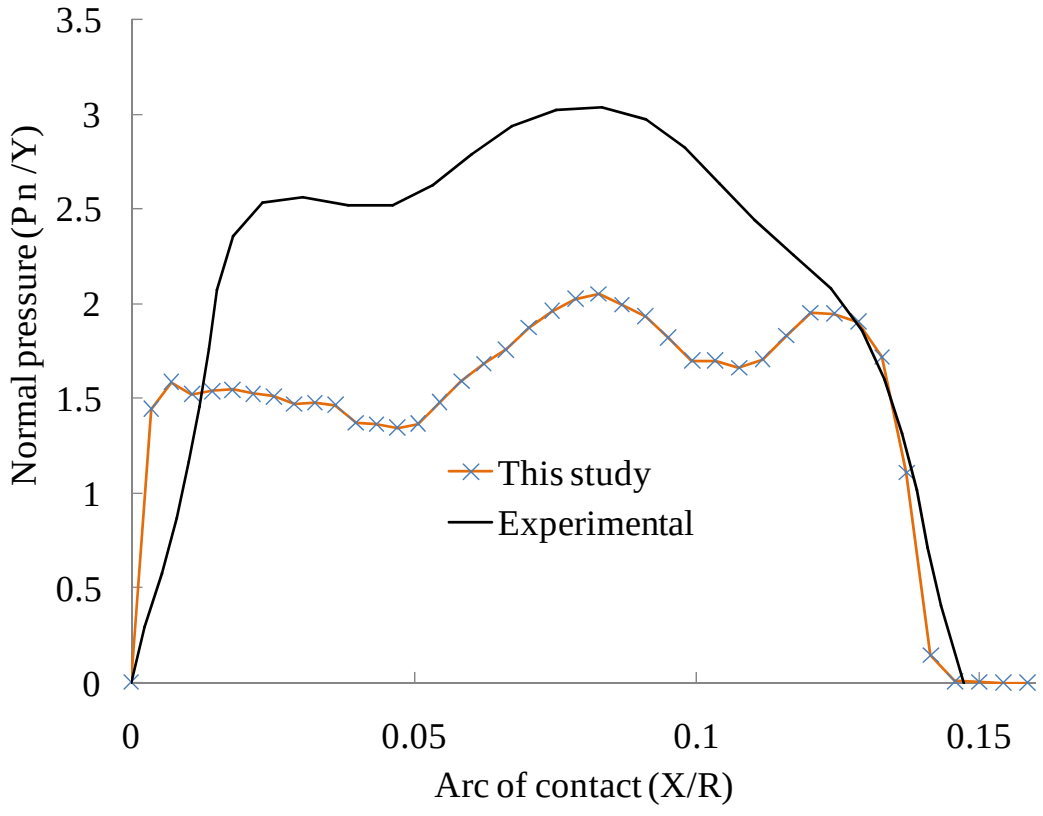

Figure 4.10: Comparison of normal pressure for 29.40% reduction

It is found that for higher thickness reduction cases, the normal pressure distributions are qualitatively similar, i.e. more peaks and drops are found both in the experiment and this study. It is noted that there are three peaks in the pressure curve for the reduction ratios 21.86% and 29.40%, which was also found in the experiments (Al-Salehi, *et al*. 1973). But overall the pressure in the experimental results was higher than this study. One of the possible reasons for this discrepancy is due to the material hardening model that was used in this study (see Eq. 4.1). Though the same material (aluminium) is used in this study and the experiment, the exact material properties of Al-Salehi *et al.*'s experiment are not available. Al-Salehi *et al*. also admitted this large discrepancy of pressure with the theoretical results was due to material hardening and when more than one pressure peak was found in the pressure distribution. Some authors (Hwu and Lenard 1988; Liu *et al.* 1985) also reported a similar discrepancy between the theoretical results and the experimental results of Al-Salehi *et al*. As an interfacial statistical rough surface is used in this study, a small pressure tail at near exit is found due to elastic unloading of asperities, where the surfaces are still in contact as discussed in the approach verification (see Section 3.4.1). The normal pressure calculated in this study may increase to some extent if the plasticity model of asperity deformation had been considered, especially near the exit region. The effects of plasticity will be discussed in more detail in Section 4.2.1.

4.2 Parametric study

Different lubricants have been used in the industry to get the desired frictional force based on operational experience. Some typical lubricants are shown in table 4.2 (Le and Sutcliffe 2006) which have been used in the analysis of the rolling process. It is noted

that the viscosity of the lubricants varies in a very wide range, say from 0.02 to 2 Pa.s (Le and Sutcliffe 2006). However, the choice of appropriate lubricants is still difficult due to lack of a reliable mixed lubrication model to analyse the real mechanics in this respect. The main purpose of this parametric study is to study the effects of different lubricants and rolling velocities in rolling. These studies may shed some light on the engineering design of rolling parameters.

Table 4.2: Lubricants used in the parametric study (Le and Sutcliffe 2006)

Lubricant name	Viscosity (Pa.s)
V68	0.0149
M320	0.671
H650	1.915

The parametric study is explored for different lubricant viscosities and rolling velocities that will be discussed in Sections 4.2.1 to 4.2.3. The parameters used in these investigations will be given in the respective sections.

4.2.1 Effect of lubricant on contact pressure

For higher viscosities (0.3 ~ 1.2 Pa.s), the significant hydrodynamic pressure P_f has been developed as shown in Fig. 4.11b. The corresponding total normal pressure P_n is shown in Fig. 4.11a. It is noted that an increase of the hydrodynamic pressure does not lead to the increase of the total normal pressure significantly.

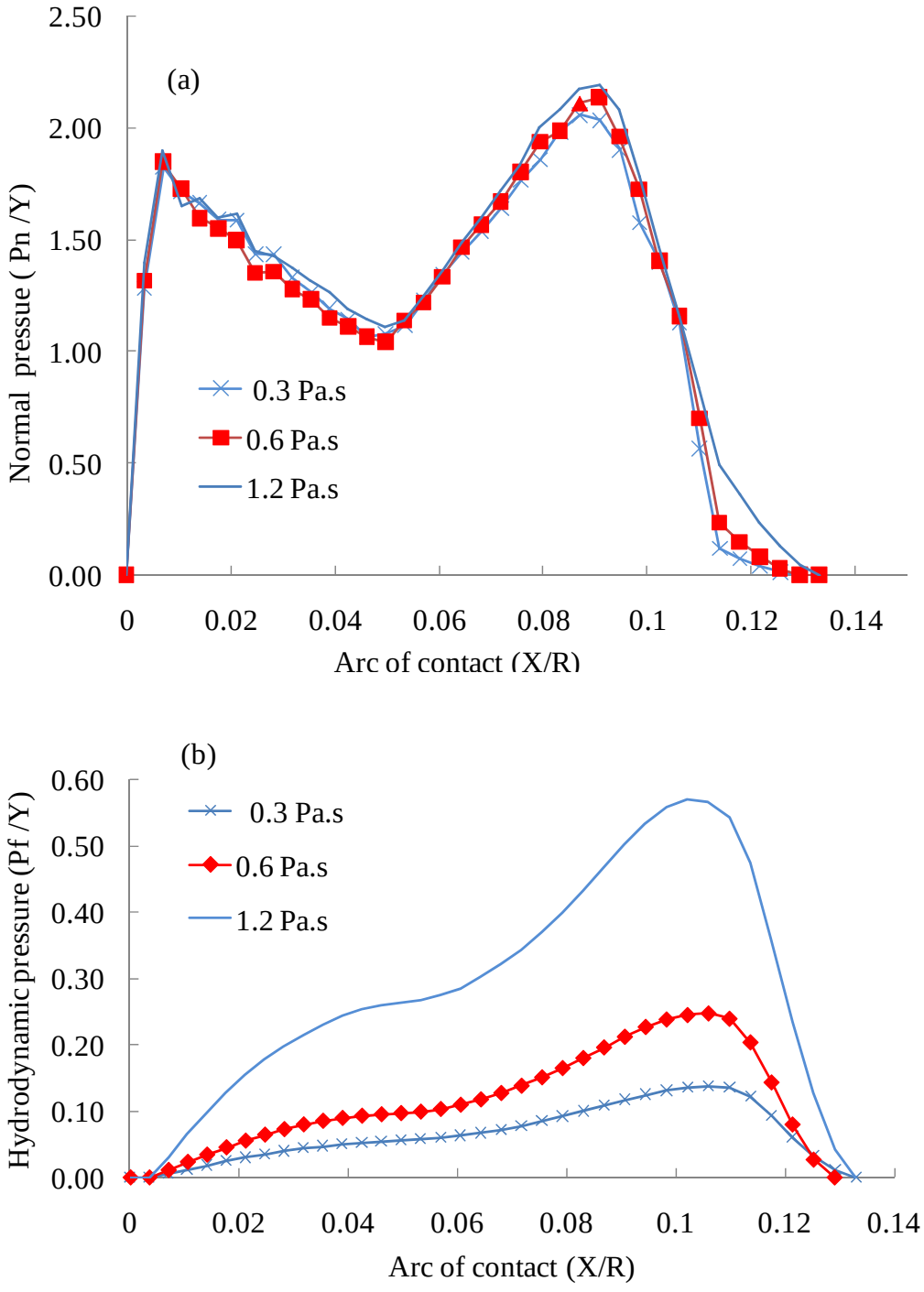

Figure 4.11: Distribution of (a) normal pressure and (b) hydrodynamic pressure

It is found that the normal pressure only increases less than 5 MPa, when the lubricant viscosity increases from 0.3 to 1.2 Pa.s as shown in Fig 4.11a. The major fraction of the total normal pressure is still due to the solid-solid asperity contact. This is due to the

dominant contribution of asperity contact pressure in load sharing. Moreover, hydrodynamic pressure does not increase at the beginning and the highest hydrodynamic pressure is generated at near the zone. Therefore, the contribution of hydrodynamic pressure comes to play effectively at near the exit zone. With an increase of hydrodynamic pressure, normal pressure in the pressure tail near the exit region increased more than when low viscosity was used. This indicates that the load sharing principle is working in the model. The higher hydrodynamic pressure at near the exit contributes a small increase of pressure in the pressure tail.

The real area of contact also plays an important role in the load sharing relation on the normal pressure distribution as shown in Fig. 4.12. It is found that the real area of contact decreases with the increase of hydrodynamic pressure, indicating that a higher viscosity leads to larger hydrodynamic pressure, less area of solid-solid asperity contact and better lubrication. Plotting the contribution of asperity contact pressure AP_a against A, as shown in the inset of Fig. 4.12, indicates that A is proportional to P_a. Therefore, the real area of contact plays a vital role in the load sharing equation. This may be the cause of a small increment in normal pressure with the application of higher hydrodynamic pressure. The decrease of real area of contact is qualitatively acceptable according to the concept of the mixed lubrication load sharing principle, where lubricants would carry some part of the total applied load and the solid-solid asperity contact would carry the rest of the load. If the asperities would carry less load in lubricated contact situation comparing to a dry contact (without any liquid) case, then there is a possibility that either fewer asperities or there will be less deformation of asperities or both would affect the real area of contact. The decrease of the real area of contact is also prompted due to the elastic deformation assumption of the GW model,

where the unloading of asperities near the exit zone leads to a decrease in the real area of contact to some extent. A decrease of the real area of contact means a decrease of asperity contact pressure. An increase of the real area of contact means either a large deformation of asperities or more asperities are in contact or both together contribute to the asperity contact pressure.

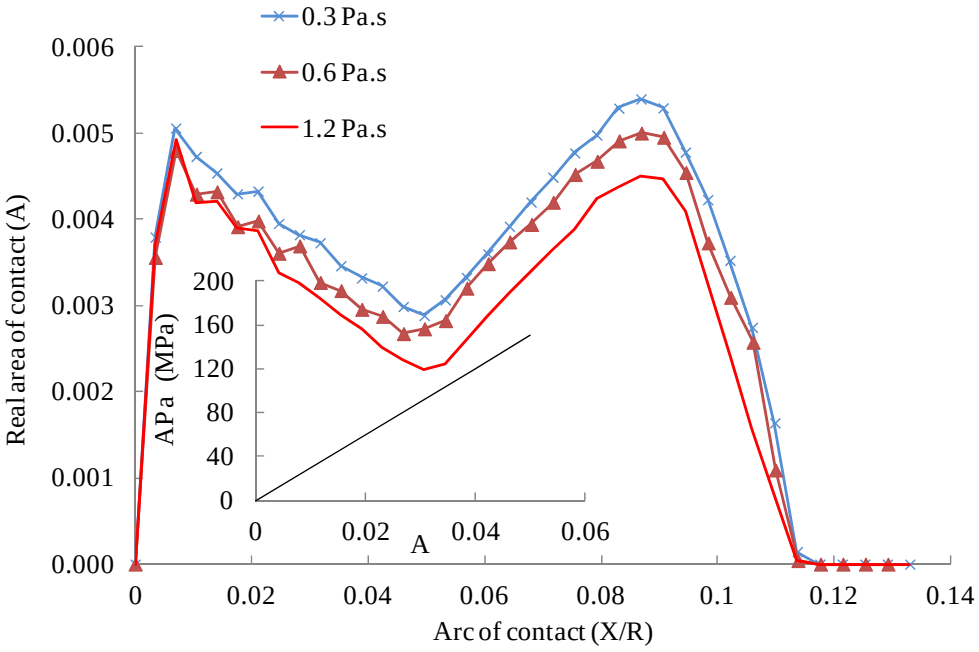

Figure 4.12: Distribution of real area of contact for different viscosity

The inclusion of the plastic deformation of asperities may contribute to increasing the overall increase of the real area of contact in the entire arc of contact according to some recent elasto-plastic asperity deformation models (Kimura and Childs 1999; Robert and Green 2005). These studies used plasticity index (ζ), which is defined by Greenwood and Williamson as

$$\zeta = \sqrt{\frac{\sigma}{\omega_c}} \tag{4.2}$$

where, ω_c is the critical interference. The critical inference ω_c is the point of initial yielding. The plasticity index may vary from 1 to 100 depending on the material properties suggested by Greenwood and Williamson. The results of the elasto-plastic asperity deformation model developed by Robert and Green (Robert and Green 2005) is shown in Fig 4.13, which confirms that the real area of contact increases significantly due to plasticity consideration.

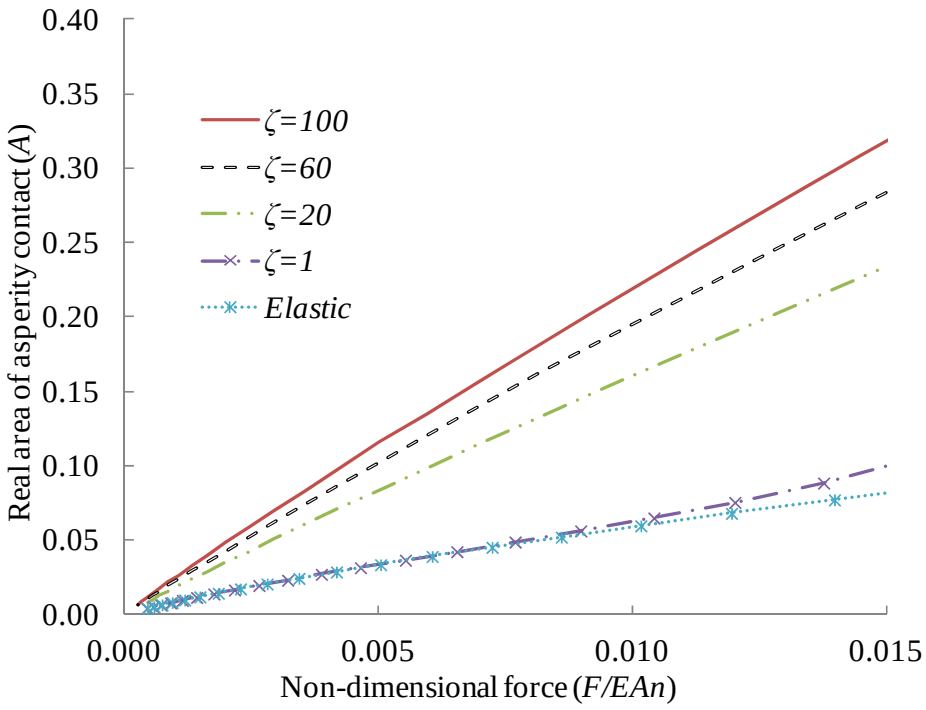

Figure 4.13: Real area of contact for different plasticity index, where A_n is the nominal area

For the same applied force, the real area of contact is almost the same for the two models (elastic and elastic-plastic), when the plasticity index is equal to 1. With the increase of plasticity from 1 to 100, the real area of contact increases significantly (see Fig 4.13). The increase of the real area of contact is very rapid at the lower plasticity index range (up to 20) and then slowly follows the increasing trend for the higher plasticity indexes. The results of the elastic-plastic asperity deformation model indicate that the real area of contact is underestimated in this study due to the elastic deformation assumption. It is expected that an increase of the real area of contact due to plasticity consideration may increase the overall normal pressure distribution. However, a decrease of the real area of contact to some extent associated with the hydrodynamic effect will be retained irrespective of either model used in the load sharing. Plasticity consideration in the asperity model may change some other parameters. The separation between the two surfaces may be different due to plasticity consideration as against the elastic assumption. If the asperities are deformed plastically, the separation between the two surfaces will become smaller gradually from the entry to the exit. The effects of separation on contact force and normal pressure are shown in Fig. 4.14a and Fig. 4.14b respectively. The contact force follows a sharp (exponentially) increase with the decrease of separation. The asperity contact pressure also increases with a decrease of separation but it does not exactly follow the trend of force increment. It is due to the real area of contact as it is also increasing with every increase of force. Here the real area of contact plays a role to change the contact pressure inversely proportional to the separation. With the monotonic increase of the real area of contact due to plasticity consideration, the separation values will be gradually smaller. The elastic unloading of the asperity deformation can be avoided totally by considering plasticity in the proposed

model of this study. However, some modification is necessary to the existing code to implement elastic-plastic asperity deformation model.

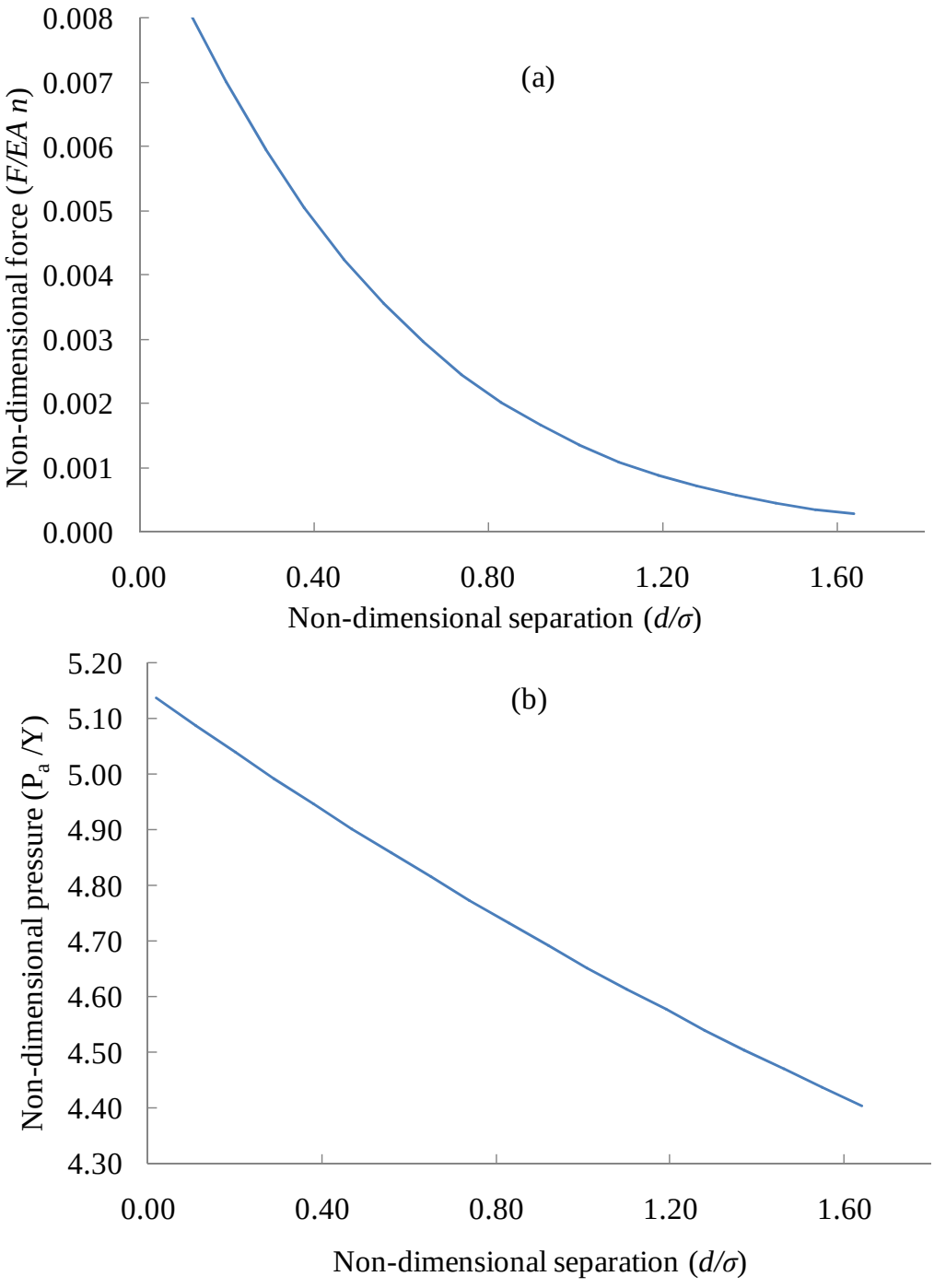

Figure 4.14: Effect of separation: (a) force and (b) normal pressure

In this study, the interfacial rough surface layer was introduced which is based on the default ABAQUS contact springs and separation values. An innovation in this direction is necessary to include the plasticity effects and the calculation of separation values with due consideration of plasticity in the model. This could be a further improvement of this developed model.

4.2.2 Effect of lubricant on frictional force

There are two parts of the frictional force (See Eqs. (3.21) to (3.22)) namely solid-solid asperity shearing and solid-liquid interaction shearing. With the increase of hydrodynamic pressure, solid-solid contact shearing will reduce as the real area of contact is reducing as shown in Fig. 4.12. The liquid shearing part will increase a little bit due to an increase of hydrodynamic pressure. But it is very small and has negligible influence on the total frictional force. The reduction of frictional force is mainly due to the reduction of the real area of solid-solid contact. This is a very important result from the mechanics of mixed lubrication point of view and also the reason why applying high-viscosity lubricant can improve the quality of the rolled surface. The distribution of friction force for different lubricants (0.3 ~ 1.2 Pa.s) is shown in Fig. 4.15. It is found that the frictional force has reduced due to the use of higher viscosity values in the simulation leading to higher hydrodynamic pressure. The neutral point is shifting to the right indicating that the positive frictional force to covers the larger arc of contact with the increase of hydrodynamic pressure, which is related to the stability issues of rolling as explained in Section 4.1.2.

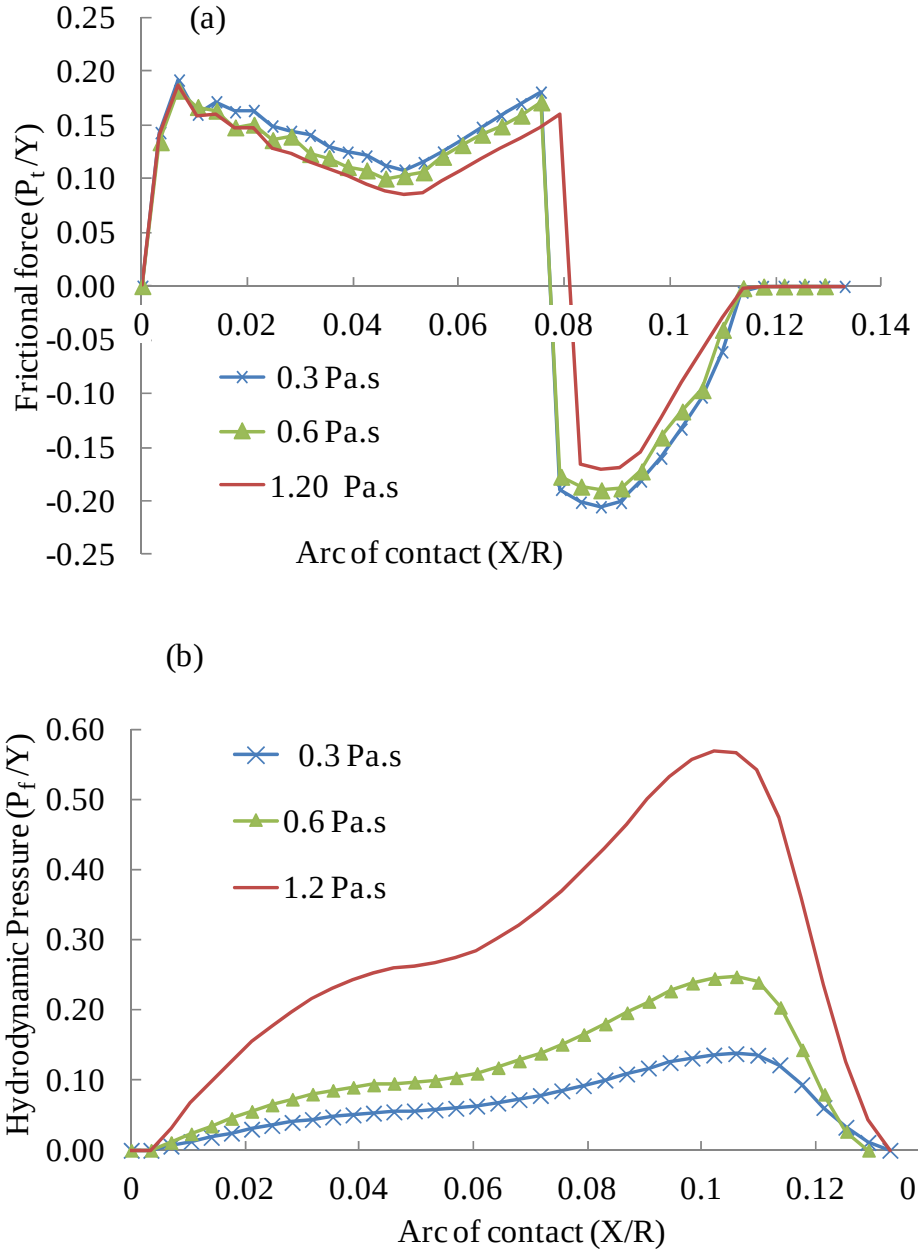

Figure 4.15: (a) The frictional force and (b) hydrodynamic pressure for different viscosity

4.2.3 Effect of lubricant on resultant friction coefficient

The resultant friction coefficient as defined in the Eqs. (3.21) to (3.23) in Chapter 3, is shown in Fig. 4.16a.

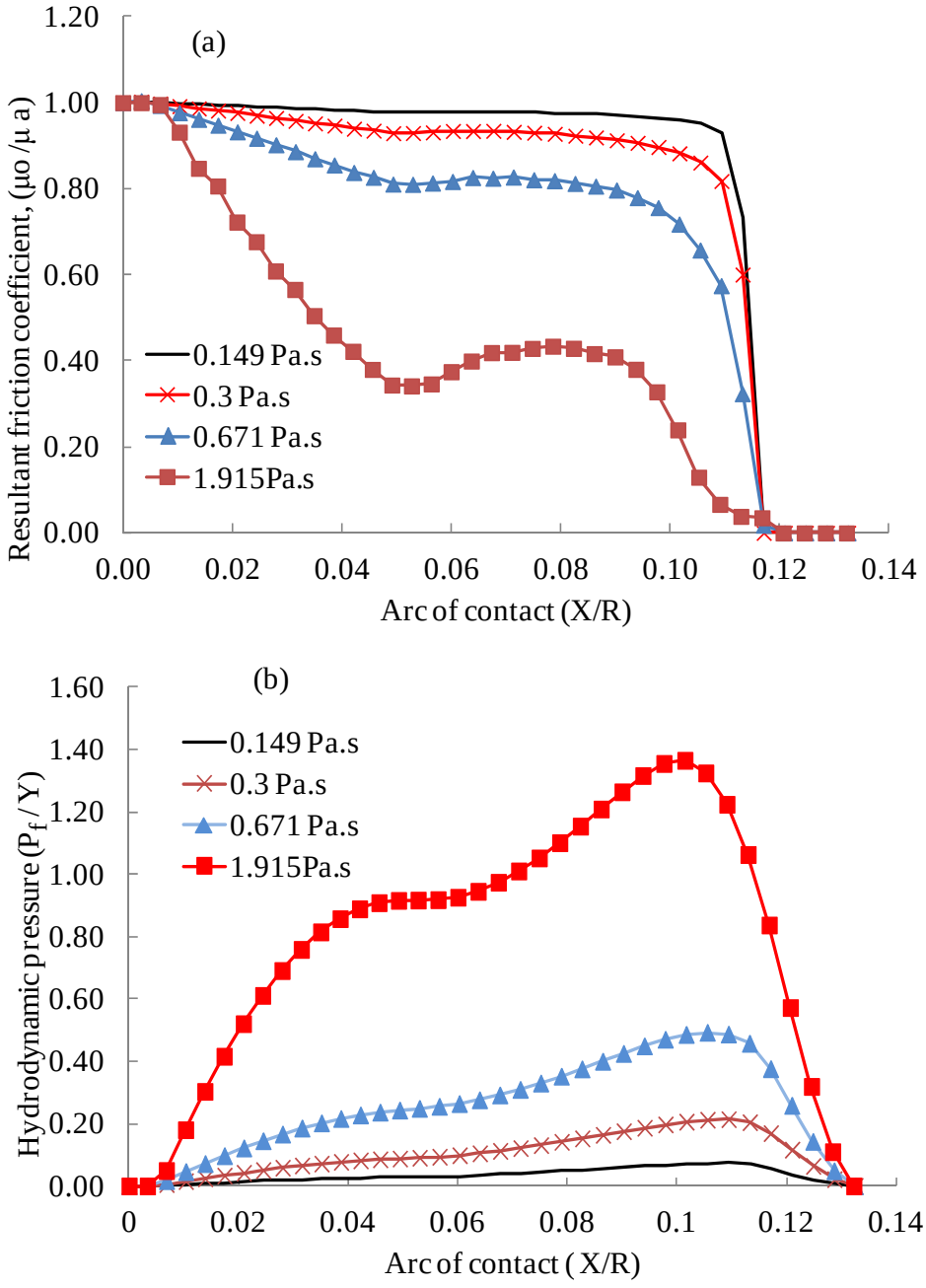

Figure 4.16: The effects of lubricants on (a) the resultant friction coefficient and (b) the hydrodynamic pressure

Applying lubricants of higher viscosity gives rise to a clear reduction of the resultant friction coefficient throughout the arc of contact. As we know, the lubricant pressure is varied according to governing Eq. (3.18), the friction reduction is more visible when the lubricant pressure is 1.915 Pa.s. The viscosity 1.915 Pa.s was 3 times higher than the viscosity 0.671 Pa.s, which leads to 3 times higher hydrodynamic pressure resulting more radical friction reduction in Fig. 4.16a. This demonstrates that a lubricant of higher viscosity is more desirable to reduce frictional force in metal rolling. Moreover, it can be seen that the reduction of friction is much more significant at the exit region. This is because the hydrodynamic pressure increases gradually along the contact arc, see Fig. 4.16b and Eq. (3.18), drops quickly at the exit region, and peaks at a point close to the exit. It is also noted that the surface finish or rolled strip quality largely depends on the frictional behaviour of the material surface at the exit.

4.2.4 Effect of rolling speed on hydrodynamic pressure

The rolling speed is also an important parameter in metal rolling. The hydrodynamic pressure increases with the increase of rolling speed. From Eq. (3.18), it is clear that hydrodynamic pressure depends on the rolling velocity, viscosity and flow factor. Varying the rolling velocities in the range of 1 ~ 9 m/s, the corresponding hydrodynamic pressure is shown in Fig. 4.17**.** It is found that the hydrodynamic pressure increases with the increase of rolling velocity. A higher rolling speed leads to higher hydrodynamic pressure. Its effect is similar to the effect of lubricant. A higher rolling speed can also increase the volume of production in the rolling process. However, the excessively higher rolling speeds than optimum can deteriorate the performance of the product quality by increasing wear in the strip surface due to the

dynamic effect. Optimization of the rolling speed is also very important for economic and quality production.

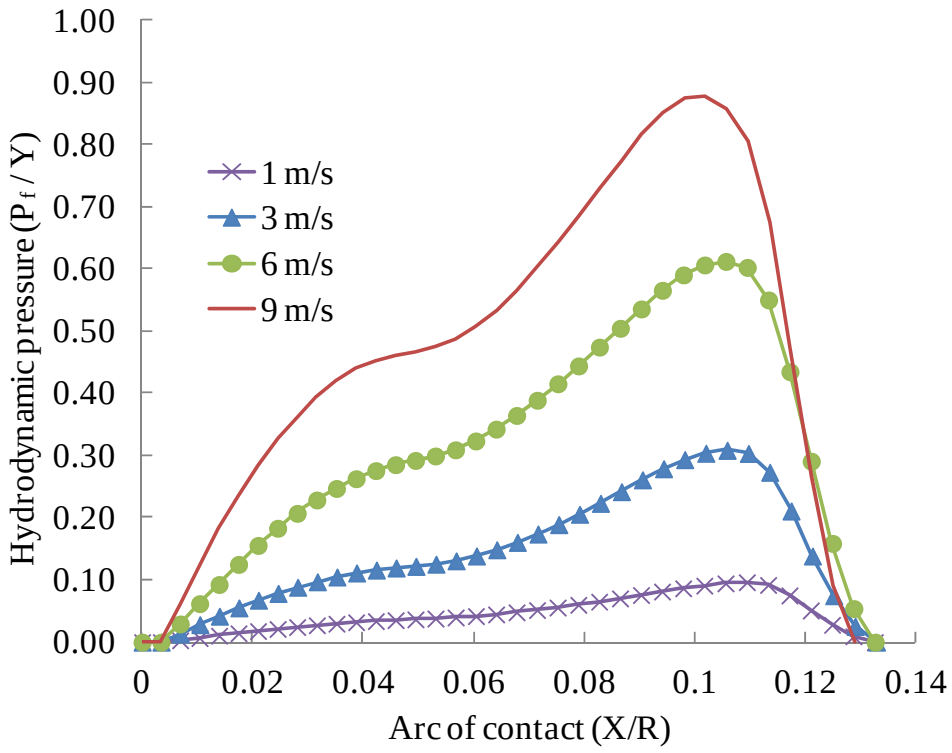

Figure 4.17: Hydrodynamic pressure for different rolling velocity

4.3 Discussion and conclusions

In this study, some quantitative results are found about mixed lubrication and the effect of different rolling parameters in rolling mechanics. The results are presented for different parameters of mixed lubrication and possible improvements of this model are also discussed in some relevant sections. Although the interface normal pressure doesn't increase much with the increase of hydrodynamic pressure, the frictional force changes significantly. The experimental evidence also shows a similar trend (Al-Salehi *et al.* 1973), where the experiment was conducted using different lubricants and also without

lubricants to investigate the effect of lubricants on normal pressure distribution. Al-Salehi *et al*. reported that there is no detectable effect of hydrodynamic pressure on normal pressure. Moreover, there is no evidence either in academic study or industry information that the normal pressure would increase significantly due to the hydrodynamic effect in strip rolling.

The shearing feature is very important and crucial for the quality of products, which can be optimized by lubricant and rolling speed in the rolling process. The quality of rolled products largely depends on the frictional behaviour of the interface. An increase of hydrodynamic pressure means the extent of direct asperity-asperity contact is less, as shown in Fig. 4.12. This is one of the important aspects of mixed lubrication that direct metal to metal contact can be avoided to some degree by using lubricants in the rolling process. It is also found that there is significant reduction of the resultant friction coefficient due to an increase of hydrodynamic pressure in the interface, as shown in Fig. 4.16a. This may be achieved either by applying a higher rolling velocity or higher viscosity in the rolling process as shown in Fig. 4.16b and Fig. 4.17. In these parametric studies, the effects of viscosity and rolling velocity are exhibited. In the industry, oil in water emulsion is used for better cooling capacity, non-flammability, low cost and environmentally friendly (Kosasih and Tieu 2007). The emulsion generally contains 1-5 % volume of natural, mineral or synthetic oil (Kosasih and Tieu 2007) and has viscosity in the range of 0.02 to 2 Pa.s (Le and Sutcliffe 2006), which allows for a fine adjustment to the frictional force. It is crucial to choose the appropriate lubricants and rolling velocity so that the desired rolling force can be developed for a stable rolling process to take place.

For the rolling industry, a combination of optimized parameters should be applied in the production process. Appropriate lubricant, roll velocity, roll dimension and thickness reduction ratio can contribute to achieve better quality and less energy consumption. Experimental investigation is also necessary using a combination of different parameters before commercial production of rolled products. If material properties and the asperity distribution of the rough surfaces can be quantified, this model can be directly used for choosing the optimized parameters in the rolling process.

CHAPTER 5

CONCLUSIONS

A new numerical approach is developed to investigate mixed lubrication in strip rolling. The new technique involves the introduction of an artificial interface layer to account for the effect of asperity contact and hydrodynamic lubrication. The load shearing principle in the interface of rolling contact is then applied by FE simulation. The integration of micro to macroscopic deformation is realized by a user subroutine integrated in FE analysis. The rough surface asperity deformation follows the Greenwood and Williamson model (Greenwood and Williamson 1966). The GW model solution is verified by the Hertz contact problem, which shows a good agreement with the analytical solution. The modified Reynolds equation is solved by the finite difference method. The solution of the Reynolds equation is also verified by an analytical calculation, which shows the correctness of the Reynolds code. The asperity deformation model and the lubricant fluid flow model are successfully coupled by our developed user subroutine. The interface real area of asperity contact, normal pressure, frictional force and hydrodynamic pressure are nicely captured by this numerical technique.

This study focuses on the effects of different rolling parameters, especially the different lubricants and rolling velocity that can influence the frictional force of the strip rolling. It is found that the hydrodynamic pressure can be increased significantly by applying either higher rolling velocity or higher viscosity, which leads to a significant reduction of the friction coefficient. However, an increase of hydrodynamic pressure does not affect the total normal pressure significantly to bring about thickness reduction. The separation between the surfaces increases due to the increase in hydrodynamic pressure, which indicates that direct metal to metal contact can be avoided to some extent by applying higher hydrodynamic pressure in the strip rolling operation.

Optimization of the rolling parameters is very important to produce high-quality roll products. It is difficult to optimize the rolling parameters by the existing approaches of mixed lubrication. Some of the unresolved issues in mixed lubrication have complicated the investigation using either theoretical or experimental approaches. The experimental studies indicated that the friction coefficient is very low in mixed lubrication, for example by Le and Sutcliffe (Le and Sutcliffe 2006). However, no reliable experiment is yet available to identify the effect of hydrodynamic pressure in details with regard to strip rolling. The earlier theoretical studies were mostly based on dry contact rolling cases. Some authors (Chang *et al.* 1996; Kosasih and Tieu 2007) attempted to apply lubricant and asperity contact features in their models but their studies were based on too many assumptions as explained in the literature review. Moreover, the frictional features of mixed lubrication were not available in those studies (Chang *et al.* 1996; Kosasih and Tieu 2007). It is believed that the friction coefficient can be measured (Le and Sutcliffe 2006) only. This study has some insightful outcomes regarding frictional force and reduction of the frication coefficient due to the hydrodynamic effect in mixed lubrication. This study can be used to optimize the appropriate lubricant and rolling velocity for the desired frictional force.

The hydrodynamic pressure can help reduce the real area of contact to some extent as the total load is shared between the asperities and the fluid. But the elastic deformation assumption of asperities also contributes to a decrease in the real area of contact near the exit zone due to elastic unloading. However, the elasto-plastic asperity deformation model of Robert and Green (Robert and Green 2005) confirms that the overall real area of contact may increase significantly with the plasticity consideration. To implement an elastic-plastic asperity deformation model in this numerical technique, further treatment

of the interfacial layer is necessary. At present, the deformations of contact springs are modelled by the GW model, which results in an elastic unloading problem near the exit zone. This unloading problem must be solved by introducing plasticity and real area of contact in the present model. This will be our next work to improve this model by applying an elasto-plastic asperity deformation model.

In this study, an innovative numerical approach has been developed, which is capable of updating any stress definition in the interface of surface to surface contact. This approach can be applied in micro to macro integration of structural contact mechanics i.e. multi-scale modelling in FE simulation. This model can be further applied to study surface wearing phenomenon by correlating the calculated frictional force and the surface quality. Moreover, the study has clearly indentified the effects of rolling parameters that need to be optimized for high-quality roll products. To the best of our knowledge, this unique approach has never been applied by any study in mixed lubrication. The metal rolling industries can benefit from the outcome of this study to optimize their rolling process.

BIBLIOGRAPHY

[1] Abo-Elkhier, M., (1997), "Elasto-plastic finite element modelling of strip cold rolling using Eulerian fixed mesh technique", *Finite Elements in Analysis and Design*, vol. 27(4), pp. 323-334.

[2] Al-Salehi, F. A. R., Firbank, T. C. and Lancaster, P. R., (1973), "An experimental determination of the roll pressure distribution in cold rolling", *International Journal of Mechanical Sciences*, vol. 15, pp. 693-710.

[3] Alexander, J. M., (1972), "On the theory of rolling", *Proceedings of the Royal Society of London*, vol. A 326, pp. 535-563.

[4] Alexander, J. M., (1955), "A slip line field for the hot rolling process", *Proceedings of the Institution of Mechanical Engineers*, vol. 169, pp. 1021-1028.

[5] Avitzur, B., (1980), "Friction-aided strip rolling with unlimited reduction", *International Journal of Machine Tool Design and Research*, vol. 20(3–4), pp. 197-210.

[6] Bertrand, C., David, C., Chenot, J. L. and Buessler, P., (1986), "Numerical methods in industrial forming processes", Rotterdam, *Balkema Press***:** 207-212.

[7] Bland, D. R. and Ford, H., (1943), "The calculation of roll force and torque in cold rolling with tension", *Proceedings of the Institution of Mechanical Engineers*, vol. 159, pp. 144-163.

[8] Chang, D.-F., Marsault, N. and Wilson, W. R. D., (1996), "Lubircation of strip rolling in the low speed mixed regime", *Tribology Transactions*, vol. 39, pp. 407-415.

[9] Chang, D., Etsion, I. and Bogy, D., (1987), "An elastic-plastic model for the contact of rough surfaces", *Journal of Tribology, ASME*, vol. 109, pp. 257-263.

[10] Chen, C. C. and Kobayashi, S., (1978), "Applications of numerical methods to forming processes", Winter meeting of ASME, San Francisco, CA.

[11] Chow, L. S. H. and Cheng, H. S., (1976), "The effects of surface rough average film thickness between lubricated rollers", *Journal of Lubrication Technology, ASME*, vol. 98, pp. 117.

[12] Christensen, H., (1970), "Stochastic models for hydrodynamic lubrication of rough surfaces", *Proceedings of Institution of Mechancial Engineers*, vol. 184, pp. 1013-1026.

[13] Christensen, H. and Tonder, K., (1971), "The hydrodynamic lubrication in rough bearing surfaces of finite width", *Journal of Lubrication Technology, ASME*, vol. 93.

[14] Cole, I. M. and Sansome, D. H., (1968), " Proceedings of the Ninth International Machine Tool Design Research Conference.

[15] Crane, F. A. A. and Alexander, J. M., (1968), "A study of friction in cold strip rolling", *Journal Institute of Metals*, vol. 96, pp. 289-300.

[16] Dawson, P. R., (1978), "Application of numerical method of forming processes", Winter Meeting of ASME, San Francisco, CA.

[17] Dewhurst, P., Collins, I. F. and Johnson, W., (1973), "A class of slip line field solution for the hot rolling of strip", *Journal of Mechanical Engineering Sciences*, vol. 15, pp. 439-447.

[18] Dixon, A. and Yuen, W. Y. D., (1995), "A computationally fast method to model thin strip rolling"**:** 239-246.

[19] Domanti, S., Edwards, W. and Thomas, P., (1994), "Application of foil rolling models to thin steel strip and temper rolling", Dussedorf**:** 422-431.

[20] Fleck, N. A. and Johnson, K. L., (1987), "Towards a new theory of cold rolling thin foil", *International Journal of Mechanical Sciences*, vol. 29(7), pp. 507-524.

[21] Fleck, N. A., Johnson, K. L., Mear, M. and Zhang, L. C., (1992), "Cold rolling of foil", *Proceedings of Institution of Mechancial Engineers*, vol. 201, pp. 119-131.

[22] Geike, T. and Popov, V. L., (2008), "Reduced description of mixed lubrication", *Tribology International*, vol. 41(6), pp. 542-548.

[23] Gratacos, P., Montmitonnet, P., Fromholz, C. and Chenot, J. L., (1992), "A plane-strain elastoplastic finite-element model for cold rolling of thin strip", *International Journal of Mechanical Sciences*, vol. 34(3), pp. 195-210.

[24] Greenwood, J. A. and Williamson, J. B. P., (1966), "Contact of nominally flat surfaces", *Proceedings of the Royal Society of London*, vol. 295, pp. 300-319.

[25] Grober, H., (1986), "Numerical methods in industrial forming processes", Rotterdam, *Balkema press***:** 225-229.

[26] Hartley, P., Sturgess, C. E. N. and Rowe, G. W., (1979), "Friction in finite-element analyses of metalforming processes", *International Journal of Mechanical Sciences*, vol. 21(5), pp. 301-311.

[27] Hartley, P., Sturgess, C. E. N. and Rowe, G. W., (1979), "Friction in finite element analyses of metal forming processes", *International Journal of Mechanical Sciences*, vol. 21, pp. 300-311.

[28] Hirakawa, T., Fujita, F. and Yamada, Y., (1984), "Advanced technology of plasticity", Tokyo**:** 1132-1137.

[29] Hollenberg, A., (1883), "Flow of metal and neutral point in rolling ", *Stahl und Eisen*, vol. 3.

[30] Hu, Y.-z., Wang, H., Wang, W.-z. and Zhu, D., (2001), "A computer model of mixed lubrication in point contacts", *Tribology International*, vol. 34(1), pp. 65-73.

[31] Hu, Y.-z. and Zhu, D., (2000), "A full numerical solution to the mixed lubrication in point contacts", *Journal of Tribology*, vol. 122, pp. 1-9.

[32] Hwu, Y. J. and Lenard, J. G., (1988), "A Finite element study of flat rolling", *Journal of Engineering Materials and Technology*, vol. 110, pp. 22-27.

[33] Jackshon, R. and Green, I., (2005), "A finite element study of elasto-plastic hemispherical contact", *ASME Journal of Tribology International*, vol. 127, pp. 343-354.

[34] Jiang, Z. Y. and Tieu, A. K., (2002), "Elastic–plastic finite element method simulation of thin strip with tension in cold rolling", *Journal of Materials Processing Technology*, vol. 130–131(0), pp. 511-515.

[35] Jiang, Z. Y., Tieu, A. K. and Zhang, X. M., (2004), "Finite element modelling of mixed film lubrication in cold strip rolling", *Journal of Materials Processing Technology*, vol. 151(1–3), pp. 242-247.

[36] Jortner, D., Osterle, J. F. and Zorowski, C. F., (1960), "An analysis of cold strip rolling", *International Journal of Mechanical Sciences*, vol. 2(3), pp. 179-194.

[37] Khayyat, F. A. and Lancaster, P. R., (1969), "Strain Analysis", *Journal of Strain Analysis*, vol. 4(4).

[38] Kimura, Y. and Childs, T. H. C., (1999), "Surface asperity deformation under bulk plastic straining conditions", *International Journal of Mechanical Sciences*, vol. 41(3), pp. 283-307.

[39] Kogut, L. and Etsion, I., (2003), "Adhesion in elastic–plastic spherical microcontact", *Journal of Colloid and Interface Science*, vol. 261(2), pp. 372-378.

[40] Kosasih, P. B. and Tieu, A. K., (2007), "Mixed film lubrication of strip rolling using O/W emulsions", *Tribology International*, vol. 40, pp. 709-716.

[41] Kumar, D. and Dixit, U. S., (2006), "A slab method study of strain hardening and friction effects in cold foil rolling process", *Journal of Materials Processing Technology*, vol. 171(3), pp. 331-340.

[42] Lai-Send, L. and Lenard, J. G., (1984), "Study of friction in cold strip rolling", *Journal of Engineering Material Technology*, vol. 106, pp. 139-146.

[43] Le, H. R. and Sutcliffe, M. P. F., (2003), "A friction model for cold strip rolling with two wavelength surface roughness in the mixed lubrication regime", *Transactions of ASME*, vol. 125(676).

[44] Le, H. R. and Sutcliffe, M. P. F., (2006), "A multi-scale model for friction in cold rolling of aluminium alloy", *Tribology Letters*, vol. 25(1), pp. 95-104.

[45] Le, H. R. and Sutcliffe, M. P. F., (2001), "A robust model for rolling of thin strip and foil", *International Journal of Mechanical Sciences*, vol. 43(6), pp. 1405-1419.

[46] Li, G. J. and Kobayashi, S., (1982), "Rigid-Plastic finite element analysis of plane strain rolling", *Journal of Engineering for industry*, vol. 104, pp. 55-64.

[47] Liu, C., Hartley, P. and Sturgess, C. E. N., (1985), "Simulation of cold strip rolling using elastic plastic finite element method", *International Journal of Mechanical Sciences*, vol. 27(11-12), pp. 829-839.

[48] Liu, C., Hartley, P., Sturgess, C. E. N. and Rowe, G. W., (1985), "Elastic-Plastic finite element modelling of cold rolling of strip", *International Journal of Mechanical Sciences*, vol. 27(7-8), pp. 531-541.

[49] Lu, C., Kiet Tieu, A. and Jiang, Z., (2003), "Modeling of the inlet zone in the mixed lubrication situation of cold strip rolling", *Journal of Materials Processing Technology*, vol. 140(1–3), pp. 569-575.

[50] Mancini, E., Campana, F., Sasso, M. and Newaz, G., (2012), "Effects of cold rolling process variables on final surface quality of strainless steel thin strip", *The international Journal of Advanced Manufacturing Technology*, vol. 61, pp. 63-72.

[51] McGregor, C. C. and Palme, R. B., (1959), "The distribution of contact pressures in rolling of metals", *Transation of ASME, Journal of Basic Engineering*, (669).

[52] Miguel, A., Marcela, B. G. and Eduardo, N. D., (2001), "Finite element simulation of the steel plates hot rolling", *International Journal for Numerical Methods in Engineering*, vol. 52, pp. 1411-1430.

[53] Mori, K., Osakada, K. and Oda, T., (1982), "Simulation of plane-strain rolling by the rigid-plastic finite element method", *International Journal of Mechanical Sciences*, vol. 24(9), pp. 519-527.

[54] Nadai, A. (1931), "Plasticity", New York, London, McGraw-Hill.

[55] Ongun, Y., André, M., Bartel, D. and Deters, L., (2008), "An axisymmetric hydrodynamic interface element for finite-element computations of mixed lubrication in rubber seals", *Journal of Engineering Tribology*, vol. 222, pp. 471-481.

[56] Orowan, E., (1943), "The calculation of roll pressure in hot and cold flat rolling", *Proceedings of the Institution of Mechanical Engineers*, vol. 150, pp. 140-167.

[57] Orowan, E., Scott, F. H. and smith, C. C., (1950), "A photoelastic dynamometer for rapidly varying forces", *Journal of Scientific Instrument*.

[58] Patir, N. and Cheng, H. S., (1979), "Application of average flow model to lubrication between rough sliding surfaces", *Journal of Lubrication Technology, ASME*, vol. 101, pp. 220-230.

[59] Patir, N. and Cheng, H. S., (1978), "An average flow model for determining effects of three dimensional roughness on partial hydrodynamic lubrication", *Journal of Lubrication Technology, ASME*, vol. 100, pp. 12-17.

[60] Peklenik, J., (1967), "New Developments in surface Characteristic Measurement By Means of Random Process Analysis.", *Proc. Inst. Mech. Eng.*, vol. 182, pp. 108.

[61] Pillinger, I., C.E.N., S. and Rowe, G. W., (1979), "Friction in finite element analyses of metal forming processes", *Internation Journal of Mechanical Sciences*, vol. 21, pp. 301-311.

[62] Ramamohana Rao, A. and Mohanram, P. V., (1994), "A study of wear characteristics of journal bearings operating under mixed-lubrication conditions", *Wear*, vol. 172(1), pp. 11-22.

[63] Rao, A. R. and Mohanram, P. V., (1993), "A study of mixed lubrication parameters of journal bearings", *Wear*, vol. 160(1), pp. 111-118.

[64] Rao, S. S. and Kumar, A., (1977), "Finite element analysis of cold strip rolling", *International Journal of Mechanical Sciences*, vol. 19, pp. 159-168.

[65] Rhow, S. K. and Elrod, H. G., (1974), "The effects on bearing load capacity of two-sided striated roughness", *Journal of Lubrication Technology, ASME*, vol. 96.

[66] Robert, L. J. and Green, I., (2005), "A statistical model of elasto-plastic asperity contact between rough surfaces", *Tribology International*, vol. 39, pp. 906-914.

[67] Roberts, W. L. (1978). "Cold rolling of steel". New York, Marcel Dekker Inc.

[68] Roelands, E. J. A., (1996), "Correlation aspects of the viscosity-temperature-pressure relationship of lubricating Oils, PhD thesis", Technische Hogeschool Delft, The Netherlands.

[69] Salimi, M. and Kadkhodaei, M., (2004), "Slab analysis of asymmetrical sheet rolling", *Journal of Materials Processing Technology*, vol. 150(3), pp. 215-222.

[70] Salimi, M. and Sassani, F., (2002), "Modified slab analysis of asymmetrical plate rolling", *International Journal of Mechanical Sciences*, vol. 44(9), pp. 1999-2023.

[71] Saniei, M. and Salimi, M., (2006), "Development of a mixed film lubrication model in cold rolling", *Journal of Materials Processing Technology*, vol. 177(1–3), pp. 575-581.

[72] Schmidt, T., André, M. and Poll, G., (2010), "A transient 2D-finite-element approach for the simulation of mixed lubrication effects of reciprocating hydraulic rod seals", *Tribology International*, vol. 43(10), pp. 1775-1785.

[73] Seibel, E. and Lueg, W., (1933), "Untersuchungen uber die spannungsverteilung in walspalt", *Mitteilungen Aus dem Kaiser-Wilhem- Institut fur Eisenforschung*, vol. 15, pp. 1-14.

[74] Serajzadeh, S., Karimi Taheri, A. and Mucciardi, F., (2002), "Unsteady state work-roll temperature distribution during continuous hot slab rolling", *International Journal of Mechanical Sciences*, vol. 44(12), pp. 2447-2462.

[75] Sheu, S. and Wilson, W. R. D., (1994), "Mixed film lubrication of stirp rolling", *Tribology Transactions*, vol. 37, pp. 483-493.

[76] Shima, S., Mori, K., Oda, T. and Osakada, K., (1980), "Rigid-Plastic finite element analysis of strip rolling", Proceedings of the 4rth International Conference on Production Engineering, Tokyo.

[77] Smith, C. L., Scott, F. H. and Sylwestrowicz, w., (1952), "Pressure distribution between stock and rolls in hot and cold flat rolling", vol. 170, pp. 347-359.

[78] Stephany, A., Ponthot, J. P., Collette, C. and Schelings, J., (2004), "Efficient approach for mixed lubrication in cold strip rolling", *Journal of Material Processing Technology*, (153-154), pp. 307-313.

[79] Stiharu, I., Demian, T. and Bhat, R. B., (1994), "Mixed lubrication model for microbearings containing microasperities of defined geometry", *Wear*, vol. 172(1), pp. 1-10.

[80] Sutcliffe, M. P. F., (1988), "Surface asperity deformation in metal forming processes", *International Journal of Mechanical Sciences*, vol. 30, pp. 847-868.

[81] Sutcliffe, M. P. F. and Johnson, K. L., (1991), "Lubrication in cold strip rolling in the mixed regime", *Proceedings of the Institution of Mechanical Engineers*, vol. 204, pp. 249-261.

[82] Sutcliffe, M. P. F. and Rayner, P. J., (1998), "Experimental measurements of load and strip profile in thin strip rolling", *International Journal of Mechanical Sciences*, vol. 40(9), pp. 887-899.

[83] Theocaris, P. S., Stassinnkakis, C. A. and Mamalis, A. G., (1983), "Stress analysis of axially stiffened shells", *International Journal of Mechanical Sciences*, vol. 25, pp. 833-844.

[84] Thompson, E. G., (1982), "Inclusion of elastic strain rate in the analysis of viscoplastic flow during rolling", *Internation Journal of Mechanical Sciences*, vol. 24, pp. 655-659.

[85] Tian, Y., Guo, Y.-h., Wang, Z.-d. and Wang, G.-d., (2009), "Analysis of Rolling Pressure in Asymmetrical Rolling Process by Slab Method", *Journal of Iron and Steel Research, International*, vol. 16(4), pp. 22-38.

[86] Tieu, A. K., Liu, Y. J., Kosasih, P. B. and Jiang, Z. Y. (2002). "Effects of elastic deformation and temperature on a mixed film lubrication model". Tribology Series. M. P. G. D. D. Dowson and A. A. Lubrecht, Elsevier. Volume 40**:** 115-120.

[87] Tonder, K., (1977), "Mathematical verification of the applicability of modified Reynolds equation to striated rough surfaces", *Wear*, vol. 44, pp. 329-343.

[88] Tzeng, S. T. and Saibel, E., (1967), "Surface roughness effectrs on slider lubrication", *ASME Transaction*, vol. 10.

[89] Van Rooyen, G. T. and Backofen, W. A., (1957), "Friction in cold rolling", *Journal of Iron Steel Institute*, vol. 186, pp. 235-244.

[90] Von Karman, T., (1925), "Contribution to the Theory of Rolling", *Zeitschrift für Angewandte Mathematik und Mechanik* vol. 5, pp. 139-141.

[91] Wang, W.-z., Hu, Y.-z., Liu, Y.-c. and Wang, H., (2007), "Deterministic solutions and thermal analysis for mixed lubrication in point contacts", *Tribology International*, vol. 40(4), pp. 687-693.

[92] Wang, W. J., Zhu, D., Cheng, H. S., Yu, T., Jiang, X. and Liu, S., (2004), "Mixed lubrication analyses by a macro-micro approach and a full scale mixed EHL model", *Journal of Tribology*, vol. 126, pp. 81-91.

[93] Wanheim, T. and Bay, N., (1978), "A model of friction in metal forming processes", *General assembly of CIRP*, vol. 27, pp. 189-194.

[94] Wilson, W. R. D. and Kalpakjian, S., (1995), "Low-Speed Mixed Lubrication of Metal-Forming Processes", *CIRP Annals - Manufacturing Technology*, vol. 44(1), pp. 205-208.

[95] Wilson, W. R. D. and Sheu, S., (1988), "Real area of contact and boundary friction in metal forming", *International Journal of Mechanical Sciences*, vol. 30(7), pp. 475-489.

[96] Yamanda, Y., Ito, K., kokouchi, Y., Tammano, T. and Ohtsubo, T., (1974), "International Symposium ", Finite Element Method in Flow Problems, swansea.

[97] Yarita, I., Mallett, R. L. and Lee, E. H., (1984), "Advanced technology of plasticity", Tokyo**:** 1126-1131.

[98] Yuen, W. Y. D., Dixon, A. and Nguyen, D. N., (1996), "The modelling of the mechanics of deformation in flat rolling", *Journal of Materials Processing Technology*, vol. 60(1–4), pp. 87-94.

[99] Zhang, L. C., (1995), "On the mechanism of cold rolling thin foil", *International Journal of Machine Tools and Manufacture*, vol. 35(3), pp. 363-372.

[100] Zhang, S. H., Zhang, G. L., Liu, J. S., Li, C. S. and Mei, R. B., (2010), "A fast rigid-plastic finite element method for online application in strip rolling", *Finite Elements in Analysis and Design*, vol. 46(12), pp. 1146-1154.

[101] Zhao, Y., Maletta, D. and Chang, L., (2000), "An asperity microcontact model incorporating the transition from elastic deformation to fully plastic flow", *ASME Journal of Tribology International*, vol. 122, pp. 86-93.

[102] Zhu, D. and Cheng, H. S., (1988), "Effect of surface roughness on the point contact EHL", *ASME Journal of Tribology International*, vol. 110, pp. 32-37.

[103] Zienkiewicz, O. C., Jain, P. C. and Onate, E., (1978), "Flow of solids during forming and extrusion: Some aspects of numerical solutions", *International Journal of Solids and Structures*, vol. 14(1), pp. 15-38.

APPENDIX

Appendix-1

FORTRAN subroutine

A FORTRAN subroutine has been developed to implement the new mixed lubrication method discussed in Section 3.2. This subroutine solves the GW model and modified Reynolds equation explicitly with the FE input model (as discussed in the Section 3.2). This subroutine follows ABAQUS Vuinter subroutine protocol. The modified Reynolds equation is solved by Finite difference method and GW integration is solved Simpson integration rule. The main subroutine vuinter links up with the ABAQUS input model. The main subroutine also works with other two subroutines, one – Calculation of Reynolds equation by finite difference method and two – Solves the GW calculation by Simpson integration rule. The full routine is given below;

C******** FORTRAN Subroutine Code **********

```
      subroutine vuinter( sfd, scd, spd, svd,
     *     stress, fluxSlv, fluxMst, sed, statev,
     *     kStep, kInc, nFacNod, nSlvNod, nMstNod, nSurfDir,
     *     nDir, nUSdv, nProps, NumTemp, NumExfv, numDefTfv,
     *     jSlvUid, jMstUid, jConMstid, timStep, timGlb,
     *     dTimCur, surfInt, surfSlv, surfMst,
     *     rdisp, drdisp, drot, stiffDflt, condDflt,
     *     shape, coordSlv, coordMst, alocaldir, props,
     *     areaSlv, tempSlv, dtempSlv, exfvSlv, dexfvSlv,
     *     tempMst, dtempMst, exfvMst, dexfvMst )

      include 'vaba_param.inc'

      character*80 surfInt, surfSlv, surfMst

      double precision a(1000), b(1000),c(1000),d(1000)

      double precision  p(1000),u(1000),a1(1000),d2(1000),pc(1000),
     * h(1000),f,Edesh,k1,a2,integral1,integral2,dx,pn,pt,phi,
```

```
     * k(200), da(200),de11(200),de12(200),slv_velocity,mst_velocity,
     * gapInit,sigma,rq, ssa, ssb,xmu, muo
      integer n,i,n1
      integer kn(200)
      dimension props(nProps), statev(nUSdv,nSlvNod),
     *    drot(2,2,nSlvNod), sed(nSlvNod), sfd(nSlvNod),
     *    scd(nSlvNod), spd(nSlvNod), svd(nSlvNod),
     *    rdisp(nDir,nSlvNod), drdisp(nDir,nSlvNod),
     *    stress(nDir,nSlvNod), fluxSlv(nSlvNod),
     *    fluxMst(nSlvNod), areaSlv(nSlvNod),
     *    stiffDflt(nSlvNod), condDflt(nSlvNod),
     *    alocaldir(nDir,nDir,nSlvNod), shape(nFacNod,nSlvNod),
     *    coordSlv(nDir,nSlvNod), coordMst(nDir,nMstNod),
     *    jSlvUid(nSlvNod), jMstUid(nMstNod),
     *    jConMstid(nFacNod,nSlvNod), tempSlv(nSlvNod),
     *    dtempSlv(nSlvNod), exfvSlv(NumExfv,nSlvNod),
     *    dexfvSlv(NumExfv,nSlvNod), tempMst(nSlvNod),
     *    dtempMst(nSlvNod), exfvMst(NumExfv,nSlvNod),
     *    dexfvMst(NumExfv,nSlvNod)
C Indices to user-defined properties (nprops=6):
      parameter ( i_prp_GW_sigma = 1,
     *          i_prp_YoungsModulus = 2,
     *          i_prp_PoissonsRatio = 3,
     *          i_prp_InitYield = 4,
     *          i_prp_HardenMod = 5,
     *          i_prp_ThickInter = 6)
Ci_prp_ initial film thickness is larger than the maximum asperity height
C      i_prp_IfcCond = 7)
C     Descriptions:
C      i_prp_GapCutOff: cut-off init. gap dist. above which slave nodes
C      are not bonded.
C      (The rest are material properties of the interface.)
C      i_prp_YoungsModulus: E
C      i_prp_PoissonsRatio: Poisson's Ratio
```

```
C     i_prp_InitYield: initial yield stress
C     i_prp_HardenMod: hardening modulus
C     i_prp_ThickInter: interface thickness
C     i_prp_IfcCond: interface conductivity
C    Indices to user-defined state variables per slave node (nUSdv=3):
      parameter ( i_usv_CompletedInit = 1,
     *     i_usv_BondStatus = 2,
     *     i_usv_CurYield = 3 ,
     *     !  previous_coordinate=4,
     *       t_previous=5,
     *       previous_vel1=6,
     *       h_value =7,
     *       pc_value=8,
     *       a1_value=9 )

C      Descriptions:
C      i_usv_CompletedInit: whether initializations have occured
C      i_usv_BondStatus: whether a slave node is bonded
C      i_usv_CurYield: current yield stress
C     Indices to the stress array:

      parameter ( i_str_S11 = 1, i_str_S12 = 2, i_str_S13 = 3 )

C      i_str_S11: normal stress
C      i_str_S12: shear traction in first tangent direction
C      i_str_S13: shear traction in second tangent direction

 parameter ( zero = 0.0, one = 1.0, half=0.5)

 double precision :: zeta=0.1D-6,
     * neu=1.0D7,pi=3.1415926,beta=0.006,
     * meu=0.35,E=70D3,nx=90, L=80,miu=0.1,
     * outputdt=1.0D-3,b2=20.0, cc=0.1
C   miu is the frictional coefficient for dry cotnact (it should an input from Inp file)
C   L and nx or dx can also be input from inp file props()
 Integer LENJOBNAME,LENOUTDIR
 character*256 filename1,filename2,outdir,jobname,thid
CALL VGETOUTDIR( outdir, LENOUTDIR )
```

```
      CALL VGETJOBNAME( Jobname, LENJOBNAME )
       filename1=outdir(1:LENOUTDIR)//'/'//Jobname(1:LENJOBNAME)
     1  //'gw.dat'
       filename2=outdir(1:LENOUTDIR)//'/'//Jobname(1:LENJOBNAME)
     1  //'other.dat'
       sigma=props(i_prp_GW_sigma)
       rq=props(i_prp_GW_sigma)
C    note rq is the cut-off thickness. I used 6*sigma for dry contact herein.
C    for mixlubrication, rq is the initial thickness of the film (i_prp_ThickInter)
C     nx=number of mesh point in x direction
C     L= total length of the strip, for this routine only
C     zt = Lubricant viscosity, for this routine only
C    Rq = Roughness of the strip surface, for this routine only
C    us = strip velocity, for this routine
C    ur = roll velocity, for this routine only
       dx = 0.5 ! dx = nominal area of contact, for this routine only
       Edesh = E/(1-meu**2) ! Edesh= Equivalent modulus of elasticity, this routine only
c***************Compute shear modulus.**********************************
       open(unit=114, file=filename1,STATUS='unknown')
       open(unit=106, file=filename2,STATUS='unknown')
       n=0      ! n= number of contact points in the arc of contact for this routine only
       if( statev(i_usv_CompletedInit,1) .eq. zero ) then
C     ****************************************************************
C     Note that state variables are initialized to zero by default outside
C     of this subroutine. Reintitialize some of them the first time VUINTER
C     is called for a contact pair.
C     ****************************************************************
       do 11 kSlv = 1, nSlvNod
       statev(i_usv_CompletedInit,kSlv) = one
       statev(i_usv_CurYield,kSlv) = props(i_prp_InitYield)
       statev(previous_coordinate, kslv)=coordslv(1,kslv)
       statev(previous_vel1, kslv)=0.0
       statev(t_previous, kslv)=timGlb
       statev(h_value, kslv)=0.0
```

```
      statev(pc_value, kslv)=0.0
      statev(a1_value, kslv)=0.0
11     continue
      else
C*************************************************************************
C*************** Main Program to calculate Normal and shear Stress***********
C*************************************************************************

      do 22 kSlv = 1, nSlvNod
      stress(i_str_S11,kSlv) = zero
      stress(i_str_S12,kSlv) = zero
      slv_velocity=statev(previous_vel1, kslv)
      if (statev(t_previous, kslv).LT.timGlb) then
       slv_velocity=0
      endif
      if (dtimCur .GT. 0.0) then
      slv_velocity=slv_velocity+(coordslv(1,kslv)-
     * statev(previous_coordinate, kslv))/dtimCur

      mst_velocity=slv_velocity-drdisp(2,kslv)/dtimcur
      endif
C  ************************************************************************
  statev(previous_coordinate, kslv)=coordslv(1,kslv)
  statev(t_previous, kslv)=timGlb
  statev(previous_vel1, kslv)=slv_velocity
C*************************************************************************
 gapInit = -rDisp(1,kSlv)
 if( gapInit .LE. rq*15.0 ) then
 n=n+1
C  n index is different from kslv, hence the correspondence between n and kslv should
be ecorded
 kn(n)=kslv
C*************************************************************************
    h(n)=gapInit ! h(n) = separation, for this routine only
```

```
      if(drDisp(2,kSlv).eq.0)   dE12(n) = 0.0
      if (drDisp(2,kSlv).gt.0)  dE12(n) = -1.0
      if (drDisp(2,kSlv).lt.0)  dE12(n) =  1.0
      u(n)=(mst_velocity+slv_velocity)
C*************************************************************************
      endif
22    continue
      endif
C*************************************************************************
      if (n .gt. zero) then
C*******************N>3*********************************************
      if (n .ge. 4) then
C*****************Cal GW pressure*************************************
      do 55 i=1,n
      if ( h(i) .LT. (SQRT(3.0))*Rq)then
      phi=(2.0*(SQRT(3.0))*rq)/(h(i))   ! phi = flow factor, for this routine only
      else
        phi=1+3.0*(Rq/(h(i)))**2
      endif
      k(i)=(phi*(h(i))**3)/zeta
C******************micro gw model symbol, for this routine only***************
C     da=dimentionless real area of contact, pc=asperity contact pressure, a1=real area of
C     contact, dx=nominal area, f=contact force, a2=lower limit, b2=upper limit
C     ***********************************************************************
      a2=h(i)/sigma   !standardized separaiton for this routine only
      call  simpson(a2,b2,integral1,integral2)
      da(i)= pi*neu*beta*sigma*integral1
      a1(i)=da(i)*dx ! a1 = real area of contact , for this routine only
      f=(4.0*neu*dx*edesh*beta**0.5*sigma**1.5*integral2)/3.0
      pc(i)=f/a1(i)


C***************Solution of Reynolds Equation by finite difference method****
C     solves a tridiagonal system using the Thomas Algorithm
C     there are n equations, in the tridiagonal form:
```

```
C    a(i)*P(i-1) + b(i)*P(i) + c(i)*P (i+1) = d(i)
C    here, a(1) and c(nn) are assumed 0, and ignored
C    P is returned in d, b is altered

55    continue
      do 99 i=2,n-1
      a(i)= (k(i-1)+k(i))/2.0                          ! coefficient of p(i-1)
      c(i)= (k(i)+k(i+1))/2.0                          !  coefficient of P(i+1)
      b(i)= -(k(i-1)+k(i))/2.0 -(k(i)+k(i+1))/2.0  ! coefficient of p(i))
      d(i)=u(i)*dx*3.0*(h(i+1)-h(i-1))              ! d=hydrodynamic pressure
99    continue
C******************Boundary conditions**********************************
      d(1)=0.0
      d(n)=0.0
      d(2)=0.0
      d(n-1)=0.0
C***************************************************************************
      CALL tridiag(a,b,c,d,n)

120   format(i3,5e15.7)
220   format(i3,9e15.7)
610   format(i3,7e15.7)

C***************n>3 finish*************************************************
      else
C******calculate GW pressure*************************************************
      do 50 i=1,n
      a2=h(i)/sigma   ! separaiton = d2(n)=h(n)
      call simpson(a2,b2,integral1,integral2)
      da(i)= pi*neu*beta*sigma*integral1 ! da= dimentionless real area of contact
      a1(i)=da(i)*dx
      f=(4.0*neu*dx*edesh*beta**0.5*sigma**1.5*integral2)/3.0
      pc(i)=f/a1(i)
50    continue
```

```
C******Calculation of  GW pressure finish**********************************
      endif
      do 60 i=1,n
C  ************* update normal and shear stress  ***************************
      pn=da(i)*pc(i)+(1-da(i))*d(i)
      ssa=pc(i)*miu*dE12(i)      ! ssa = shear stress of solid-solid contact
      ssb=(zeta*(mst_velocity-slv_velocity)/h(i))*dE12(i)   !ssb=shear stress of fluid
      pt=da(i)*ssa+(1-da(i))*ssb
      stress(i_str_S11,kn(i))=pn
      stress(i_str_S12,k n(i))=pt
      muo = pt/pn      ! muo = overall coefficient of friction, for this routine only
      muo= sign(muo, pn)
      if ((timGlb-floor(timGlb/outputdt)*outputdt).LT.dtimCur) then
       write(114,220)kn(i),
     *      timGlb,
     *      coordslv(1,kn(i)),
     *      pn,
     *      pt,
     *      muo,
     *      da(i),
     *      u(i),
     *      h(i),
     *      d(i)
      endif
 60   continue
      endif
      return
      end
C*****************Main subroutine complete*****************************

      Subroutine tridiag(a,b,c,d,nn)

C     solves a tridiagonal system using the Thomas Algorithm
C     there are nn equations, in the tridiagonal form:
```

```
C    a(i)*x(i-1) + b(i)*x(i) + c(i)*x(i+1) = d(i)
C    here, a(1) and c(nn) are assumed 0, and ignored
C    x is returned in d, b is altered

 double precision a(nn),b(nn),c(nn),d(nn)
 integer  nn, j ,st,ed
      st=2                    ! st=Start value, for this routine only
     ed=nn-2                 ! ed=end value, for this routine only
     if(ed .eq. st) then
     d(st)=d(st)/b(st)
     return
     end if
     do 10 j = st+1,ed
     km1 = j - 1
     if(b(j-1) .eq. 0.0) then
     write(6,100) km1
     stop
     end if
    xm = a(j)/b(km1)
      b(j) = b(j) - xm*c(km1)
      d(j) = d(j) - xm*d(km1)
  10   continue
      d(ed) = d(ed)/b(ed)
      do 20 i = st+1, ed
      j= ed +st – i
      d(j) = (d(j) - c(j)*d(j+1))/b(j)
  20   continue
      return
 100   format(/3x,'diagonal element .eq. 0 in tridiag at J = ',i2/)
      end
```

```
      Subroutine simpson(a2,b2,integral1,integral2)
      double precision  f1,f2

C     *****************Simpson integration*********************************
C      Integration of f(x) on (a,b)
C      Method: Simpson rule for n intervals
C     f   - Function to integrate (supplied by a user)
C     a  - Lower limit of integration
C     b  - Upper limit of integration
C     n   - number of intervals
C     d -OUT:
C     integral - Result of integration
C     ************************************************************************
      double precision a2, b2,integral1,integral2,s1,s2
      double precision h, x
      integer n1, i
C     if n is odd we add +1 to make it even
C     if((n1/2)*2.ne.n1) n1=n1+1
C      loop over n (number of intervals)
      n1 = 20000
      s1 = 0.0
      s2 = 0.0
      if (a2.lt.b2) then
      h = (b2-a2)/2.0D4
      x=a2
      do i=2, n1-2, 2
      x   = a2+i*h
     s1 = s1 + 2.0*f1(x,a2) + 4.0*f1(x+h,a2)
     s2 = s2 + 2.0*f2(x,a2) + 4.0*f2(x+h,a2)
     end do
    integral1 =0.0D0
     *      +(s1 + f1(a2,a2) + f1(b2,a2) + 4.0*f1(a2+h,a2))*h/3.0
      integral2=0.0D0
     *      +(s2 + f2(a2,a2)+ f2(b2,a2)+ 4.0*f2(a2+h,a2))*h/3.0
```

```
      else
      integral1=0.0D0
      integral2=0.0D0
      endif
      return
      end subroutine simpson
C*********************************************************************
     double precision function f1(x,k1)
      double precision  x,k1
      f1=(1.0/(sqrt(2.0*3.14)))*((x-k1)*exp(-0.5*x**2))
       return
       end
C*********************************************************************
      double precision function f2(x,k1)
      double precision  x,k1
      f2=(1.0/(sqrt(2.00*3.14)))*((x-k1)**1.5*exp(-0.5*x**2))
      return
      end
C**********************************Subroutine complete***************
```

Appendix-2

List of publication

1. Mohammad N. Khan, Haihui Ruan, Liangchi Zhang, X.M. Zhao and X.M. Zhang," A new approach to the numerical investigation of mixed lubrication in strip rolling", *7th Australasian Congress on Applied Mechanics, ACAM 7 , 9-12 December 2012, Adelaide, Australia.* - Accepted**.**